

DISS. ETH NO. 25230

***EXPLORING FUNDAMENTAL ASPECTS OF  
BIO-MODIFIED RECLAIMED  
ASPHALT BINDER***

A thesis submitted to attain the degree of  
DOCTOR OF SCIENCES of ETH ZURICH  
(Dr. sc. ETH Zurich)

presented by

***MARIA CHIARA CAVALLI***

*Laurea Magistrale in Ingegneria Civile  
Università degli Studi di Parma*

born on *15.10.1988*

citizen of Italy

Accepted on the recommendation of

*Prof. Dr. Edoardo Mazza, ETH Zürich, examiner*

*Prof. Dr. Nicole Kringos, KTH, co-examiner*

*Dr. Lily Poulidakos, Empa, co-examiner*

2018



*This dissertation is dedicated to my family*

*“Ethic is not how we may make ourselves happy,  
but how we may make ourselves worthy of happiness”.*

*Immanuel Kant*

## Acknowledgments

As conclusion of this Ph.D. thesis, I have to mention that this work would have not been possible without the support and contribution of many people.

First of all, my deep gratitude goes to my main supervisor Dr. Lily Poulikakos for putting trust in me every day through these years. In the same way, she provided the best supervision a student could have with constant discussions and a precious help in finalizing the thesis. Last but not least, I'm deeply thankful for the great support during a personal very challenging time.

I would like to thank Prof. Dr. Edoardo Mazza for bringing his knowledge into this project and for acting as my doctoral father. From my side, a thank for having me taught how to apply a critical thinking and to go beyond the results.

Further, I want to express my gladness to Prof. Dr. Niki Kringos from KTH for accepting to act as my external examiner and for her interest in my Ph.D. thesis.

I sincerely thank Prof. Dr. Chiara Daraio from the California Institute of Technology who inspired me to open the way to my doctoral studies. Without her enthusiasm, I most probably would have not gone through this process.

I thank all the members in the road engineering/sealing components at Empa who have actively participated in the project and provided me help and support, in particular Dr. Salomé dos Santos, Dr. Martins Zaumanis, Prof. Dr. Manfred Partl and Christian Meierhofer. In addition, I'd like to thank all the members of our research group at Empa for nice memories and experiences during these years.

The financial support by the Swiss federal office for the environment as well as BHZ Baustoff Verwaltungs AG and Ammann Group is greatly acknowledged.

On a personal note, a big thank to the group of Italian friends for the wonderful moments and for having sweetened this Swiss experience.

Last but most important, my immense gratitude goes to my family for being always an important source of encouragement and Francesco for standing by me all these years.

# Table of Contents

<b>ACKNOWLEDGMENTS</b> .....	<b>5</b>
<b>LIST OF FIGURES</b> .....	<b>8</b>
<b>LIST OF TABLES</b> .....	<b>13</b>
<b>ABBREVIATIONS</b> .....	<b>14</b>
<b>SUMMARY</b> .....	<b>15</b>
<b>SOMMARIO</b> .....	<b>17</b>
<b>1. INTRODUCTION AND OBJECTIVE</b> .....	<b>19</b>
1.1 MOTIVATION .....	19
1.2 OUTLINE OF THE DISSERTATION .....	22
<b>2. THEORETICAL AND EXPERIMENTAL BACKGROUND</b> .....	<b>23</b>
2.1 SUMMARY .....	23
2.2 BITUMEN’S CHEMISTRY AND ITS SARA FRACTIONS.....	23
2.3 TOWARDS A MICROSTRUCTURAL MODEL OF BITUMEN.....	26
2.4 RHEOLOGICAL BASIC MODELS.....	29
2.2 RHEOLOGICAL PROPERTIES OF BITUMINOUS MATERIALS .....	39
2.3 FRACTURE TOUGHNESS .....	42
2.4 LOW TEMPERATURE CRACKING BEHAVIOUR OF BITUMINOUS BINDERS.....	44
2.5 INFRARED SPECTROSCOPY .....	46
2.6 CHROMATOGRAPHIC ANALYSIS.....	47
2.7 APPLICATION OF FTIR-ATR AND GPC FOR THE CHARACTERIZATION OF BITUMEN .....	49
2.8 ATOMIC FORCE MICROSCOPY .....	52
2.9 BITUMEN’S OBSERVATIONS BY USING ATOMIC FORCE MICROSCOPY .....	60
<b>3. MATERIALS</b> .....	<b>65</b>
<b>4. INFLUENCE OF REJUVENATORS ON THE MECHANICAL PERFORMANCES OF RECLAIMED ASPHALT BINDER</b> .....	<b>67</b>
4.1 SUMMARY .....	68
4.2 INTRODUCTION.....	68
4.3 MATERIALS AND METHODS .....	69
4.4 RESULTS AND DISCUSSION .....	70
4.5 CONCLUSIONS AND PERSPECTIVES .....	81
4.6 APPENDIX.....	83
<b>5. LOW TEMPERATURE CRACKING BEHAVIOUR OF RECLAIMED BINDER WITH REJUVENATORS</b> .....	<b>87</b>

5.1	SUMMARY .....	88
5.2	INTRODUCTION.....	88
5.3	MATERIALS AND METHODS.....	89
5.4	RESULTS AND DISCUSSION .....	90
5.5	CONCLUSIONS AND PERSPECTIVES .....	96
5.6	APPENDIX.....	97
<b>6.</b>	<b>SURFACE NANO-MECHANICAL PROPERTIES OF BIO-MODIFIED RECLAIMED ASPHALT BINDER.....</b>	<b>99</b>
6.1	SUMMARY .....	100
6.2	INTRODUCTION.....	100
6.3	MATERIALS AND METHODS .....	101
6.4	RESULTS AND DISCUSSION .....	104
6.5	CONCLUSIONS AND OUTLOOK .....	118
<b>7.</b>	<b>OVERALL CONCLUSIONS AND OUTLOOK.....</b>	<b>119</b>
	<b>BIBLIOGRAPHY .....</b>	<b>122</b>
	<b>CURRICULUM VITAE .....</b>	<b>136</b>

## List of Figures

Figure 1 Goals of this Ph.D. Thesis. ....	21
Figure 2 Multiscale approach used in this Ph.D. thesis: from rheological measurements towards micro-scale topography. ....	22
Figure 3 Example of an asphaltene molecule according to (Lesueur 2008). ....	24
Figure 4 Bitumen's fractions according to SARA by their atomic mass according to (Lesueur 2008). ....	25
Figure 5 Structure of bitumen according to SARA fractioning: "sol" type (left) and "gel" type (right) according to the model proposed by Pfeiffer and Salt (Pfeiffer and Saal 1940) ....	25
Figure 6 A simplified view of the colloidal structure of bitumen. (Lesueur 2008) ....	26
Figure 7 Derived micromechanical model of asphalt. (Eberhardsteiner et al. 2015b) ....	27
Figure 8 Maxwell Model. ....	30
Figure 9 Voigt Kelvin Model. ....	31
Figure 10 Example of Burger's model. ....	32
Figure 11 E' and E'' represented in an imaginary plane with indication of the phase angle $\delta$ . ....	33
Figure 12 Stress and strain over time in case of sinusoidal loading for a viscoelastic material. ....	34
Figure 13 Example of construction of a sol called "master curve". ....	36
Figure 14 Example of a material response for a strain sweep. ....	36
Figure 15 Dynamic shear rheometer apparatus (left) and example of mastercurve obtained with a dynamic shear rheometer (right). ....	38
Figure 16 Complex shear modulus and phase angle at various temperatures/frequencies for a typical asphalt binder and corresponding master curve at 25 °C. (Jongepier et al. 1969) ....	40
Figure 17 Complex modulus and phase angle for bitumen with different percentages of waxes. (Edwards and Redelius 2003) ....	40
Figure 18 Influence of different percentages of rubber on neat asphalt. (S.-C. Huang 2008) ....	41
Figure 19 Plot showing strength–toughness relationships for engineering materials where $Kc$ is the fracture toughness and $\sigma_y$ the yield strength. (Ritchie 2011) ....	42
Figure 20 Schema of the fracture toughness test setup. ....	43
Figure 21 Temperature vs deflection plot and the corresponding force-deflection curve for temperature $T_2$ (satisfying the FTT requirement of 0.3 mm). ....	44
Figure 22 Example of work to fracture for RAP + 5% A at -10° C. ....	44
Figure 23 Example of ATR-FTIR spectroscopy. ....	46
Figure 24 FTIR spectrum for a virgin binder 50/70. ....	47



Figure 25 Scheme of gel permeation chromatography (left) and example of GPC results for a RAP binder (right). .....	48
Figure 26 Relation between $G^*$ and LMS. (Zhao et al. 2014).....	49
Figure 27 FTIR spectra analysis of an asphalt binder before and after laboratory aging. (Yao et al. 2013).....	50
Figure 28 ATR-FTIR of different binders. Red arrows highlight changes in the spectra due to aging. Blue arrows highlight differences between asphaltenes of asphalt binder and pure bio-rejuvenator (BR). (Pahlavan et al. 2018).....	51
Figure 29 Scheme of an atomic force microscopy according to (Das et al. 2016a).....	52
Figure 30 Force-distance curve with its corresponding cantilever position. Adapted from (Cappella and Dietler 1999) .....	53
Figure 31 AFM topography image of a bitumen. Adapted from (Pahlavan et al. 2016). .....	55
Figure 32 Example of Hertzian contact with indication of the tip radius $R$ , the indentation $\delta$ , the elastic modulus $E$ and the Poisson's ratio $\nu$ of the sample. Adapted from (S. H. Kim, Dugger, and Mittal 2010). .....	57
Figure 33 Force-distance curve with indication of the Peak Force ( $F_{tip}$ ); deformation (indentation $\delta$ ); adhesion force ( $F_{ad}$ ) and the DMT modulus ( $E$ ). .....	58
Figure 34 Example of a $10 \times 10 \mu\text{m}$ image of virgin binder 50/70 corresponding to $512 \times 512$ pixels. .....	59
Figure 35 Force-distance curve obtained for the virgin binder 50/70 at designed point in Figure 34. ....	59
Figure 36 Example of bitumen's morphology with catanaphase, paraphase and periphase. (Lyne, Wallqvist, and Birgisson 2013).....	61
Figure 37 An example AFM height image ( $5 \mu\text{m} \times 5 \mu\text{m}$ ) with corresponding scheme of a "bee" (Hung and Fini 2015). .....	62
Figure 38 AFM height images of the surface of (a) undoped bitumen and bitumen doped with (b) 1% amide, (c) 1% acid, (d) 1% amide and +1% acid. (Hung et al. 2017).....	63
Figure 39 AFM images $9 \times 9 \mu\text{m}$ of the control asphalt binder (left) and a RAP binder (right). (Nazzal et al. 2014) .....	64
Figure 40 Rejuvenator dosage vs. penetration grade. The values presented were obtained following the European standard EN 1426. ....	66
Figure 41 Dynamic shear moduli master curves for reference temperature of $20^\circ\text{C}$ (left) and phase angle measurements (right) from frequency sweeps (0.1-20 Hz). The presented values are an average of four measured values.....	71
Figure 42 Master curves of complex shear moduli results of the aged materials measured (left) and phase angle measurements (right) at reference temperature of $20^\circ\text{C}$ and at frequency sweeps (0.1-20 Hz). The presented values are an average of four measurements.....	72

Figure 43 Example of the calculation of the crossover temperature at 1Hz. ....	72
Figure 44 The crossover temperatures for the aged and unaged materials, at the frequency of 1 Hz for the different binders tested between -10° C and +40° C.....	73
Figure 45 Principle of the rheological aging index calculation using the area between the aged and unaged master curve at reference temperature of 20° C.....	74
Figure 46 Variation of the rheological aging index for the different binders. ....	75
Figure 47 ATR-FTIR spectra of the plain rejuvenators A, B and C before aging.....	76
Figure 48 ATR-FTIR spectra of the virgin binder 50/70, the RAP binder and the RAP binders with rejuvenators A, B and C (5% by mass of RAP binder each). ....	77
Figure 49 Comparison between the CAI of the virgin binder, RAP binder and RAP binder plus 5% by mass of rejuvenators before and after aging. ....	78
Figure 50 GPC spectra with UV (left) and RI-signals (right) of the RAP binder and the RAP binder with rejuvenator A, B and C (5% by mass of RAP binder each).....	79
Figure 51 SARA fractioning of the virgin binder, the RAP binder and the rejuvenated RAP binder before and after aging. ....	79
Figure 52 Colloidal index for the virgin binder, the RAP binder and the rejuvenated RAP binder before and after aging. ....	80
Figure 53 Complex modulus variation at different shear strains at 40° C.....	83
Figure 54 Data shifting to obtain a mastercurve according to the sigmoidal model with the WLF shift factor.....	84
Figure 55 Mastercurves with indication of the standard deviation as average for four measurements. ....	85
Figure 56 Comparison between the carbonyl and sulfoxide index of the virgin binder, RAP binder and RAP binder plus 5% by mass of rejuvenators before aging (top part) and after aging with RTFOT and PAV (bottom part). ....	86
Figure 57 FTT moulds with paper to impose a pre-notch.....	89
Figure 58 Example of force vs. deflection curves for all the unaged (left) and aged (right) binders at -10° C. The curves presented are averaged of four measurements and standard deviation is presented for each point. ....	90
Figure 59 Work to fracture at crack initiation at -10° C before and after aging. ....	91
Figure 60 Deflection variation with temperature for all the binders tested at unaged state. Average and standard deviation were calculated for four measurements per sample. ....	92
Figure 61 Fracture toughness temperature for the different materials at unaged/aged state. Average and Standard deviation was calculated for four measurements.....	93
Figure 62 Modulus and phase angle master curves for all the unaged binders (on top) and the aged ones (on the bottom). Values presented are averages of four measurements. ....	94

Figure 63 Example of elastic and viscous components of the complex modulus ( $G'$ , $G''$ ) together with the crossover frequency. The data plotted are average of four measurements.....	95
Figure 64 Crossover modulus and crossover frequency (log-log scale) for all materials tested before and after aging.....	95
Figure 65 Example of output data for unaged binders at $-10^{\circ}$ C.....	97
Figure 66 Example for output data for aged binders at $-10^{\circ}$ C. ....	98
Figure 67 Corresponding grey scale image (right) of the phase image from the virgin binder 50/70 (left). Size was $10 \times 10 \mu\text{m}$ each image corresponding to $512 \times 512$ pixels.....	102
Figure 68 Histogram showing each pixel its corresponding grey scale value. On the y axis the colour intensity is reported.....	102
Figure 69 Histogram with the threshold to obtain a black and white image.....	103
Figure 70 Black and white image of the virgin binder 50/70 after the application of the threshold. ....	103
Figure 71 AFM height morphology image of the virgin binder 50/70 (left) and phase visualization (right) (image size $10 \times 10 \mu\text{m}$ ). ....	104
Figure 72 AFM height image showing present structures in the virgin binder 50/70. The scan size is $10 \times 10 \mu\text{m}$ . ....	105
Figure 73 AFM height morphology image of the RAP binder with 22% asphaltenes (left) and its phase visualization (right) ( $10 \times 10 \mu\text{m}$ ).....	106
Figure 74 AFM height morphology image ( $10 \times 10 \mu\text{m}$ ) of the RAP plus 5% A (a) and corresponding phase image (b); RAP plus 5% B (c) and its phase image (d); and RAP plus 5% C (e) and its phase image (f). Branches are indicated with a dotted line while salphases are outlined with arrows.....	107
Figure 75 AFM morphology of the different rejuvenated RAP binder after aging ( $10 \times 10 \mu\text{m}$ ). From top left to bottom (clockwise): a) Aged virgin binder 50/70; b) Aged RAP binder; c) Aged RAP + 5% A; d) Aged RAP + 5% B and e) Aged RAP + 5% C. Branches are indicated with a dotted line while salphases are outlined with arrows. ....	108
Figure 76 Area dark (relatively soft) and area white (relatively hard) for each binder and its relative standard deviation. The standard deviation was calculated over five areas in five different images. ....	109
Figure 77 $G^*$ and ratio between the dark are and the white area for each binder. ....	110
Figure 78 AFM QNM images ( $10 \times 10 \mu\text{m}$ ). a) Virgin binder 50/70 unaged; b) RAP binder unaged; c) Virgin binder 50/70 aged; d) RAP binder aged. ....	111
Figure 79 AFM QNM images ( $10 \times 10 \mu\text{m}$ ). From top left clockwise: a) RAP + 5% A b) RAP + 5% B c) RAP + 5% C d) RAP + 5% A aged e) RAP + 5% B aged f) RAP + 5% C aged. ....	112

Figure 80 Gaussian distribution and cumulative frequency curve for unaged binders (A, left) aged binders (B, right). Data were obtained as average of five different images per binder. ....113

Figure 81 50<sup>th</sup> percentile elastic modulus for all binders with standard deviation calculated as average of five measurements. ....113

Figure 82 Top part: AFM topography image of the virgin binder 50/70 with corresponding measurement of wavelength  $\lambda_0$  and maximal amplitude  $2A_0$  of the “bee” structure. Bottom part: representation of the “bee” structure with corresponding wavelength  $\lambda_0$  and the maximum amplitude  $2A_0$ . ....114

## List of Tables

Table 1 Parameters obtained after application of the sigmoidal model to all binders. ....	84
Table 2 Results obtained from the rheological measurements with corresponding elastic modulus as well elastic modulus obtained after AFM QNM. ....	117

## **Abbreviations**

AFM Atomic force microscopy

ATR-FTIR Attenuated Total Reflection Fourier Transform Infrared Spectroscopy

BSP Boltzmann superposition principle

CT Computed tomography

DMT Derjaguin-Muller-Toropov

DSR Dynamic shear rheometer

ESEM Environmental scanning electron microscope

FTIR Fourier transforms infrared spectroscopy

FTT Fracture toughness test

GPC Gel permeation chromatography

HMA Hot mix asphalt

LVE Linear viscoelastic

QNM Quantitative nano-mechanical mapping

RAP Reclaimed asphalt pavement

SARA Saturates, aromatics, resins, asphaltenes

T<sub>FT</sub> Temperature fracture toughness

TTS Time temperature superposition

WLF Williams-Landel-Ferry

## Summary

Because of the increasing environmental awareness, reclaimed asphalt pavement (RAP) has become more and more important in road engineering as renewable source. Despite that, RAP cannot be used as it is because it is more brittle than virgin asphalt concrete thus it needs to be modified with additives known as rejuvenators. Modified reclaimed asphalt pavement is a novel composite material that has gained interest from some decades ago. This thesis explores the potential of using bio-based rejuvenators in RAP binder from different perspectives. Three different bio-based rejuvenators have been used: a sunflower seed oil which is known for its antioxidant properties, a cashew-nut shell based oil and a tall oil. The latter two are commercially available products commonly used in the asphalt industry as rejuvenators.

In the first part of the thesis, I have evaluated the rheological as well the chemical properties of the bio-modified RAP binder before and after aging. By using SARA fractioning, I have highlighted how rejuvenators caused a change in RAP binder's polar/non-polar compositions. Nevertheless, from Fourier transform infrared spectroscopy I have detected how rejuvenators did not cause any changes at functional group level to the RAP binder. Analyses with the dynamic shear rheometer have shown how after the addition of rejuvenators an improvement in the mechanical performances of the RAP binder has been observed. Furthermore, I have shown how aging is an important parameter to be considered when evaluating the effectiveness of rejuvenators when studying the rheological performances. I have demonstrated how a holistic approach combining chemo-mechanical analysis is fundamental to understanding the behaviour of these bio-modified binders.

In the second part of the thesis, I focused on the low temperature cracking performances of bio-modified RAP. High RAP mixtures are susceptible to cracking therefore; strong cracking resistance is desirable when producing such roads thus, it is fundamental for a bio-modified pavement to fulfil the required mechanical performances at low temperatures. By utilizing a so called fracture toughness test, I have observed how aging has a prominent effect on the fracture toughness. By combining rheological measurements and cracking experiments, the effectiveness of rejuvenators in restoring the properties of the RAP binder can be evaluated from different angles.

In the third part of the thesis, I have analysed the microstructure of binders with atomic force microscopy (AFM). New features on the surface of the RAP binder and different mechanical properties have been observed when rejuvenators were added to the RAP binder. Quantitative nano-mechanical mapping (QNM) showed how aging caused a significant increase in terms of elastic moduli of all the binders. A qualitative correlation between bulk complex moduli (from rheological measurements) and phase images (from atomic force microscopy) has been shown. This correlation was found valid after the direct measurements of the elastic moduli at the samples' surface with

QNM. Furthermore, I have shown that the microstructures forming on the surface of the virgin binder due to wrinkling of the surface that has a higher measured modulus in comparison to the bulk.

In the framework of this thesis, a multi-scale approach on the evaluation of rejuvenated binders has been proposed. It was demonstrated how a holistic approach is vital when solving questions addressing fundamental aspect of bio-modified reclaimed asphalt binder, thereby improving our understanding of challenges when producing high RAP mixtures and solutions to obtain the required performance of such mixtures.



## Sommario

Il fresato sta diventando sempre più un materiale di primaria importanza a causa del sempre maggiore interesse nella tutela delle risorse non rinnovabili e il rispetto dell'ambiente. Nonostante ciò, il fresato non può essere utilizzato senza l'aggiunta di particolari prodotti chiamati rigeneranti affinché si possano ripristinare le sue proprietà reologiche andate perdute a causa del fenomeno dell'invecchiamento. Il fresato modificato è un nuovo materiale composito che ha assunto notevole rilevanza negli ultimi decenni. Questa tesi di dottorato analizza il potenziale nell'uso dei rigeneranti sotto diversi aspetti. In particolare, tre diversi rigeneranti sono stati utilizzati: un olio di semi dalle elevate proprietà antiossidanti, un olio di semi di arachidi e un olio di pino; questi ultimi due prodotti sono stati scelti poiché rigeneranti commercializzati per il solo asfalto.

Nella prima parte di questa tesi sono state studiate le proprietà chimiche e reologiche del fresato modificato prima e dopo il processo di invecchiamento. È stato dimostrato come i rigeneranti potessero essere in grado di modificare la composizione del fresato in termini di elementi polari grazie all'utilizzo della tecnica definita SARA fractioning. Nonostante ciò, i rigeneranti non hanno inficiato i legami molecolari formati a causa dell'invecchiamento come è emerso a seguito delle analisi con spettroscopia infrarossa in trasformata di Fourier. Tuttavia, il binder del fresato ha mostrato notevoli miglioramenti dal punto di vista delle prestazioni reologiche a seguito dello studio delle proprietà reologiche con la tecnica del reometro. Un aspetto chiave sviluppato in questo capitolo è stato l'analisi dell'effetto dell'invecchiamento sui vari bitumi testati. È stato possibile dimostrare come un approccio multi-scala sia fondamentale quando si voglia dimostrare l'efficacia dei rigeneranti prima e dopo i fenomeni di invecchiamento.

Nella fase successiva sono state analizzate le prestazioni del fresato modificato a basse temperature. La resistenza a basse temperature è una qualità importante per il fresato in quanto a basse temperature le pavimentazioni stradali sono più soggette a fenomeni di fessurazioni. Le proprietà meccaniche del materiale nonché la tenacità sono state analizzate grazie all'utilizzo delle prove di frattura a basse temperature. Un approccio che unisce proprietà reologiche a basse temperature e proprietà meccaniche si è rivelato efficace nell'individuazione di rigeneranti che potessero migliorare le funzionalità meccaniche del fresato e allo stesso tempo mantenere le giuste prestazioni meccaniche a basse temperature.

A conclusione di questa tesi di dottorato, è stata analizzata la microstruttura dei bitumi con il microscopio a forza atomica. È stato così possibile osservare caratteristiche differenti dal punto di vista morfologico dei vari bitumi. Con la procedura definita quantitative nano-mechanical mapping (QNM) è stato possibile identificare il modulo elastico di ogni bitume in corrispondenza della superficie. È stata poi proposta una correlazione tra il modulo complesso ottenuto dalle analisi reologiche, le immagini a contrasto di fase e il modulo elastico in superficie ottenuto con QNM. È

stato altresì dimostrato come strutture superficiali di differente modulo elastico si sviluppino solo sulla superficie del bitume vergine.

In sintesi, in questa tesi è stato proposto un approccio multi dimensionale per l'analisi di bitumi modificati. E' stato altresì dimostrato come sia fondamentale un'analisi olistica affinché si possano risolvere aspetti fondamentali inerenti all'utilizzo dei bitumi modificati.

# 1. Introduction and objective

## 1.1 Motivation

Asphalt concrete, which is a composite material consisting of approximately 95% mineral aggregates and 5% bitumen, is the most used building material in road construction. Hot mix asphalt mixtures (HMA) generally require high mixing and installation temperatures for heating both the mineral aggregates and the bitumen. Hence, researchers started to put efforts to develop low energy consumption solutions as well as to increase sustainability when using asphalt concrete. In the past, the importance of environmental protection has not been considered a priority, but more recently this has changed to become indisputably a subject of serious and persistent concerns as well as to assume a much wider scope. Nowadays, it is fundamental to save raw materials such as virgin bitumen and virgin aggregates and try to reuse materials from old roads. To do so, reclaimed asphalt is used which is defined as the “removed or reprocessed pavement materials containing asphalt and aggregates” (National Asphalt Pavement Association 2010). The most economical use of RAP is in the intermediate and surface layers of flexible pavements because the less expensive RAP binder can replace a portion of the more expensive virgin binder; nevertheless a mixture is considered as a high RAP content mixture when it contains RAP in the range of 25% of the weight of the mixture (B. Huang et al. 2005). Flexible pavements are made of several layers of carefully selected materials designed to gradually distribute loads from the pavement surface to the layers underneath. The design ensures the load transmitted to each successive layer does not exceed the layer’s load-bearing capacity. However, 100% RAP content mixes are perceived to be more susceptible to fatigue and thermal cracking failures than traditional mixtures. For this reason, so called “rejuvenators” are used for restoring the properties of the RAP binder. To this extent, in order to have a complete picture of the effect of rejuvenators, the viscosity reducing capacity as well as changes at molecular level are generally analysed (dos Santos, Partl, and Poulidakos 2015). Firstly, this complex composite material needs to be understood at its fundamental level. A broad understanding on the correlation between chemical composition, polar/non-polar components, microstructural properties and the macro-scale properties is still largely missing. The understanding of these connections will lead to strengthen the scientific approach needed in this field. Thus, the larger motivation behind this study is to demonstrate how a multi-scale approach can be used to obtain a holistic understanding when investigating recycled asphalt binder with bio-based additives. This dissertation is part of a larger project funded by the Swiss Federal Office for the Environment (BAFU) titled “Fully sustainable asphalt concrete” involving two industrial partners: Ammann Switzerland AG (asphalt plant manufacturer) and BHZ Baustoff Verwaltungs AG

(an asphalt mixing plant owner). The global goal of this project has been to develop a multiscale methodology, from nano-scale characterization to field scale to study bio-modified RAP mixtures. Results acquired through this Ph.D. study have been used to conduct evaluations on 100% reclaimed asphalt pavement mixture performance and are the subject of other publications. Specifically, the Ph.D thesis has evaluated rejuvenators and methods to ensure full recycling of asphalt binder. Results of this part have been used to develop performance-based mixture design methodologies for 100% recycled asphalt as well as advancing 100% recycled asphalt manufacturing technologies to ensure safe and reliable production of the designed mixtures. Subsequently, an evaluation of environmental effects of 100% recycling and rejuvenator use to ensure safe asphalt recycling for the people and environment have been carried out. In the last part of the project, the performance of plant-produced 100% recycled asphalt pavement in comparison to conventional asphalt has been determined. Author of this Ph.D. thesis has focused on the characterization of reclaimed asphalt binder with different bio-based rejuvenators. The goal was to use a multi scale approach to investigate bio-modified RAP as can be seen in Figure 1. In order to reach this goal, several techniques have been used. To detect any changes at molecular scale/functional groups level caused by oxidation and rejuvenation, Fourier transform infrared spectroscopy has been used. The creation of covalent bonds (i.e. C=O and S=O) have been seen as fundamental to detect effect of oxidation (Marsac et al. 2014). Changes at larger scale, can be detected with techniques such as gel permeation chromatography and SARA fractioning. As it will be outlined in the thesis, rejuvenator additions in RAP binder did not cause any changes at molecular scale level but rather at larger scale (i.e. polar components). Rheology and low temperature cracking have been found to be a fundamental step to show the effectiveness of rejuvenators as well as for the evaluation of the effect of aging. In the end, surface microstructures of all binders have been analysed before and after aging. Atomic force microscopy has been utilized to characterize both topography and quantitative nano-mechanical information along the surfaces.

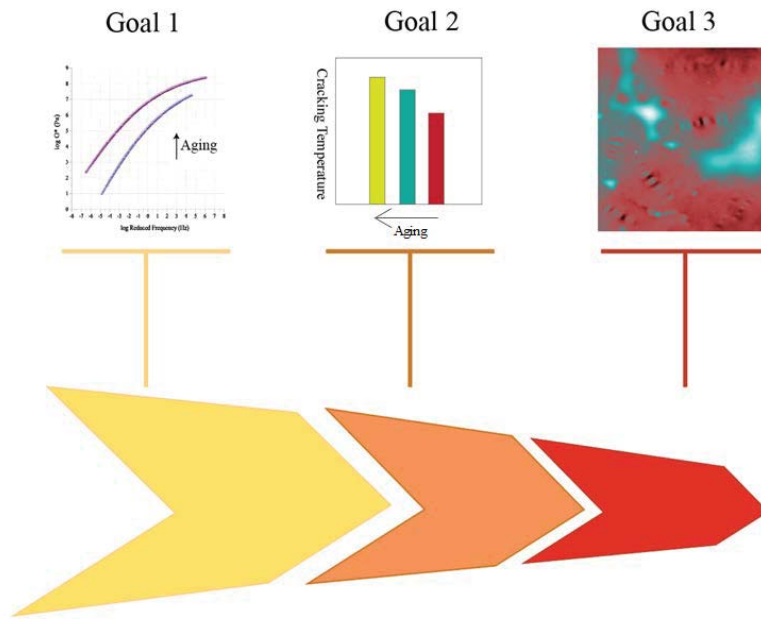


Figure 1 Goals of this Ph.D. Thesis.

## 1.2 Outline of the dissertation

As outlined in Figure 2, the general goal of this thesis is to develop a comprehensive understanding at fundamental scale on RAP binder with bio-based rejuvenators. In particular, several objectives have been identified:

Chapter 1 has given an overview of this Ph.D. thesis. Chapter 2 describes the theoretical and experimental background used to assess the bio-based RAP modification.

Chapter 3 focuses on the materials and their preparation for the purpose of this study.

Aim of Chapter 4 is to understand if RAP binder treated with different bio-based rejuvenators can have the same mechanical performances in terms of rheological properties at different temperature/frequencies conditions. The objective of this study is also to characterize and understand the effects of aging of bio-modified RAP from different points of view: molecular level, polar/non-polar compounds, and rheology.

Goal of Chapter 5 is to analyse the low temperature cracking behaviour of the modified RAP and to identify which rejuvenators could enhance its cracking behaviour at low temperature.

Chapter 6 presents phase variations as well as topography information on the bio-modified RAP. Moreover, effect of aging on the surface is also analysed. Topography and quantitative nano-mechanical properties by means of elastic moduli at the surface of all the materials were compared. In the end, Chapter 7 shows the main conclusions of this dissertation and describing the contributions of this work to create a milestone when producing bio-based pavement and how future perspectives can be evaluated.

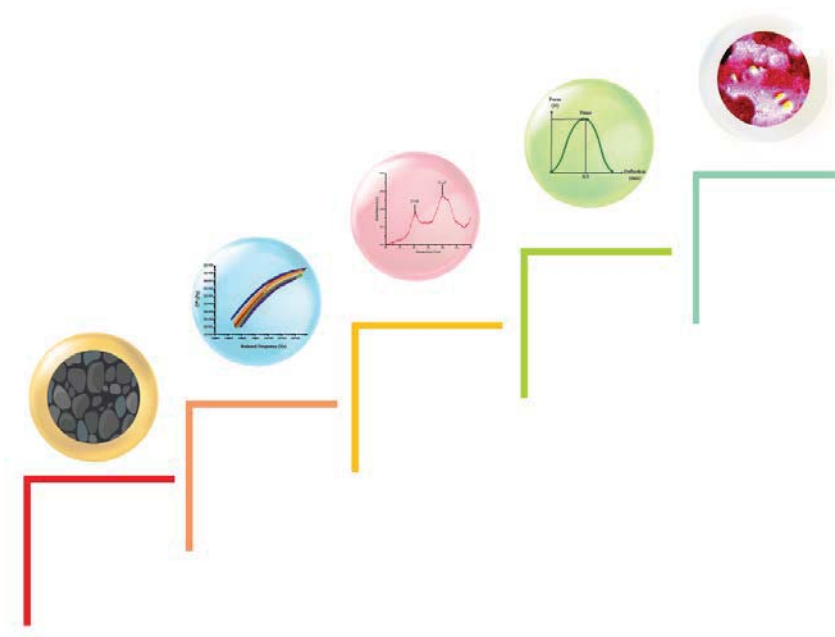


Figure 2 Multiscale approach used in this Ph.D. thesis: from rheological measurements towards micro-scale topography.

## 2. Theoretical and Experimental background

### 2.1 Summary

This chapter summarizes the background of this thesis. Specifically, rheology, mechanics and chemistry of bitumen together with its microstructure is presented. In the last part of each paragraph, the state of the art is presented. Understating the phenomena occurring from microscale to performance properties is fundamental in order to produce asphalt mixtures with 100% reclaimed asphalt.

### 2.2 Bitumen's chemistry and its SARA fractions

The first mention on the use of bitumen in road construction dates back to the construction of Babylon (625–604 BC). However, bitumen essentially disappeared from the pavements until the early 19th century, when the rediscovered European sources of natural bitumen led to the development of the modern applications for this material. The use of natural bitumen in road construction started to decay in 1910 with the advent of vacuum distillation which made it possible to obtain bitumen from crude oil and nowadays, paving grade bitumen is almost exclusively obtained as the vacuum residue of petroleum distillation. In particular, bitumen is defined as “adhesive and waterproofing material derived from crude oil, which is completely or nearly completely soluble in toluene, and very viscous at ambient temperatures” (Lesueur 2008). Bitumen's density at room temperature lies typically between 1.01 g/cm<sup>3</sup> and 1.04 g/cm<sup>3</sup>, depending on the crude source (Read et al. 2003). However, the complexity of bitumen chemistry lies in the fact that many different chemicals are present. As an overall description, the chemical nature of the crude oil is described by the nomenclature commonly used in the petroleum industry that describes bitumen components as belonging to the paraffinic, naphthenic, or aromatic fractions (Pedersen, Fredenslund, and Thomassen 1989).

Generally, the components of the heavy fraction of a petroleum fluid can be separated into four groups: saturates, aromatics, resins, and asphaltenes (SARA). Particularly, the following fractions can be observed:

- i. Saturates are non-polar long hydro carbons chains containing paraffin (C<sub>n</sub>H<sub>2n+2</sub>). They are a viscous liquid and consist of C<sub>20</sub>-C<sub>50</sub> paraffin hydrocarbons with an averaged molecular weight of 110 g/mol (Freund and Mozes 1982).

- ii. The aromatics are viscous liquids with non-polar chains of carbon able to plasticize the material; they are the dispersive matrix with average molecular weight of 400-900 g/mol (Eicher, Hauptmann, and Speicher 2003).
- iii. The resins are semi-solid polar materials which can cause the binder to be viscous and fluid; they are the dispersive agent for the asphaltenes. They are made of polar long alkane's chains with adsorbed molecules such as sulphur, nitrogen or oxygen with average molecular weight of 600-1000 g/mol as proposed in (Speight 2014).
- iv. The asphaltenes are polar amorphous solids which cause the stiffening in the binder. The polar components belong to condensed aromatics with additional heteroatoms such as sulphur, oxygen and nitrogen with averaged molecular weight of 5000 g/mol (Mitchell and Speight 1973) as can be seen in Figure 3.

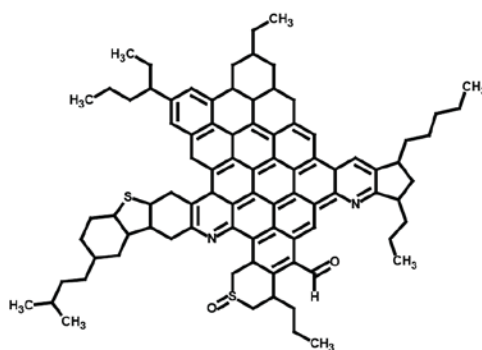


Figure 3 Example of an asphaltene molecule according to (Lesueur 2008).

- v. Saturates, aromatics and resins form the matrix, the so called maltene phase (Klein et al. 2006).

Petroleum waxes are the bitumen fractions having a crystalline form such as paraffinic waxes which are n-alkane with low molecular weight. A depiction of the all the fractions composing asphalt can be seen in Figure 4.



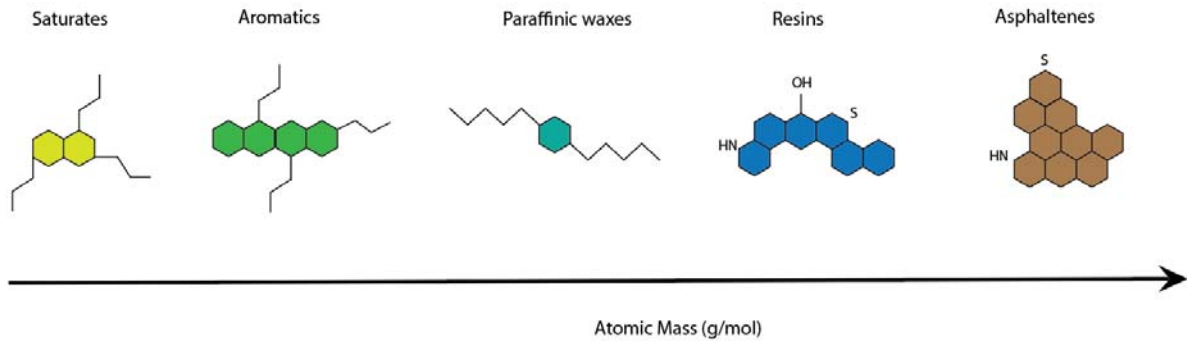


Figure 4 Bitumen's fractions according to SARA by their atomic mass according to (Lesueur 2008).

Bitumen's microstructure consists of a contiguous matrix of maltenes with saturates and aromatics, and clusters of asphaltenes as proposed in Figure 5 following what previous work had enlightened (Pfeiffer and Saal 1940). It is known that virgin bitumen is less affected by aging in terms of the formation of asphaltenes, thus, resulting in a so called "sol" type structure with majority of resins and maltenes and less asphaltenes. On the contrary, aged bitumen is supposed to be stiffer than the virgin binder, having a "gel" structure with asphaltenes forming agglomerations between the resins and the maltenes (Bonemazzi and Giavarini 1999).

Within the framework of this thesis, SARA fractioning has been chosen as it is known for being reliable in terms of repeatability and in addition, it's the most widely used test for asphalt components (Lesueur 2008).

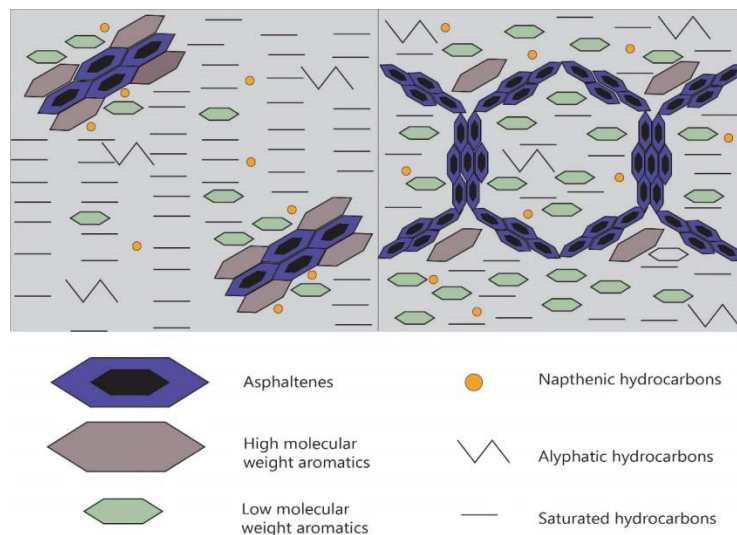


Figure 5 Structure of bitumen according to SARA fractioning: "sol" type (left) and "gel" type (right) according to the model proposed by Pfeiffer and Salt (Pfeiffer and Saal 1940) .

## 2.3 Towards a microstructural model of bitumen

For a complex composite material such as bitumen, examining the material's structure is a reliable way to better understand at fundamental level changes in the mechanical behaviour. As already mentioned, SARA fractioning separates bitumen into saturates, aromatics, resins and asphaltenes. The first colloidal model was developed by Pfeiffer (Pfeiffer and Saal 1940) to show the difference in rheological properties between what was defined as sol or gel bitumen's. As can be seen in Figure 6, asphaltenes were identified as forming clusters. Sol bitumens exhibited Newtonian behaviour, whereas gel bitumens are generally highly non-Newtonian.

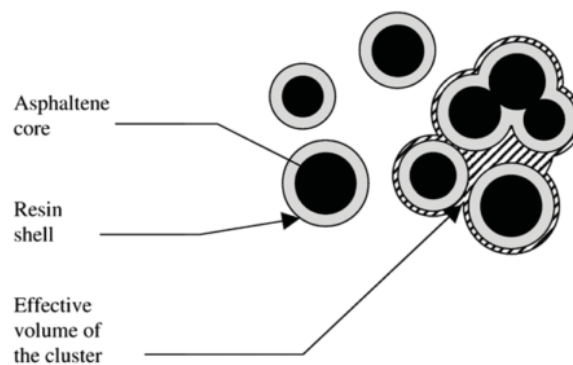


Figure 6 A simplified view of the colloidal structure of bitumen. (Lesueur 2008)

The physical and rheological properties of bitumen are influenced especially by the asphaltenes' content. Aging is known to cause an increase in asphaltene content contributing to an increase in the stiffness (Weigel and Stephan 2017b). Oxidation is a fundamental parameter to be considered when dealing with asphalt material thus, it is fundamental to investigate changes at polar/non-polar components level. RAP for example can be seen as the oxidized version of a virgin binder in which asphaltenes molecules are more clustered and agglomerated. An increase in the gel properties of bitumen causes firstly an increasing in stiffness as well as an increasing in viscosity.

It has been documented that as a result of oxidative aging the ratio of polar to nonpolar components increases, as evidenced in (Mangiafico et al. 2016). The commonly accepted explanation for these observations is that some aromatics evolve into resins, which in turn generate asphaltenes. The low reactivity of saturates is the reason for their lack of important variations after aging (Mangiafico et al. 2016).

In recent years, an asphalt model was proposed by combining SARA analysis with rheological measurements (Lackner and Spiegel 2005). As a further step, Eberhardsteiner et al. (Eberhardsteiner et al. 2015b) developed another model by creating a contiguous matrix of aromatics and resins with embedded saturate and asphaltenes as can be seen in Figure 7. The net-

work-like structure built up by the micelle mantles is represented by an interaction phase appearing as needles, being oriented in all directions.

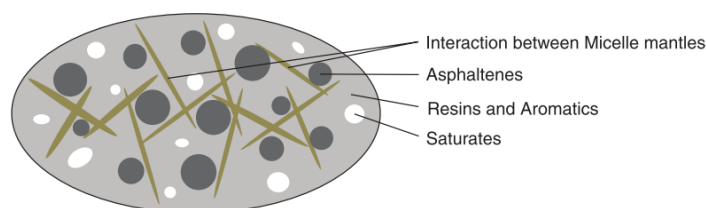


Figure 7 Derived micromechanical model of asphalt. (Eberhardsteiner et al. 2015b)

Small angle X-Ray scattering (SAXS) can confirm that asphaltenes form micelles in organic solvents (Storm, Sheu, and DeTar 1993). The colloidal model is also consistent with results obtained by thermal analysis. For example, bitumen undergoes a glass transition at a temperature very close to the one of its aromatics. This shows how asphaltenes exist as dispersed solid particles and do not directly participate to the glass transition (Petersen 2000). So far, various geometrical shapes were indeed proposed for the asphaltenes micelles in the literature. Swanson et al. firstly showed that asphaltenes precipitate when mixed with only the oily components of bitumen and how resins could help disperse asphaltenes in benzene, highlighting their key role in asphaltenes stabilization inside bitumen (Swanson 1942). More recently, Lian et al. (Lian, Lin, and Yen 1994) showed that the resins could stabilize asphaltenes. The role of the resins as a stabilizer for the asphaltenes has been further studied and it was confirmed how asphaltenes precipitate from the oily bitumen components without the resins (Mitchell and Speight 1973). Despite that, the role of the resins in asphaltenes micelles stabilization remains to be fully understood. If a reasonable agreement exists concerning the size of the asphaltenes micelles, their organisation at a higher scale remains quite hypothetical due to experimental difficulties (Gawrys and Kilpatrick 2004). In the model proposed by Petersen (Petersen and Glaser 2011), asphaltenes strongly aggregate at low temperature (60 °C), thus preventing oxygen to diffuse inside the aggregates which in turn lowered the oxidation rate. At high temperature however (130 °C), a better dispersion was found. In addition to that, waxes naturally present within bitumen, can crystallize. The consequences of wax crystallizations on the structure of bitumen are still not clear. Generally, the viscosity may suddenly decrease the melting temperature range of the crystallized wax. Other feared effects due to waxes are brittleness, physical hardening, poor ductility and poor adhesion (Edwards and Redelius 2003). (Hofko et al. 2016) outlined the influence of the SARA fractions and the interactions of these fractions on the bitumen microstructure and thus on the viscoelastic behaviour. However, (Yu et al. 2014) showed that the contents of the SARA fractions are not solely sufficient to capture the bitumen behaviour. Instead, a further characterization of the SARA fractions is necessary. In

(Weigel and Stephan 2017a), SARA fractions were linearly combined with standard engineering tests such as penetration and softening point. It was found that by increasing the content of resins, the softening point decreased. Redelius (Per G. Redelius 2006), has outlined how to avoid confusion in using the term “asphaltenes” in that it should only be used for the material precipitated with n-heptane. In his research, it is hypothesized that rather than with a colloidal model, bitumen should be described in terms of three component solubility parameters like Hansen solubility parameters which have proven to give a reasonable good model of bitumen (P.G Redelius 2000). Although it is extremely difficult to account for a complete array of chemical reactions occurring during oxidation, it is possible to evaluate the chemical reactivity of the molecules that compose current models of petroleum asphalt as well as bio-modifiers. Such evaluation can help developing guidelines for evaluating and selecting promising additives to enhance the long-term performance of asphalt. In conclusion, a full-scale characterization of the bitumen structure would be needed in order to draw a complete description of asphalt’s structure. In a future perspective, molecular modelling and computational chemistry could be useful tools to filter the most dominant processes which are relevant for understanding the mechanical properties so that it will be possible to better control the entire asphalt mix design procedure.

## 2.4 Rheological Basic Models

Rheology is the science that deals with materials' flowing. The rheological characteristics of bitumen depend mostly on its source affecting its chemical composition as well (Read et al. 2003). The word rheology is from the Greek words "ρεω", which can be translated as "flowing" and "λογος" meaning "science" and, therefore, literally means "the study of the flow" (G.D. Airey 1997). Ancient users of bitumen observed the strong effect of temperature on its consistency (Murali Krishnan and Rajagopal 2003). Asphalt binders which flow easily might be susceptible to rutting while stiffer ones can be susceptible to fatigue and cracking (Daniel et al. 2002; Y. R. Kim 2009). The first attempt to measure the viscosity of a bituminous-like substance was probably done by Von Obermayer, who used three rheometers (sliding plate, parallel plate and torsion plate) to characterize a tar as early as 1877 (Lesueur 2008). Pfeiffer and co-workers correctly attributed the non-Newtonian effects to viscoelasticity, and interpreted it as a consequence of the gel structure of the materials (Pfeiffer and Saal 1940). In modern terms, their measurements would account for the presence of delayed elasticity together with non-linearity, a behaviour now known to be present in bitumen (Lesueur 2008). The analysis of the mechanical response, due to the application of a certain load, can identify the existence of two systems: the elastic solid and the viscous fluid. The first one identifies a solid with a linear relation between stress and strain while the second one is characterized by a certain flow. In subsequent sections, models which are suitable for viscoelastic materials will be described.

### 2.1.1 Linear elastic solid

Hooke's Law is the basic principal used for determining the linear elastic response of a solid.

$$\sigma = E \times \varepsilon \quad (1)$$

with  $\sigma$  the applied stress [Pa],  $E$  the elastic modulus [N/mm<sup>2</sup>] and  $\varepsilon$  the strain [mm/mm].

The material gives a response which is linear with respect to the applied strain and independent by the time. This model was firstly proposed by Hooke (Hooke 1678). Stresses and strains of the material inside a continuous elastic material are linked by a linear relationship similar to Hooke's spring law.

### 2.1.2 Viscous Fluid

The proportional relation between an applied stress and the rate, at which the fluid deforms, is giving by the Newton relationship:

$$\sigma = \lambda \frac{d\varepsilon}{dt} \quad (2)$$

where  $\sigma$  is the applied stress [Pa]. The variation of the strain  $\varepsilon$  over time  $t$  is proportional to the factor  $\lambda$  which is the viscosity of the fluid [Pa  $\times$  s]. The model is suitable for considering time dependent fluid as well as materials which display irreversible strain when unloaded (Bird, Stewart, and Lightfoot 2007).

### 2.1.3 Maxwell Model

In the case of a viscoelastic material, the dependence between time and constitutive equation does not let the possibility to identify a linear relation between stress and strain. Therefore, it is necessary to create functional relation in which the stress at a certain time  $t$  does not only depend on the value of deformation but also on the entire history of deformation (Tschoegl 1989).

The model proposed by Maxwell, shows a spring in series with a dashpot as shown in Figure 8, thus having the total strain which will be the sum of each strain. In the case of Maxwell's model, the spring and the dashpot are connected in series, implying that the stress  $\sigma$  is equal for the two elements, thus  $\sigma_e$  is equal to  $\sigma_v$ , and that the total displacement results from the sum of the relative displacements. So that the following equation holds:

$$\frac{d\varepsilon}{dt} = \frac{d\sigma}{dt} \times \frac{1}{E} + \frac{\sigma}{\lambda} \quad (3)$$

where the variation of the strain  $\varepsilon$  over time is given by the variation of the applied stress  $\sigma$  [Pa] over time  $t$  divided per  $E$  which is the elastic modulus [N/mm<sup>2</sup> ] and the contribution given by the dashpot which is the ratio between the applied stress  $\sigma$  [Pa] and the viscosity  $\lambda$  [Pa  $\times$  s].

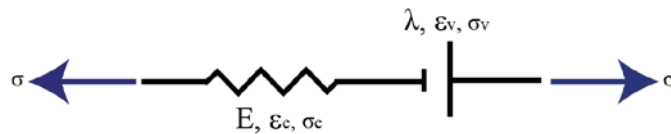


Figure 8 Maxwell Model.

### 2.1.4 Kelvin Voigt Model

This model consists of a spring and dashpot in parallel, simulating a viscoelastic solid. Unlike the case of Maxwell model, for this model a spring and a dashpot are connected in parallel implying that the strain of the two elements is the same.

The total stress is given by the sum of the applied stress to the spring and to the dashpot.

As can be seen in Figure 9, in this configuration, the dashpot reacts very slowly bearing all the stress initially and gradually transferring it to the spring. The deformation of the spring  $\varepsilon_e$  is equal to the deformation of the dashpot  $\varepsilon_v$ .

Thus, the following holds:

$$\sigma = E\varepsilon + \lambda \frac{d\varepsilon}{dt} \quad (4)$$

where the total stress  $\sigma$  [Pa] is given by the contribution of the spring  $E\varepsilon$  and the contribution of the dashpot  $\lambda \frac{d\varepsilon}{dt}$ .  $E$  is the elastic modulus [N/mm<sup>2</sup>] while the viscosity is designated by  $\lambda$  [Pa x s].

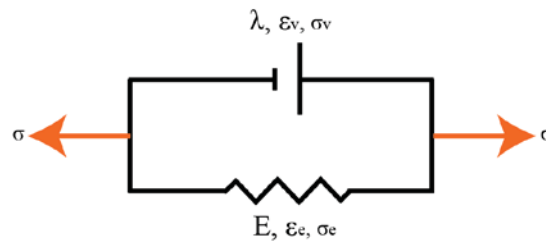


Figure 9 Voigt Kelvin Model.

### 2.1.5 Burger Model

The Burger's model provides a Kelvin model acting in series with a Maxwell model, in both the normal and shear direction. The model aims at replicating the behaviour of a viscoelastic material where strain and stress are functions of four parameters  $E_1$ ,  $E_2$ ,  $\lambda_1$  and  $\lambda_2$  (Mainardi and Spada 2011).

As in

Figure 10, this kind of material is defined as “memory fluid” as it tends to regain its original shape during unloading.

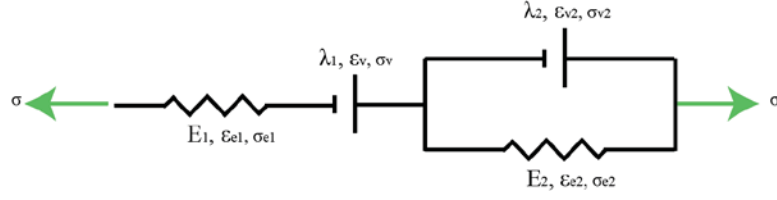


Figure 10 Example of Burger's model.

### 2.1.6 Viscoelastic systems during sinusoidal loading

When a viscoelastic material is subjected to a sinusoidal varying stress, a steady state will eventually be reached in which the resulting strain is also sinusoidal, having the same angular frequency but retarded in phase by an angle  $\delta$  (Roylance 2011).

A sinusoidal strain is proportional to the angular frequency  $\omega$ , which is the frequency of the strain oscillation over a certain cyclic frequency  $f$ .

$$\omega = 2\pi f \quad (5)$$

With  $\epsilon_0$  the amplitude of the strain, it is conceivable the following:

$$\epsilon(t) = \epsilon_0 \sin(\omega t) \quad (6)$$

If a sinusoidal strain is applied to a viscoelastic material, it creates a phase response in terms of:

$$\sigma(t) = \sigma_0 \sin(\omega t + \delta) \quad (7)$$

where  $\delta$  is the phase lag in time; with  $\sigma_0$  the amplitude of the stress;  $\omega$  is the angular frequency which is a measure of how rapidly the disturbance changes over a given time  $t$ .

For a viscoelastic material, the time dependent elastic modulus can be written as follows:

$$E(t) = \frac{\sigma(t)}{\epsilon(t)} = \frac{\sigma_0}{\epsilon_0} [\cos(\delta) + \tan(\omega t) \sin(\delta)] \quad (8)$$

By using the theorem of addition  $\{\sin(\alpha + \beta) = \sin\alpha \cos\beta + \cos\alpha \sin\beta\}$  it is possible to obtain the following:

$$\sigma(t) = \sigma_0 \cos(\delta) \sin(\omega t) + \sigma_0 \sin(\delta) \cos(\omega t) \quad (9)$$



where  $\omega$  is than angular frequency,  $\delta$  is the phase lag in time,  $\varepsilon_0$  and  $\sigma_0$  the amplitude of the strain and stress respectively.

By introducing the notations  $E'$  and  $E''$  :

$$\varepsilon_0 E' = \sigma_0 \cos(\delta) \quad (10)$$

$$\varepsilon_0 E'' = \sigma_0 \sin(\delta) \quad (11)$$

Equation (9) can be written with the new notation resulting in:

$$\sigma(t) = \varepsilon_0 E' \sin(\omega t) + \varepsilon_0 E'' \cos(\omega t) \quad (12)$$

with  $E'$  representing the so called storage modulus while  $E''$  is defined as loss modulus.

Furthermore, it is also possible to represent  $E'$  and  $E''$  as vectors in an imaginary plane by using the phase angle  $\delta$  as can be seen in the following Figure 11.

Therefore, it is possible to define a so called complex modulus:

$$\vec{E}^* = \vec{E}' + \vec{E}'' \quad (13)$$

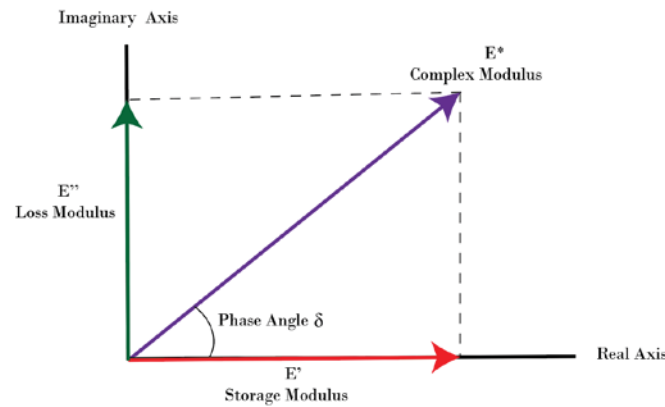


Figure 11  $E'$  and  $E''$  represented in an imaginary plane with indication of the phase angle  $\delta$ .

Hence it results that the phase angle is equal to the following:

$$\delta = \tan^{-1} \frac{E''}{E'} \quad (14)$$

where the viscoelastic material shows a phase angle between  $0^\circ$  (completely elastic) and  $90^\circ$  (completely viscous).

The result above shows how a viscoelastic material's response to a sinusoidal loading is a sinusoidal stress response characterized by a phase lag  $\delta$  in time as can be seen by the following as in Figure 12. (Christensen 1982)

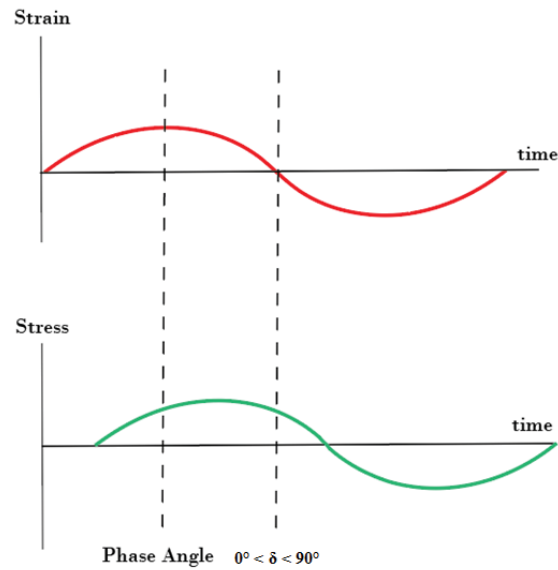


Figure 12 Stress and strain over time in case of sinusoidal loading for a viscoelastic material.

### 2.1.7 Boltzmann Superposition Principle

Generally, the evolution of deformations over time of a viscoelastic material depends on the applied stress. In this way, it can be hypothesized that the stress trend over time depends on the applied deformation and certain material parameter such as the elastic modulus. Boltzmann (Boltzmann 1871) could generalize the above mentioned hypothesis as listed below.

- i. In case of creep: the history of the total strain due to stress steps, results from the sum of the corresponding individual creep curves.
- ii. In case of relaxation: the history of the total stress, due to strain steps, results from the sum of the corresponding individual relaxation curves.

Thus, each loading step makes an independent contribution to the final strain, so that the total strain is obtained by the addition of all the contributions. In other words, the Boltzmann superposition principle (BSP) states that the effect of a compound cause is the sum of effects of the individual causes. (Kolarik and Pegoretti 2008)

The above-mentioned principle persists as long as some assumptions hold:

- i. The deformations have small rate.

- ii. The material properties are independent of the mechanical loading (strain and stress are proportional).
- iii. The material properties are independent of time of loading (time invariance).
- iv. The test temperature is constant.

The importance of Boltzmann's principle to the study of viscoelasticity is providing a starting point for mathematical models that can be used to predict the behaviour of a material (Christensen 1982).

### 2.1.8 Time-temperature superposition Principle

Bitumen, because of its viscoelasticity, exhibits a behaviour which is both temperature and time (frequency) dependent. Like other viscoelastic materials, it shows linearity between applied stress and induced strain at sufficiently low deformations (linear viscoelastic region). The "time-temperature superposition" (TTS) principle aims at overcoming the difficulty of extrapolating limited laboratory tests at shorter times to longer term. The TTS principle is well grounded in theory and can be applied to the rheological data obtained from oscillation experiments relating time to temperature for viscoelastic materials within the linear viscoelastic region at constant strain amplitude (Desseaux et al. 2018).

This technique uses temperature dependent shift factors for the magnitude of measured stresses (vertical shift factors) and time/frequency (horizontal shift factor) on plots of material's properties such as the elastic modulus (Dealy and Plazek 2009).

Several researchers have investigated the temperature dependent behaviour of the horizontal shift factor and proposed various empirical formulas.

In particular, the WLF equation (Williams, Landel, and Ferry 1955) is often used.

This equation reads as follow:

$$\log a_T = \frac{-C_1(T-T_0)}{(T-T_0)+C_2} \quad (15)$$

where  $C_1$  and  $C_2$  are material related constants.

$T_0$  is the test reference temperature.

$T$  is the temperature which has to be compared with the reference temperature.

As depicted in Figure 13, if time-temperature superposition is obeyed, the use of shift factors will yield a so called "master curve" showing viscoelastic behaviour over a much larger range of fre-

quencies. This implies that viscoelastic functions shown on a double- logarithmic plot, show data at various temperatures which can be shifted horizontally by a constant (independent of time) distance identified as  $\log a_T$  to obtain a single master curve. Thus, the master curve displays data over a wide range of frequencies "reduced" to a reference temperature,  $T_0$ , which means a unique curve that can intrinsically have both time and temperature effects.

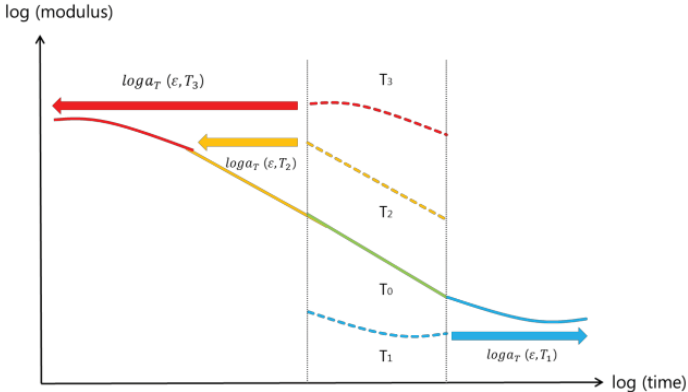


Figure 13 Example of construction of a sol called “master curve”.

As shown in Figure 14, the resulting rheological parameters are obtained under linear viscoelastic (LVE) conditions meaning that the rheological properties have to be independent of the strain amplitude (Ferry 1980).

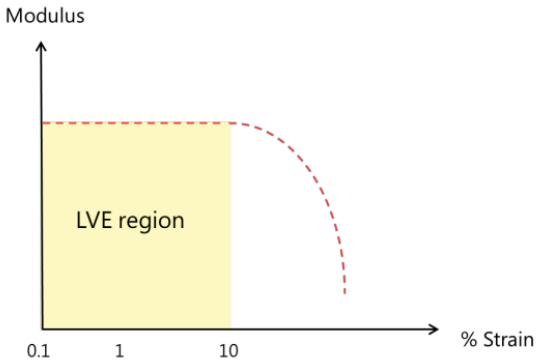


Figure 14 Example of a material response for a strain sweep.

When applying the TTS principle to viscoelastic materials such as bitumen, the material should be considered as thermo-rheologically simple, i.e. temperature affecting the motion of the molecules only. This implies that the temperature does not affect the material’s structure (Rodríguez-Alloza, Gallego, and Giuliani 2017). It has been observed that addition of certain products in asphalt binder experienced a deviation from the TTS principle as at higher temperatures the modification controlled the rheology (Desseaux et al. 2018).

### 2.1.9 Sigmoidal master curve

The amount of shifting at each temperature required to form the mastercurve, describes the temperature dependency of the material. In general, the master curves can be mathematically modelled by a sigmoidal function described as:

$$\log G^* = \zeta + \frac{\alpha}{1 + e^{\beta - \gamma(\log f_R)}} \quad (16)$$

where  $G^*$  is the complex modulus (this parameter will be discussed in the following section),  $\zeta$  is the minimal value of  $G^*$ ,  $f_R$  is the reduced frequency for the defined temperature while  $\alpha$  is the span between the maximum and minimum value of  $G^*$ .

$\beta$  and  $\gamma$  are parameters describing the form of the sigmoidal function.

As proposed in (Witczak and Fonseca 1996), sigmoidal function for fitting is based essentially on the physical observations of the asphalt mixture behaviour. The upper part of the sigmoidal function approaches asymptotically to the maximum stiffness of the bitumen, which is dependent on the limiting stiffness at cold temperatures.

### 2.1.10 Complex moduli in sinusoidal regime

Dynamic mechanical properties of bitumen may be expressed in terms of a complex shear modulus  $G^*$  that is composed of two components  $G'$  and  $G''$  representing the dynamic storage and loss modulus respectively and are either time or frequency and temperature dependent. They can be determined through sinusoidal loading in a dynamic shear rheometer (DSR) from the phase angle  $\delta$  between sinusoidal input load or deformation and material response together with the corresponding amplitudes of shear stress  $\tau_0$  and shear strain  $\gamma_0$ . Hence, the following equations hold:

$$\blacktriangleright G^* = |G^*|(\cos \delta + i \sin \delta) = G' + G'' \quad (17)$$

with the norm  $|G^*|$  or stiffness modulus (Di Benedetto et al. 2001):

$$\blacktriangleright |G^*| = \sqrt{G'^2 + G''^2} \quad (18)$$

### 2.1.11 Dynamic shear rheometer

The rheological properties of bitumen are usually determined using an oscillatory type testing apparatus known as DSR. A known oscillatory shear stress is applied to the temperature controlled

test geometry, in which the bituminous test specimen is held. The binder's strain response to the stress is measured. As in Figure 15, test specimens are installed between parallel metal plates. The principle used with the DSR is to apply sinusoidal, oscillatory stresses and strains over a range of temperatures and loading frequencies to a thin disc of bitumen, which is sandwiched between the two parallel plates of the DSR. One of the parallel plates (the upper one) is oscillated with respect to the other at pre-selected frequencies and angular deflection (or torque) amplitudes. Oscillatory loading frequencies using this standard can range from 0.1 to 20 rad/s by varying the temperature of the inner plate. The test is carried out in the linear viscoelastic regime as already discussed before. In the end, the complex modulus  $G^*$  and phase angle  $\delta$  are calculated by the rheometer using a specific software. According to European standard 14770, an 8 mm plate-plate geometry with 2 mm gap has to be used in the temperature range  $-10^\circ\text{C}$  to  $+40^\circ\text{C}$  while a 25 mm plate-plate geometry with 1 mm gap has to be utilized for the temperature range  $+40^\circ\text{C}$  to  $+80^\circ\text{C}$ .

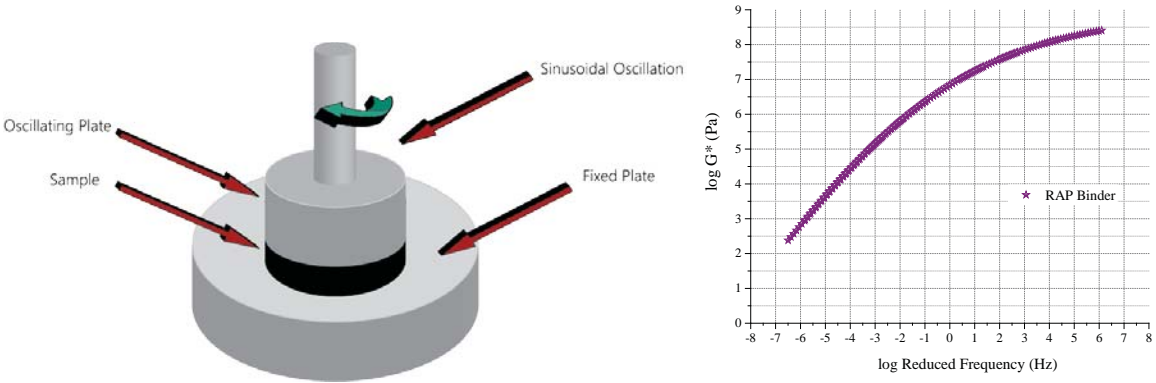


Figure 15 Dynamic shear rheometer apparatus (left) and example of mastercurve obtained with a dynamic shear rheometer (right).

## 2.2 Rheological properties of bituminous materials

As described earlier, the first attempt to measure the viscosity of a material was proposed by Von Obermayer. Trouton derived the ratio between tensile and shear viscosity describing the non-Newtonian behaviour of pitch a viscous residue, based on the shift from linearity of the early deformation rate in tensile creep and on its non-proportionality to stress (Lesueur 2008). The first modern description of bitumen viscoelastic properties was done by Van der Poel who combined static creep measurements with dynamic experiments at various temperatures (Poel 1954). Although bitumen is considered a complex material, it is commonly considered a thermo-rheologically simple material as extensive researches have shown that experimental results obtained on several bitumens validate the TTS principle (Lu and Isacsson 2002a; Loeber et al. 1998; Mastrofini and Scarsella 2000). The LVE rheological characteristics of bituminous binders and asphalt mixtures have been intensely studied over the past years. The linearity limits of bituminous binders and mixtures under transient and dynamic loading conditions have been studied from different angles. For example, it was discovered that under steady-state conditions the transition from linear to non-linear behaviour was stress dependent within a stress range of approximately 50–500 kPa (Cheung and Cebon 1997). In another work, it was shown how LVE strain limit versus testing temperature decreases with bitumen modification such as the addition of a mineral filler to the neat bitumen (G.D. Airey 1997). Most of the later studies concerning asphalt were dedicated to the development of simple linear viscoelastic models. The first attempts at modelling the viscoelastic behaviour of bitumen were the works of Pfeiffer & Saal (Pfeiffer and Saal 1940). They proposed analogical models with two springs and two dashpots to describe bitumen viscoelasticity. Nowadays, the Burger's model is the most commonly used as it shares both viscoplasticity and non-linearity of bitumen. Past researches have established relationships between the dynamic modulus and phase angle as in Figure 16 (Jongepier et al. 1969) as well as master curves for the complex shear modulus with frequency and temperature (Dobson et al. 1969) or linear viscoelastic models for thin bituminous films in tension and compression (Dickinson and Witt 1974). However, it is not surprising that definite conclusions regarding the mechanical response of different chemical species that constitute asphalt are not yet in place.

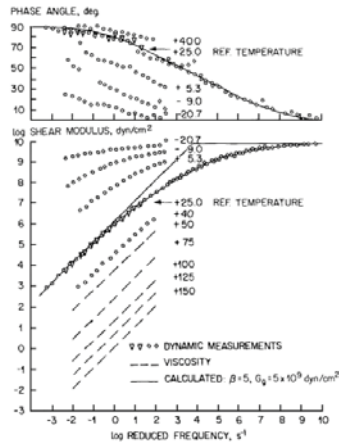


Figure 16 Complex shear modulus and phase angle at various temperatures/frequencies for a typical asphalt binder and corresponding master curve at 25 °C. (Jongepier et al. 1969)

Different studies have addressed the issues related to the existence of waxes in asphalt and their role in affecting the mechanical properties. Most of these studies have concluded that the low temperature properties of asphalt binders depend to a large extent on the amount of crystallisable fractions and which influence the phase angle as well as outlined in (Edwards and Redelius 2003) and can be observed in Figure 17. In summary, as the temperature is reduced, one phase of the mixture starts crystallizing while the other remains in the amorphous phase.

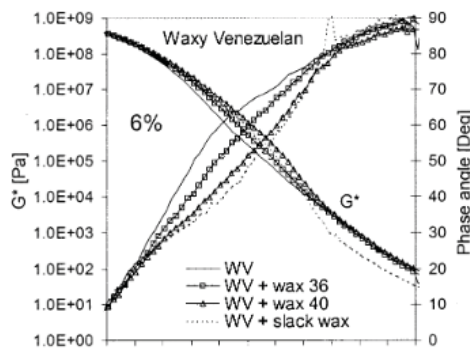


Figure 17 Complex modulus and phase angle for bitumen with different percentages of waxes. (Edwards and Redelius 2003)

Changes in viscosity has been widely studied also when bitumen have been modified. Understanding the effect of modification regarding rheological properties is fundamental when evaluation the efficiency of certain asphalt additives. The rheological properties of bitumen can normally be improved with the addition of modifiers such as polymers or rejuvenators. For example, the use of polymer modified bitumens (PMBs) helps improving its rheological properties over a wide range of temperatures and times of loading. Generally, by adding polymer into the neat bitumen, the stiffness modulus and elasticity values significantly increased (Gordon D. Airey, Rahimzadeh, and



Collop 2004). In (Al-Khateeb and Ramadan 2015), it was shown the influence of crumb rubber content on rheological properties of aged bitumen, reporting that the rheological changes in bitumen binder led to improving the mechanical properties of rubberised bitumen binder.

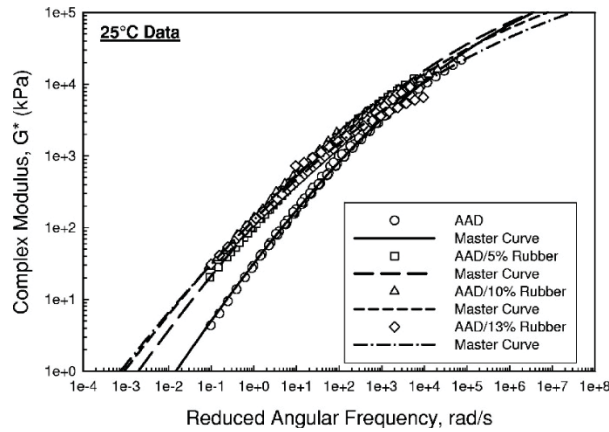


Figure 18 Influence of different percentages of rubber on neat asphalt. (S.-C. Huang 2008)

In addition, the effectiveness of rejuvenators to restore aged binder rheological properties to virgin-like condition, thus balancing the effects of RAP addition to mixture, is a fundamental parameter to be known from rheological measurements. For instance, the addition of the bio-based oil as recycling agent was observed to generally lower the complex moduli and improve fatigue performances of mixtures with a RAP content equal to or greater than 40% (Mangiafico et al. 2017). In another study, rubbers have been seen as cause of change in terms of complex modulus at low frequencies range as can be observed in Figure 18 (S. C. Huang et al. 2015). Recently, waste vegetable oil, waste vegetable grease, organic oil, distilled tall oil, and aromatic extract were compared and analysed. All products have been seen to be improving rheological properties of RAP binder however, fundamental parameter have been seen to be the percentage of rejuvenator as too high concentration could reduce the RAP binder viscosity excessively (Zaumanis, Mallick, and Frank 2014). Laboratory addition of waste vegetable oils into RAP binder as rejuvenators have shown that the use of such oils can reduce the viscosity to reach the target grade, ensure similar rheology to virgin binder as measured with DSR, reduce the mixture stiffness to a level of virgin mix and improve the resistance to aging compared with virgin binder by 20% (Bailey and Zoorob 2012). In summary, several studies have explored effects of various rejuvenators on bitumen's mechanical properties and reported that all rejuvenators were effective in enhancing mechanical properties. However, a better understanding of these mechanisms is vital for the development of more effective rejuvenators. Furthermore, the majority of the researches available analyse restoration of mechanical properties as the sole indicator for rejuvenation. On the contrary, aim of this Ph.D. thesis is the investigation of the efficacy of different bio-based rejuvenator while using a combination of rheological, chemical and morphological properties as metrics for rejuvenation.

## 2.3 Fracture toughness

Strength (or hardness) is invariably a characteristic representing a material's resistance to non-recoverable (for example, plastic) deformation at least in ductile materials. Toughness is a material's resistance to fracture and as such is a measure of the energy needed to cause fracture.

Traditionally, toughness is considered to represent the combination of strength and deformability (ductility). The ability of a material to undergo limited deformation is a critical aspect of conferring toughness, as this feature enables the local dissipation of high stresses that would otherwise cause the material to fracture; this is the reason that hard materials tend to be brittle and lower strength materials, which can deform more readily, tend to be tougher as can be seen in Figure 19. (Ritchie 2011)

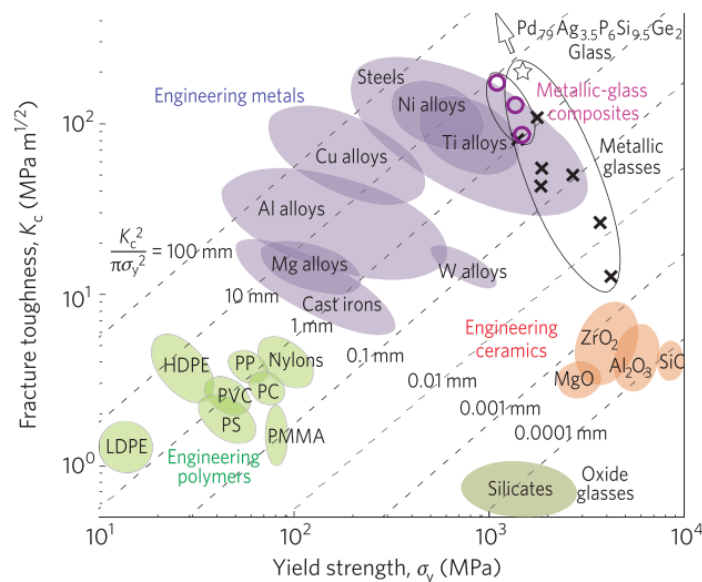


Figure 19 Plot showing strength–toughness relationships for engineering materials where  $K_c$  is the fracture toughness and  $\sigma_y$  the yield strength. (Ritchie 2011)

For asphalt binders, the fracture toughness test (FTT) is a low temperature cracking test based on a European standard (European Committee for Standardization CEN TS15963, 2010). As shown schematically in Figure 20, it is a three-point bending test where the test sample is a beam with a thin notch in the middle. The samples are tested in a temperature controlled 99.5% ethanol bath in order to cool the sample from room temperature down to the one desired for testing (range  $-10^\circ\text{C}/0^\circ\text{C}$ ). The use of ethanol as cooling fluid has been studied previously and it was considered having less influence on bitumen's surface characteristics as compared to other cooling media (i.e. potassium acetate) (Cannone Falchetto, Turos, and Marasteanu 2012).

Subsequently, a vertical load is applied with a constant displacement rate of 0.01 mm/s until failure of the specimen.

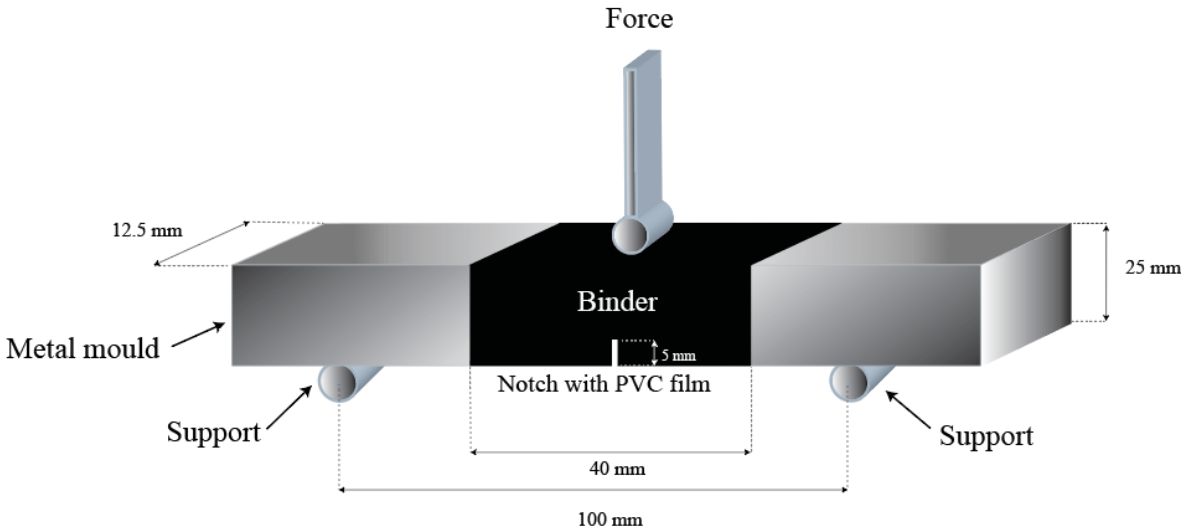


Figure 20 Schema of the fracture toughness test setup.

The fracture toughness temperature ( $T_{FT}$ ) of a bituminous binder is defined in the standard (CEN/TS 15963:20) as the temperature at which the deflection in the middle span at maximum force is equal to 0.3 mm.

In order to calculate such temperature, the fracture toughness test can be repeated at different temperatures until a deflection  $\geq 0.3$  mm is measured. As Figure 21 demonstrates, for each temperature the force vs. deflection curve can be measured. In this case  $T_2$  is satisfying this criterion but not  $T_1$  and  $T_3$ , thus,  $T_2$  corresponds to the fracture toughness temperature.

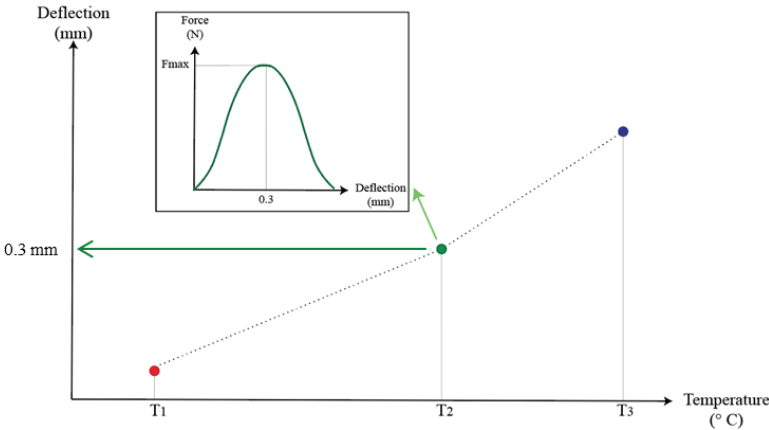


Figure 21 Temperature vs deflection plot and the corresponding force-deflection curve for temperature  $T_2$  (satisfying the FTT requirement of 0.3 mm).

By considering the force deflection curve, it is also possible to calculate the area corresponding to the work to fracture which is defined as the work necessary to crack the material as can be seen in the following Figure 22. As outlined in the standard (CEN/TS 15963:20), it corresponds to the area under the force-deflection curve from the beginning of the test to the break of the sample, i.e. at the maximum force.

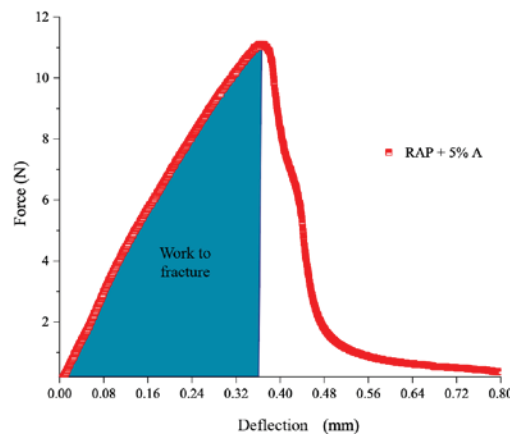


Figure 22 Example of work to fracture for RAP + 5% A at  $-10^{\circ}$  C.

## 2.4 Low temperature cracking behaviour of bituminous binders

Due to exposure to cold temperatures, asphalt binders shift from time dependent ductile to brittle behaviour, increasing the risk of crack formation (Baek et al. 2011).

Low temperature cracking of asphalt pavements is attributed to thermal stresses developed during cooling. If the stress is equal to or greater than the tensile strength of the pavement, a micro-crack may develop on the pavement surface, and, after additional low temperature cycles, this crack will propagate downward through the pavement. Water entering the crack may freeze during winter and result in the formation of ice lenses, which in turn can produce frost heave. Pumping of fines through the crack may produce voids under the pavement, which means that the bearing capacity may be reduced. Consequently, the cracking process described above may cause poor ride quality, reduced service life and increased costs for maintenance of roads, unless measures are taken to decrease the risk of low temperature cracking. (Lu and Isacson 2002b)

This is even more detrimental with asphalt mixture with RAP materials which contain hard RAP binder (the binder around RAP's aggregates) with has potentially higher susceptibility to crack

formation than virgin binders (Cavalli, Partl, and Poulikakos 2017). As described in the previous section, time-temperature behaviour and possible mechanical restoration achieved by rejuvenators may be determined with the DSR whereas resistance to failure at low temperature may be characterized by fracture toughness, derived from the energy for causing fracture (Kang et al. 2017). A previous research showed that the application of bio-binder from swine manure could alleviate the effect of RAP while improving the overall low temperature fracture properties of the asphalt mixture (Oldham et al. 2018). Test results demonstrated how mixtures composed by bio-based additives had superior physical properties in terms of fracture resistance and creep compliance (Hill et al. 2018). Generally, tests showed positive effects of the bio-based rejuvenating agent especially at low temperature to restore flexibility (Porot et al. 2017). In road engineering field, the bending beam rheometer (BBR) is a traditional asphalt test method to determine the low temperature properties. It consists in loading an asphalt binder beam and subsequently measuring the deflection at the centre of the beam obtaining the so called “creep stiffness”. The BBR is designed to measure this stiffness and the rate of stress relaxation. As for example in (Shen, Amirkhanian, and Tang 2007), the fracture properties were observed to be better for asphalt mixtures containing the rejuvenated binder than virgin asphalt mixtures. Recently, in (Lu, Uhlback, and Soenen 2017) it was investigated how the BBR test results were difficult to connect to the DSR results due to high discrepancy in sample size. In addition, BBR is generally limited to certain test conditions (limiting temperature at 300 MPa stiffness) as well as it is known for being highly time consuming.

Thus, in the framework of this Ph.D. thesis, an FTT test is used as a possible alternative to traditional test method such as for example BBR, for determining low temperature properties and crack susceptibility of modified RAP binders with rejuvenators. This approach has been used to have a broader study on the low temperature cracking behaviour of the bio-based binders.

Further investigations are needed before more definitive conclusion can be drawn in particular, how bitumen chemistry may have a significant influence on the mechanical performances thus being related with the low temperature behaviour as well.. As it has been mentioned above, FTT appears to be capable of predicting asphalt behaviour at low temperature. However, even in this area, more experience is required. Finally, correlation between laboratory studies and field tests are necessary before the possible practical importance of the results presented in this section can be determined.

## 2.5 Infrared Spectroscopy

The objective of Fourier transform infrared spectroscopy (FTIR) is to measure the absorption spectrum of a particular substance. This phenomenon happens when the substance absorbs energy in the form of light at different wavelengths. The conventional method consists of using a monochromatic source, varying the wavelength gradually and subsequently by measuring the amount of light absorbed by the sample. Nowadays, it has been generally used broadband sources, which contain all the frequencies needed to be studied. To distinguish the absorption of the different wavelengths by the sample it is then necessary to use a specific instrument, which is called Michelson interferometer. Firstly, the spectrum is measured without any sample. This operation is called “background collection”. In this way it is possible to measure the amount of light transmitted by the apparatus at different frequencies, by performing a Fourier transform of the resulting spectrum. Subsequently, the sample which has to be analysed is inserted between the source and the interferometer. This measurement, after the Fourier transform and the subtraction of the background, will correspond to the desired absorption spectrum. The whole operation can be done in rapid timing, as the Fourier transform calculation is very fast. (Lindon, Tranter, and Koppenaal 1999)

### 2.5.1 Attenuated Total Reflection Fourier Transform Infrared Spectroscopy (ATR-FTIR)

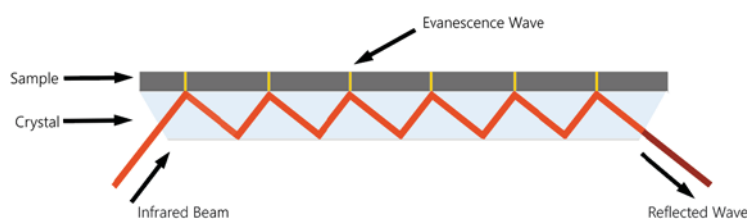


Figure 23 Example of ATR-FTIR spectroscopy.

Attenuated total reflection Fourier transform infrared spectroscopy (ATR-FTIR) is suitable both for liquids and solid samples. Since bitumen is a viscous material, ATR-FTIR was found suitable to analyse its chemical functionalities corresponding to the different bonds/functional groups, as a function of the wavenumber. As shown in Figure 23, a beam of infrared light is passed through the ATR crystal. This reflection forms an evanescent wave which extends itself into the sample.

The beam is collected by a detector as it exits the crystal. Depending on the application, different materials are used as ATR crystals such Germanium or diamond (Lindon, Tranter, and Koppenaal

1999). A bitumen FTIR spectra example can be seen in Figure 24. The intensity of the peaks is a function of the concentration of the bonds/functional groups.

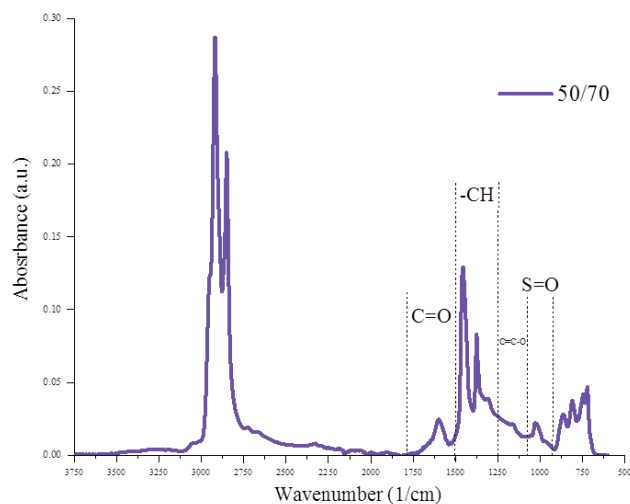


Figure 24 FTIR spectrum for a virgin binder 50/70.

## 2.6 Chromatographic analysis

Chromatography systems employ a column, capillary or other container that is filled with a mobile and a stationary phase, which can be solid, liquid or gas. The stationary phase remains in position and does not move during the analysis, whereas the mobile phase moves through the container. The concentration by weight of the substance in the eluting solvent may be monitored continuously with a detector such as concentration sensitive detectors which includes UV absorption, or refractive index (RI) detectors (Fleig 1969).

Chromatography uses the chemical and physical properties of sample molecules and mobile phases to detect their presence as they elute from a column to differentiate all compounds. Detectors may respond to a change in the mobile phase due to the presence of the sample, or to a property of the sample alone. The ability to scatter light, molecular viscosity and the adsorption of ultraviolet (UV) or infrared (IR) are all used as measurement parameters.

### *Refractive Index Detector*

These detectors work by assessing the difference in refractive index between the mobile phase and the pure solvent. RI detectors are sometimes referred to as ‘universal’ detectors, as they tend to give a usable response for all types of polymers. (Fleig 1969)

### Ultraviolet detector

The most sensitive detector is the differential UV photometer. These are optical instruments for measurement of the absorption of light of a given wavelength of substances in solution. (Fleig 1969)

#### 2.6.1 Gel permeation chromatography (GPC)

As can be seen in Figure 25, this technique separates dissolved macro-molecules by size, based on their elution from columns filled with a porous gel. The smaller molecules shown in red spend more time in the column and therefore will elute last. Conversely, larger molecules shown in purple will spend less time in the pores and will be eluted earlier (Tung 1966). The resulting chromatogram is therefore a weight distribution of the substance as a function of retention volume (Tung 1966) as in Figure 25. GPC gives information regarding the size of molecules in solution that are converted into molecular weights using a calibration.

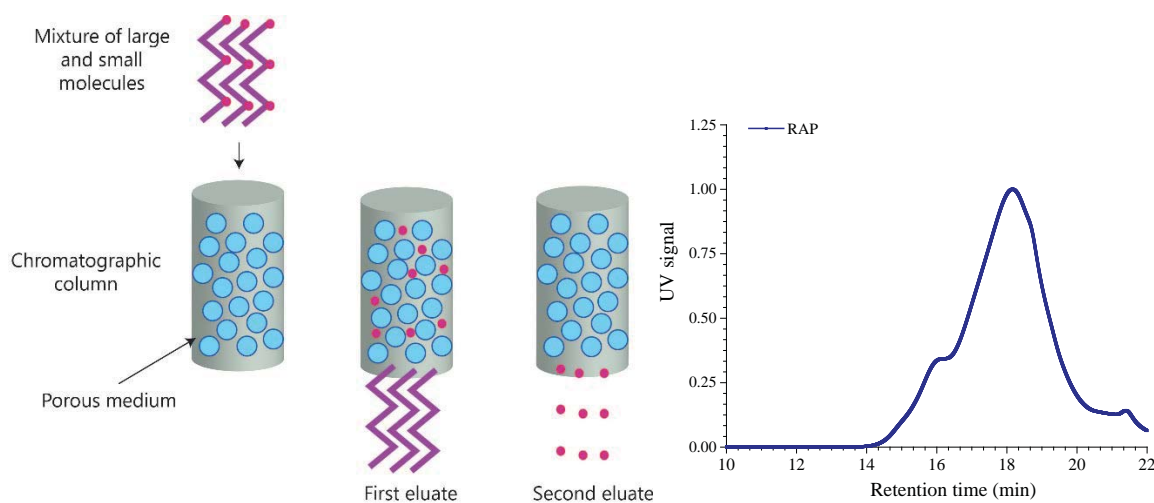


Figure 25 Scheme of gel permeation chromatography (left) and example of GPC results for a RAP binder (right).



## 2.7 Application of FTIR-ATR and GPC for the characterization of bitumen

It is known that molecules may irreversibly evolve through chemical aging which is generally thought to be a sum of oxidation reactions and polymerisation, and to a lesser extent, lighter volatilization (Lesueur 2008).

The use of gel permeation chromatography (GPC) for asphalt dates back to the 1960s. In 1969 Snyder described GPC as a method to characterize molecular separation in asphalt with average molecular weight in the 700–2400 Dalton range (Snyder 1969). Bowers et al. (Bowers, Huang, and Shu 2013) used GPC as a method of detecting asphalt contamination in fine aggregate particles by examining the molecular weight change. In Jennings et al. (Jennings et al. 1992) it was found that, the most damaged asphalt pavement was the one with the highest number of large molecules (LMS) the stiffening of asphalt binder due to oxidation and aging there is an increase of large molecular sizes LMS. In addition, they found that the critical percentage of LMS is 20%. In another study, the percentage of LMS was related to the viscosity and thus a stiffening of the asphalt binder in the mixture by increasing the percentage of LMS (K. W. Kim et al. 2006). Recently, the complex modulus,  $G^*$ , of a virgin asphalt binder blended with reclaimed asphalt shingles (RAS) binder was correlated to the percent of LMS. The test results showed that the percentage of LMS was highly correlated with the complex shear modulus ( $G^*$ ) of asphalt binder as in Figure 26 (Zhao et al. 2014).

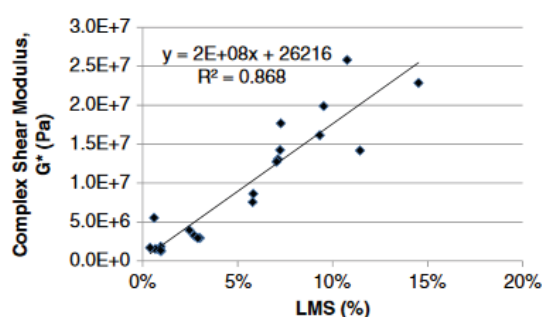


Figure 26 Relation between  $G^*$  and LMS. (Zhao et al. 2014)

Chemical functional groups are groups of atoms which are responsible for different reactions within a compound. Lu and Isacsson (Lu and Isacsson 2002a) studied the effects of aging on bitumen chemistry and rheology. It was found that the C=O double bond, the carbonyl group, and the S=O sulfoxides groups, tend to grow as the material ages. Ouyang et al. (Ouyang et al. 2006) studied the effects of adding antioxidants to styrene butadiene styrene in asphalt during the oxidative aging process. By use of FTIR-ATR they found an increase in the carbonyl group as the asphalt

binder aged. In the same way, in (Yao et al. 2013) it was outlined as FTIR was fundamental when studying aging at different laboratory stage (RTFOT and PAV) as can be seen in Figure 27.

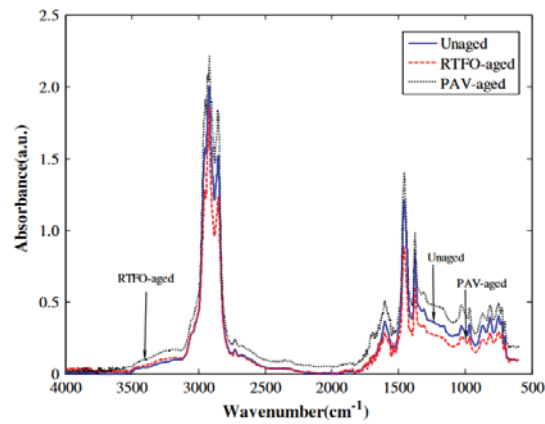


Figure 27 FTIR spectra analysis of an asphalt binder before and after laboratory aging. (Yao et al. 2013)

In another research, by testing asphalt binders from different sources at different temperatures and aging periods it was found that the carbonyl and sulfoxide functional group's increased with aging time, however the sulfoxide group decreased after severely aging (S.-C. Huang and Grimes 2010). Various methods are used to quantify the aging related evolutions of the bitumen spectrums at the sulfoxide ( $1030\text{ cm}^{-1}$ ) and carbonyl ( $1,700\text{ cm}^{-1}$ ) wavenumbers specifically. In order to minimise the influence of sample thickness and IR radiation path length, the general principle is to normalise the absorption values obtained for these specific wavenumbers by calculating a ratio of a value obtained at a reference wavenumber which is supposed not to be significantly affected by oxidation (i.e. methyl group  $\text{CH}_2$  and  $\text{CH}_3$  group with peak centred at  $1455\text{ cm}^{-1}$ ). FTIR has been a promising method for understanding the effect of rejuvenator in reclaimed binder as it seems suitable for monitoring the diffusion process involved in mixtures, providing differences in IR absorption between the different components (Karlsson and Isacson 2003). Rejuvenators are generally created for restoring the physical and chemical properties of oxidized binder by rebalancing the colloidal structure as well as restoring the aged asphalt's original viscosity (Gong et al. 2016). Recently, it was noted that the carbonyl and sulfoxide functional groups were shown to increase with aging however, the modification due to the addition of rejuvenators did not cause any significant alteration in the FTIR absorbance of the carbonyl and sulfoxide groups (Elkashef et al. 2017).

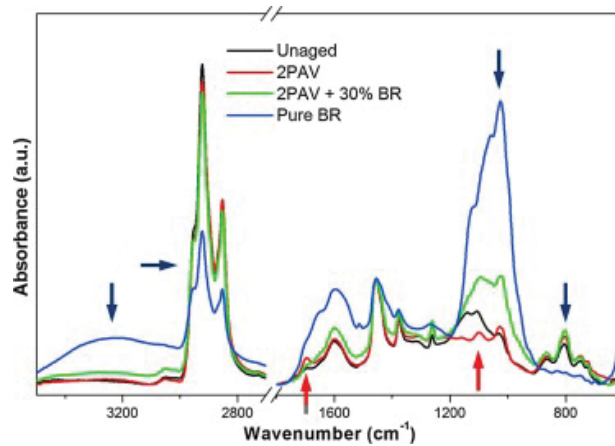


Figure 28 ATR-FTIR of different binders. Red arrows highlight changes in the spectra due to aging. Blue arrows highlight differences between asphaltenes of asphalt binder and pure bio-rejuvenator (BR). (Pahlavan et al. 2018)

FTIR has been seen as promising when dealing with bio based materials as can be seen in Figure 28. Mokhtari et al. showed changes in the sulfoxide index after the addition of petroleum based rejuvenator in an aged binder with PAV-aged samples (Mokhtari et al. 2017). In (Lin et al. 2014) rejuvenator-seal materials have been used in reclaimed asphalt and have the potential of decreasing the carbonyl index. By comparing diffusion coefficients obtained using a DSR with results obtained using FTIR-ATR, it was shown that diffusion detected chemically by FTIR-ATR is accompanied by a change in rheological properties (Karlsson, Isacsson, and Ekblad 2007). Generally, it can be stated that laboratory aging techniques are attempting to simulate both short term aging and long term aging. However, the understanding of all processes behind aging is still largely missing. As described before, asphalt molecules may irreversibly evolve through chemical aging which is generally thought to be a sum of oxidation reactions and polymerisation, and to a lesser extent, lighter components evaporation (Lesueur 2008). This process includes loss of volatile components which include migration of oily components from the bitumen into the aggregate. In addition, when monitoring the viscosity (or any mechanical property) of a bitumen versus time around room temperatures, a very slow heat-reversible hardening is indeed observed and generally referred to as steric hardening (Lu and Isacsson 2002a). In a future perspective, a broader analysis including other techniques such as molecular dynamics in combination with FTIR and GPC can contribute to better understanding of the oxidation and the rejuvenation mechanisms.

## 2.8 Atomic Force microscopy

In the 1980s, scanning tunnelling microscope was invented. This was a precursor of atomic force microscopy (AFM) which was realized few years later (Binnig, Quate, and Gerber 1986).

The principle of the AFM is represented in the following figure.

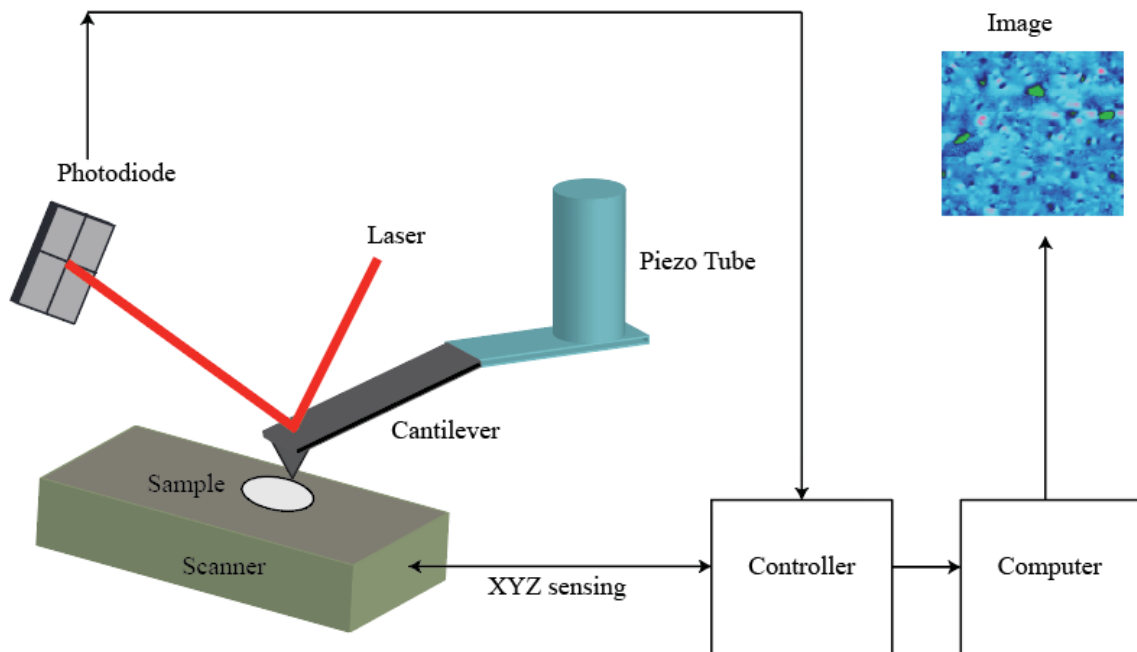


Figure 29 Scheme of an atomic force microscopy according to (Das et al. 2016b).

As depicted in Figure 29, AFM is composed of a cantilever carrying a sharp tip that interacts with a sample surface, the laser path and the piezo transducer. The cantilever interacts with the surface of a sample which is moved in the x, y and z directions by the piezo actuators. A laser beam focused at the end of the cantilever is reflected into a detector and when the cantilever experiences a force, by a topographical, chemical or electrical feature on the sample, the cantilever is deflected leading to a deviation of the laser beam from its original position on the detector. This deviation is measured as a voltage, which can be translated into a force or a relative height (Binnig, Quate, and Gerber 1986). The field of view can vary from the atomic and molecular scale up to sizes larger than 125  $\mu\text{m}$ . The AFM can also examine rough surfaces because its vertical range can be up to 8-10  $\mu\text{m}$  with a minimum resolution of 0.1 nm (Binnig, Quate, and Gerber 1986).

The most important tip-sample force in the AFM is the van der Waals interaction. It is responsible for a variety of physical phenomena and they consist of three components (D. Tranchida and Piccarolo 2007):

- Dipole-dipole interactions: permanent dipole moments in polarized molecules interact together.
- Dipole-induced dipole interactions: a dipole polarizes a non-dipole.
- Dispersion forces: these arise when a nonpolar atom or molecule exhibits fluctuating dipoles due to quantum fluctuations in the ground state. These create rapidly fluctuating dipole fields that can propagate through the medium.

### 2.8.1 The deflection curve and the force curve

In order to be able to image with AFM in the most generally applicable mode, the tip must be brought into contact with the surface. The total forces, plotted as a function of the tip-sample distance, give rise to a force curve. In the following Figure 30 a deflection curve of a cantilever is schematically shown.

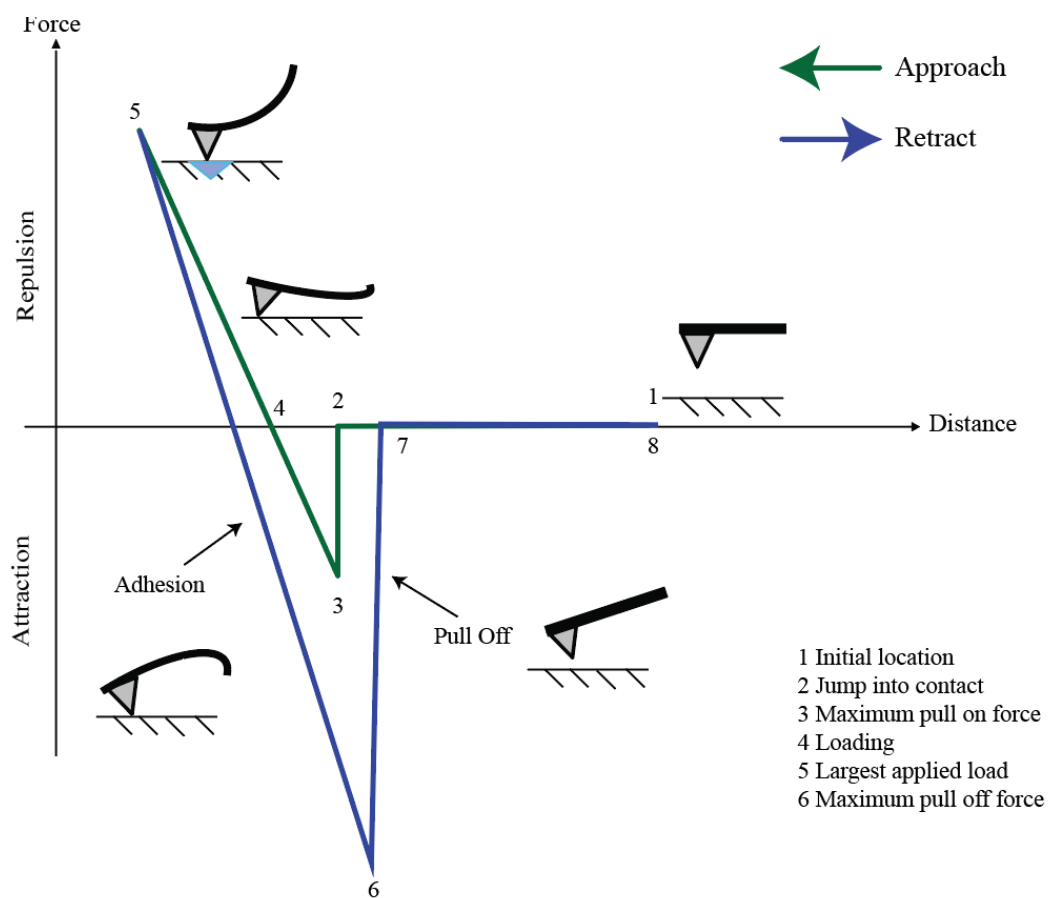


Figure 30 Force-distance curve with its corresponding cantilever position. Adapted from (Cappella and Dietler 1999)

As the tip approaches the sample, the cantilever shape changes also. As can be seen in Figure 30, from point 1 to point 2 there is no change in the deflection of the cantilever, because there is still no interaction between tip and sample. From 2 there is a “jump to contact”: the tip rapidly deflects and comes into contact with the sample. This is caused by instability in the system. After point 3 the upwards deflection of the cantilever begins, as the tip is pressed against the surface. This corresponds to the hard interaction of the tip and the surface, and, in a force curve would be nearly vertical. After point 5 the piezo begins to go down again, and the measured cantilever deflection also decreases again. Afterwards, the cantilever goes through zero deflection and subsequently it gradually bends downwards because of the attractive forces between tip and sample until the spring force equals the adhesive force (point 6) and the cantilever jumps back to its starting position (D. Tranchida and Piccarolo 2007).

### 2.8.2 *Operational modes*

The AFM is used predominantly in three different modes.

- **Contact mode:** by observing Figure 30, when the tip is far from the sample surface, the cantilever is considered to have zero deflection, on the contrary, as the tip approaches the surface, it normally feels firstly an attractive force, and a ‘snap-in’ occurs, as the tip becomes unstable and jumps into contact with the surface. As the instrument continues to push the cantilever towards the surface, the interaction moves into the ‘repulsive’ regime, i.e. the tip is applying a force to the sample, and the sample applies an opposite force to tip. In this regime, a combination of cantilever bending and sample compression will be occurring according to the relative compliances of the sample surface and AFM probe. It is within the repulsive regime that contact-mode imaging usually occurs. (Eaton and West 2010)
- **Non-contact mode:** to achieve non-contact AFM, the tip must be close enough to the sample surface without passing into the repulsive regime. Non-contact AFM is therefore carried out in the attractive regime, as shown previously in Figure 30. These effects are caused by a change in the cantilever resonant frequency which is in turn caused by forces from the surface (as the previously mentioned van der Waals forces) acting on the tip.
- **"Tapping mode":** during this mode, feedback is usually based on amplitude modulation and the tip–sample interaction passes from the ‘zero-force’ regime, through the attractive regime, and into the repulsive regime, as described in (García, Tamayo, and Paulo 1999)

and shown in Figure 30. The result is that the probe touches the surface only for a short time, thus avoiding the issue of lateral forces and drag across the surface. The cantilever is driven to oscillate up and down at its resonance frequency. The motivation for the use of the tapping mode AFM is to overcome the difficulty of operating the non-contact mode AFM thus, the oscillation amplitude, and therefore, the energy associated with the oscillation, is made to be sufficient to overcome the stickiness of the surface, making this method appropriate for bitumen imaging.

### 2.8.3 *Topography imaging*

As described in the previous paragraph, topographic imaging can be conducted either by continuous contact of the tip with the surface (contact mode) or by allowing the tip to tap the surface periodically (tapping mode or non-contact). In either of the above mentioned modes, the tip is allowed to scan the surface. During the scan, the oscillation amplitude, which is smaller than the free amplitude, is used as the feedback signal by the electronic controller. The variation of surface topography alters the oscillation amplitude of the cantilever. The topographic contrast is then generated by the vertical movement of the scanner, which moves to maintain the pre-set oscillation amplitude. (García, Tamayo, and Paulo 1999)

Example of topographic image can be seen in the following figure.

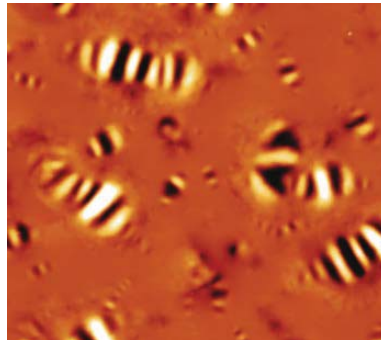


Figure 31 AFM topography image of a bitumen. Adapted from (Pahlavan et al. 2016).

The tapping mode essentially produces topographic contrast as can be observed in Figure 31. This mode can also be used to generate a phase images as described in the following paragraph.

### 2.8.4 *Phase imaging with AFM*

‘Phase imaging’ in AFM refers to recording the phase shift signal in tapping AFM mode.

In 1995, the phase signal was described as being sensitive to variations in composition, adhesion, friction, viscoelasticity as well as other factors. Later on, it was suggested that the phase signal in soft materials is sensitive to viscoelastic properties and adhesion forces. From that moment, it has been a common assumption that phase contrast is related to viscoelastic properties. This is because the phase is an indirect measure of the energy dissipation involved in the contact between the tip and the sample, which can be seen as depending on a number of factors, including features as viscoelasticity. (Gómez Castro et al. 2006)

The average energy released by the cantilever to the medium  $E_{med}$  (air or liquid) and the sample surface must match the average energy supply by the external driving force. Then, the phase shift  $\phi$  between the cantilever excitation and the probes response is related to the oscillation amplitude  $A$ , the amplitude of its free value  $A_0$ , and the average energy dissipated in the sample  $E_{dis}$  and in the environment  $E_{med}$  by the following equation:

$$\sin\phi \cong \frac{A}{A_0} \left( 1 + \frac{E_{dis}}{E_{med}} \right) \quad (19)$$

The pre-factor  $\frac{A}{A_0}$  and  $E_{med}$  remain constant during amplitude modulation AFM imaging ( $A = \text{constant}$ ). Consequently, any change of the phase shift is directly related to a local change in the energy dissipated in the sample and remaining independent of the topography. The oscillation amplitude is kept constant by the feedback system with only small instantaneous variations because of the finite response of the electronics. (Garcia et al. 2006)

### 2.8.5 Quantitative nano-mechanical properties

During quantitative nano-mechanical mapping (QNM) analysis in tapping mode, the cantilever is intermittently contacting the sample. The QNM oscillation is performed at frequencies well below the cantilever resonance, thus avoiding the filtering effect and dynamics of a resonating system. The difference with a conventional force curve (and force volume imaging) are that the z-position is modulated by a sine wave, thus avoiding unwanted resonances at the turnaround points. Continuous force curves can be executed at frequencies between 1 kHz and 10 kHz. (D. Tranchida and Piccarolo 2007).

The sample deformation and its associated stress is calculated by the Derjaguin Muller Toropov Model (DMT) which assumes that the contact profile remains the same as in Hertzian contact (Hertz, H. R. 1882) as shown in Figure 32 but with additional attractive interactions outside the area of contact (Derjaguin, Muller, and Toporov 1975).



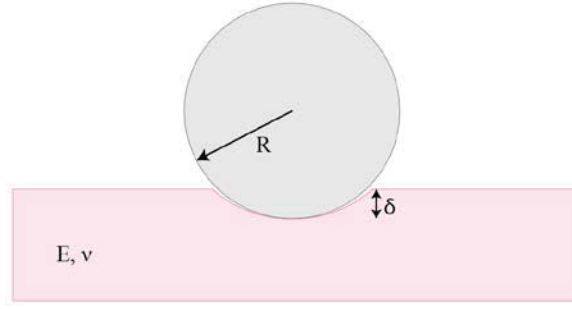


Figure 32 Example of Hertzian contact with indication of the tip radius  $R$ , the indentation  $\delta$ , the elastic modulus  $E$  and the Poisson's ratio  $\nu$  of the sample. Adapted from (S. H. Kim, Dugger, and Mittal 2010).

If  $F_{tip}$  is considered the peak force (from the force curve as in Figure 33) acting on the tip, thus, the following holds:

$$F_{tip} = F_{herz} + F_{ad} = \tilde{E}R^{1/2}\delta^{3/2} + F_{ad} \quad (20)$$

where  $F_{tip}$  is the Peak Force as shown in Figure 33.

$F_{herz}$  is the contact force (hertzian contact) and  $F_{ad}$  is the adhesion force. In addition,  $\delta$  is the deformation (thus the indentation),  $\tilde{E}$  is the effective elastic modulus the so called "DMT modulus", and  $R$  is the tip radius.  $F_{ad}$  is given by several contribution as the capillary forces as well as van der Waals forces and it can be obtained from the force-curve as in Figure 33 (D. Tranchida and Piccarolo 2007).

It follows that  $\tilde{E}$  is obtained by fitting the retracting curve using the force-distance curve obtained as outlined in paragraph 2.10.1. as can be observed in the following Figure 33.

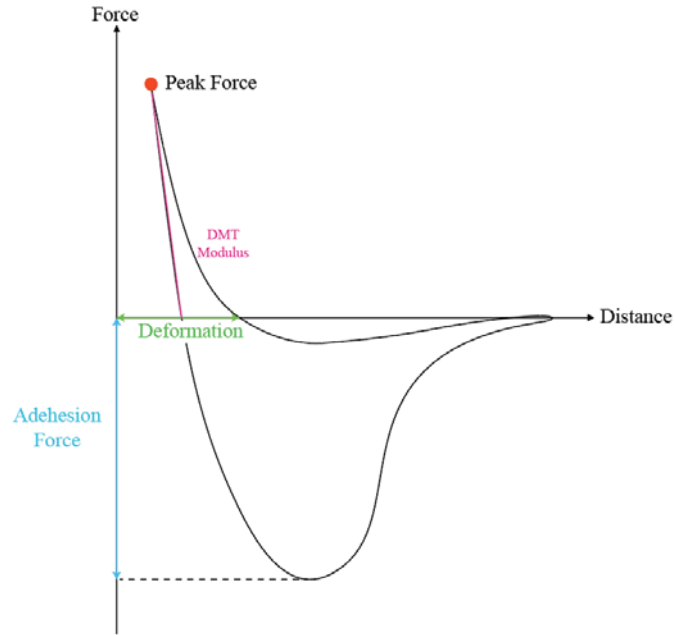


Figure 33 Force-distance curve with indication of the Peak Force ( $F_{tip}$ ); deformation (indentation  $\delta$ ); adhesion force ( $F_{ad}$ ) and the DMT modulus ( $\tilde{E}$ ).

The DMT modulus is calculated under the following assumption:

- i. The strains are small and within the elastic limit.
- ii. The surfaces are continuous implying that the area of contact is much smaller than the characteristic dimensions of the contacting bodies.
- iii. Each body can be considered an elastic half-space.
- iv. The surfaces are frictionless.

### 2.8.6 QNM method applied to bitumen's sample.

As described previously, QNM uses tapping mode to acquire information on nano-mechanical properties. The method is non-destructive to both tip and sample since it directly controls the peak normal force. QNM mode measurements is generally performed as follows: the probe is oscillated in the z-direction; at the same time the sample is scanned line by line at a rate of 1 Hz. Every image is built up by 512 per 512 pixels each. As mentioned in the previous paragraph, a force curve is obtained to gain information on the elastic modulus. To acquire such information, the AFM tip works in step mode so that it creates a force curve each step (corresponding to each pixel). In particular, as it will be outlined in Chapter 6, the tip radius is calibrated so that the value of radius used respects the hypothesis of Hertzian contact as in Figure 32.

By taking as example the following Figure 34, it is possible to observe how a 10x10  $\mu\text{m}$  topography image corresponded to a 512x512 pixels image. Thus, 1 pixel corresponded to 0.019  $\mu\text{m}$  having an area corresponding to 361  $\text{nm}^2$ .

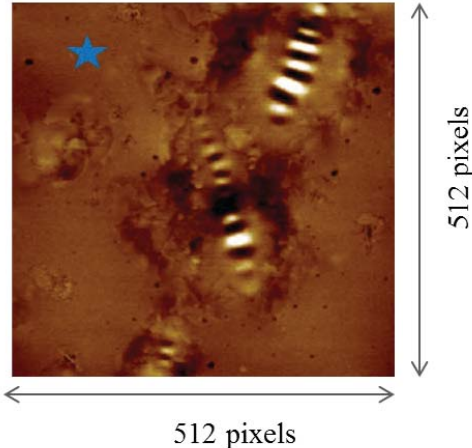


Figure 34 Example of a 10x10  $\mu\text{m}$  image of virgin binder 50/70 corresponding to 512x512 pixels.

This step-operation was repeated for the entire 10x10  $\mu\text{m}$  figure having one force-curve each pixel and the corresponding elastic moduli measurements. From Figure 34 and its corresponding point designated by a star (the star symbol is not in scale), the following force-distance curve can be obtained as shown in Figure 35.

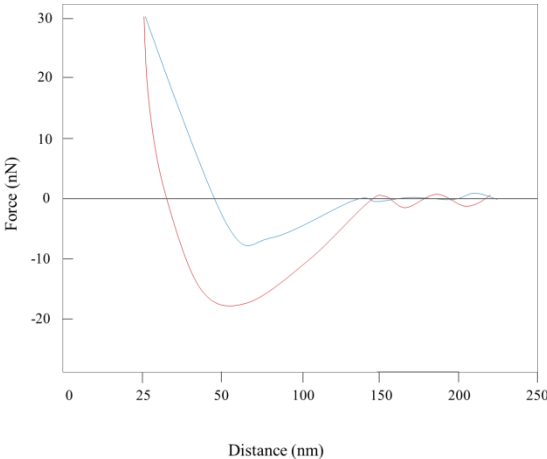


Figure 35 Force-distance curve obtained for the virgin binder 50/70 at designed point in Figure 34.

As was outlined in the previous section, to obtain the elastic modulus  $\tilde{E}$  at the sample surface, the retraction curve was then fitted by using a specific software with the DMT model (Derjaguin, Muller, and Toporov 1975) as was shown in Figure 33. As shown before, the DMT model is used by

default when fitting the AFM retraction curve and it was firstly developed when studying the interaction between an elastic ball and a rigid flat substrate (Derjaguin, Muller, and Toporov 1975). These assumptions could not fully reproduce the interaction between the silicon tip and a viscoelastic material such as bitumen which has in addition the disadvantage of having many asperities as well not being perfectly flat. However, it has been shown how this system is also applicable in such cases by using proper calibration method (Dokukin and Sokolov 2012) as will be outlined in Chapter 6.

## **2.9 Bitumen's observations by using atomic force microscopy**

### *2.9.1 Sample preparation techniques*

Special attention is needed in sample preparation as surface topography can be highly influenced by the preparation process itself. For viscous material like asphalt binder, surface preparation becomes an even more important factor for avoiding any artefacts. As described in the previous chapter, binder shows ageing due to oxidation and also collects dust or other airborne particles with time if not stored in a dust-free environment. Thus, the sample preparation techniques had always been a concern while conducting AFM scanning of binders. Nowadays, there are two main techniques used for samples preparation: the spin casting and heat casting. (Das et al. 2016a)

In the spin casting method, the sample is produced by dissolving asphalt binder in a solvent and subsequently the solution is cast on a spinning plate. After evaporation of the solvent, the resulting film thickness of the sample is in the micrometre range depending on the binder concentration in the solvent. In order to eliminate residual of solvent used during the sample preparation, generally specimen are placed in an airtight heated vacuum desiccator followed by ultra-high purity dry nitrogen to pass through a purifier (Allen et al. 2014). Annealing is also important to enable the micro-structure of the asphalt binder to return to its original form and eliminate any artefacts that may be attributable to the solvent cast spin-coating process. However, in (Pauli et al. 2011) it was shown how the nanometre range sample can have a direct impact on the AFM images, as the size and shape of the micro-structures change significantly with the relative film thickness. In addition, steric hardening effects in the spin-casting and can also alter the bitumen microstructure (Pauli et al. 2011).

In the heat casting method, the asphalt binder needs to be mixed properly by stirring around  $120 \pm 10^\circ\text{C}$  (depending on the types of binder) to avoid biases due to samples' inhomogeneity (Das et al. 2016a). A sample holder can be used to place approximately 20–30 mg of hot liquid binder and keeping it on a hot plate for 5 min at the same temperature. This will allow the binder to spread

out by creating a smooth surface. Afterwards, the specimens need to be left horizontally and be covered to prevent dust pick up for at least 24 h at 25°C prior to test. Since all specimens generally go through the same preparation process, it can be assumed that oxidation during sample preparation can be ignored or is at least constant amongst all specimens (Das et al. 2013).

### 2.9.2 “Bee” shapes and bitumen microstructure

The first attempt at investigating bitumen's microstructures using AFM was done by Loeber et al. (Loeber et al. 1996). They reported rippled micro-structures on surface of a thin film of bitumen and coined the term “bee” structures to describe the undulated patterns that resemble the yellow and black stripes of a bumble bee. Although “bee” structures are a common feature in bitumen, their shape and size can differ depending on the source of the crude oil (Pauli et al. 2011). In addition, micro-structures with fine domains, flake-like domains, and flower-like domains also appear on surfaces of other bitumens (Menapace et al. 2018). In all cases, as depicted in Figure 36, bitumen presents common features called catanaphase (“bee”-shaped), periphase (around catanaphase), paraphase (solvent regions) and salphase region (high phase contrast spots).

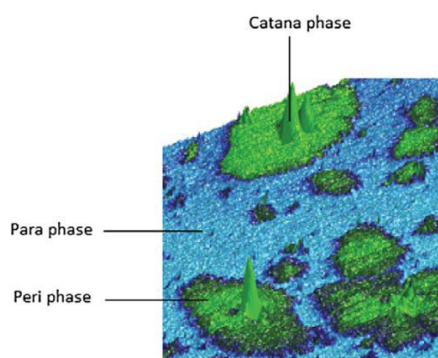


Figure 36 Example of bitumen’s morphology with catanaphase, paraphase and periphase. (Lyne, Wallqvist, and Birgisson 2013)

The effect of thermal history on bitumen microstructures is often related to the crystallized fractions in bitumen, which can be paraffin waxes or certain ratio of the polar components. For instance, it was reported how the “bee” structures were absent from its non-annealed film, which was prepared by merely buttering the bitumen at room temperature with no heat treatment (dos Santos, Partl, and Poulidakos 2015). For waxy bitumen subjected to heating and cooling cycles in the temperature range from room temperature to 80° C, the “bee” structures changed considerably (Pauli et al. 2011). In another study, it was demonstrated how “bee” structures appearing at room temperatures were completely dissolved into the matrix phase at 70° C while reappearing upon cooling (Soenen et al. 2014). Firstly, some authors (Jäger et al. 2004) indicated that the “bees”

could be composed by polar fraction, namely the asphaltenes; then Masson et al. (Masson, Leblanc, and Margeson 2006) reported a good correlation between the presence of the “bee” and the metal contents. Recently, the “bee” structures has been attributed mainly to clustering of the non-polar waxes (Pauli et al. 2011).

“Bee” structures have been seen as temperature dependent (Soenen et al. 2014). Therefore, the interaction between the waxes and the asphaltenes could be the key to the interpretation of the presence of the “bees”. It is known that the maltene phase does not show any “bee” structures (Hofko et al. 2016). However, it was seen how by changing the percentage of asphaltenes, the quantity of the “bees” changes. Thus, it can be hypothesized that the “bee” formation is linked to a process in which asphaltenes and paraffinic waxes are involved (and not the matrix phase composed by the maltenes). The “bee” like structure might be caused by defined quantities of asphaltenes and paraffin (Xu et al. 2016) with the result that “bees” are not influenced by extraction process with compounds such as toluene. The aging of asphalt increases the contents of asphaltenes and decreases the contents of paraffinic waxes which corroborates other research results (Eberhardsteiner et al. 2016).

A detailed AFM microscopy study of bitumen samples under mechanical strain and under different sample preparation and storage conditions showed how “bee” structures are very thin (ca. 10 nm) with hills being harder than the valleys in terms of elastic modulus as can be observed in Figure 37 (Hung and Fini 2015). In addition, it was observed how AFM imaging revealed relevant topological evolution of the bitumen with water exposure at elevated temperature (Hung, Goodwin, and Fini 2017).

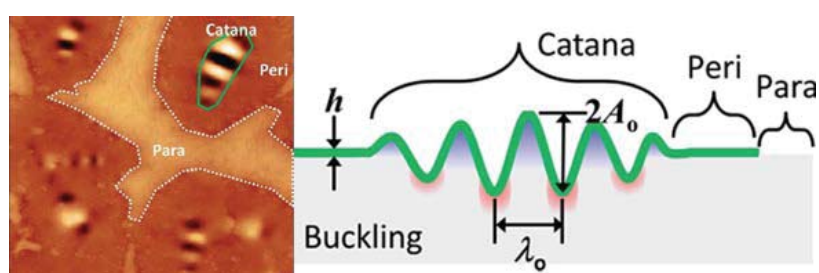


Figure 37 An example AFM height image (5  $\mu\text{m}$  x 5  $\mu\text{m}$ ) with corresponding scheme of a “bee” (Hung and Fini 2015).

In addition to chemical composition, questions remain as to the origin, properties, and subsurface structure of these features as well as their relation to material performance. Several studies have analysed the surface properties of reclaimed asphalt binder after the addition of rejuvenators. For example addition of additives have caused a drastic change in the binder’s morphology as shown in Figure 38 (Hung et al. 2017).

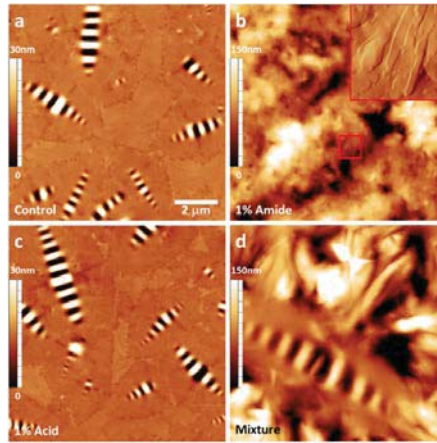


Figure 38 AFM height images of the surface of (a) undoped bitumen and bitumen doped with (b) 1% amide, (c) 1% acid, (d) 1% amide and +1% acid. (Hung et al. 2017)

Huang and Pauli studied the effect of crumb rubber on bitumen. The morphology of the rubber phase and its interaction with the asphalt binder network structure in various concentrations at different particle sizes was investigated in (S. C. Huang and Pauli 2008). They showed how rubber-modified asphalt had different phase images, which led to the findings that some fractions of the rubber particles may be dissolved in the asphalt. The temperature effect on morphology of asphalt binder modified with polymers was studied in (Navarro et al. 2007) where it was shown how the polymer addition leads to “bee”-shaped micro-structure regions with lower thermal susceptibility. AFM is capable also of giving information on the micro-mechanical properties such as elastic modulus, adhesion and sample deformation quantitatively as described in the previous paragraphs. Jäger et al. (Jäger et al. 2004) were the first ones to investigate the relative stiffness of different phases in asphalt binder. It was observed how the micro-structure and its surrounding matrix showed different relative stiffness. In another study, AFM was used to relate the “bees” to local stiffness and elastic recovery. Indentations were performed at different points on the surface and a significant variation of elasticity was observed between the points on the “bee” shaped micro-structures and the matrix (Dourado et al. 2014). In (Lyne, Wallqvist, and Birgisson 2013), the adhesive forces were measured in the region (periphase) surrounding the “bees” (catanaphase). In the “bee” areas, adhesion was lower than in the smooth matrix (para phase). Likewise, elastic moduli in the region surrounding (periphase) the ‘bees’ (catanaphase) and in the “bees” were higher than elastic modulus of the smooth matrix (para phase). Generally, when rejuvenators are added in a binder, the surface microstructure changes consistently. Microstructural investigations with AFM have also been performed on recycled binders and blends of base and recycled binders. RAP binders commonly present a microstructure which is different from the neat virgin binder. As can be seen in Figure 39, RAP binder shows dispersed “bee” structures compared to the virgin

binder. For example, as reported in (Yu et al. 2014) the microstructure depended largely on the specific binder-rejuvenator combination and the rejuvenated blends duplicated the surface microstructures of the virgin binders. Bio-based rejuvenators have been seen as promising for revealing how bio-oil mitigates the number of “bee” structure in the binder’s surface. This could be an indication how rejuvenators are effectively able to enhance the diffusion of certain asphalt compounds (Ali et al. 2016). The inclusion of recycling agents in the rejuvenated blends generally caused rounder dispersed domains, smoother domain borders, a larger matrix, and in some cases roughness decrease and phase contrast increase (Menapace et al. 2018).

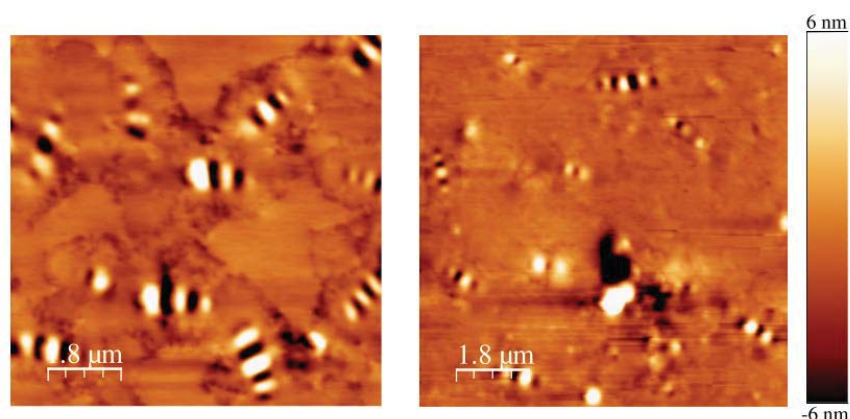


Figure 39 AFM images  $9 \times 9 \mu\text{m}$  of the control asphalt binder (left) and a RAP binder (right).

(Nazzal et al. 2014)

Mainly, the effects of time, temperature and aging in modified RAP’s binders are still not univocally identified. Nowadays, it is still to be demonstrated how the morphologic changes can affect the mechanical performances of asphalt binder. Generally, it can be seen how a systematic approach is missing especially regarding the measurement of the mechanical properties with AFM. In addition, conclusive results concerning the elastic moduli at the surface are largely missing as well. A better understanding of the “bees” formation as well as bitumen’s mechanical properties at the surface might offer new insights for the molecular basis of bitumen mechanical properties. The aim of Chapter 6, will be to better understand the changing of the microstructures in RAP binder after the addition of rejuvenators before and after aging and compared it to the virgin binder.



### **3. Materials**

As outlined in Chapter 1, this Ph.D. thesis was part of a larger study project titled “Fully sustainable recycled asphalt concrete”. The materials used to analyse fundamental aspects of modified RAP binder were the same for all tests campaign. Thus, in this section is reported a description of each material used together with its preparation method if required.

#### **i. RAP and virgin binder**

As this is part of a cooperative project with industries, the materials RAP and virgin binder were provided by the company BHZ in Switzerland. The RAP binder was extracted from the RAP mixture, with toluene and recovered following the European Standard 12697. It is hypothesized that the total evaporation of the toluene does not influence the properties of the recovered RAP binder (Amani, Gray, and Shaw 2014). The extracted binder content from RAP was 5.60% by weight of the mixture. Standard engineering tests have been performed showing a needle penetration of  $22 \times 10^{-1}$  mm at  $25^{\circ}$  C (European Standard 1426) and a Ring & Ball softening point temperature equal to  $65.7^{\circ}$  C (European Standard 1427). A virgin penetration graded bitumen 50/70 with a measured penetration of  $62 \times 10^{-1}$  mm at  $25^{\circ}$  C and a softening point temperature of  $49^{\circ}$  C was used as reference as prescribed by the project’s partners.

#### **ii. Rejuvenators’ selection**

Three commercial bio-based rejuvenators were used: rejuvenator “A” based on natural seed oil, rejuvenator “B” based on cashew nut shell oil and rejuvenator “C” based on tall oil. Rejuvenators B and C are commercial products marketed in Switzerland for the purpose of asphalt rejuvenation. Several studies have indicated the importance of proper dose of rejuvenators and its effect on binder and mixture properties (Oliveira et al. 2013; S. C. Huang et al. 2015). For this study, the rejuvenator’s dosage was chosen to be 5% by mass of recovered RAP binder to have a direct comparison between the effects of each rejuvenator. However, the softening efficiency of rejuvenators was also determined using penetration test (EN 1426) at room temperature. In order to duplicate the needle penetration of the virgin binder 50/70, the targeted penetration was set as equal to 50  $\text{mm}^{-1}$ . As can be seen in Figure 40, the starting point on the y axis was set as  $22 \times 10^{-1}$  mm which corresponded to the RAP’s binder penetration with 0% rejuvenators. Afterwards, 5% of each rejuvenator was added and the corresponding penetration grade was calculated. Subsequently, the

targeted penetration equal to  $50 \times 10^{-1}$  mm was calculated by using exponential fitting as proposed in (Zaumanis, Mallick, and Frank 2014).

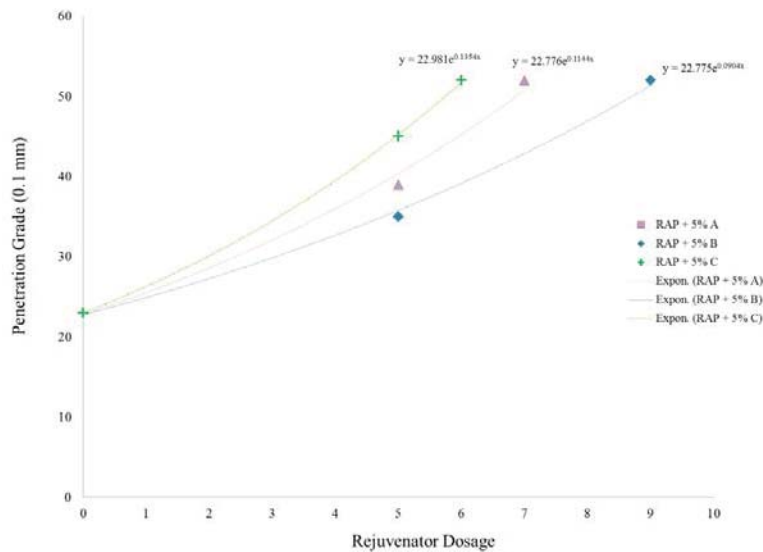


Figure 40 Rejuvenator dosage vs. penetration grade. The values presented were obtained following the European standard EN 1426.

### iii. Binder mixture preparation

The extracted RAP binder was placed in the oven at a temperature equal to the softening point temperature plus  $80^{\circ}$  C for 40 minutes as prescribed in the European standard EN 1426. This amount of time was found to be the minimum for the RAP binder to become liquid. Subsequently, 5 grams of each rejuvenator, which were at room temperature, were added to 100 g of hot RAP binder and processed in a Speed Mixer<sup>TM</sup> for one minute at 3500 rounds per minute. One minute was found experimentally suitable for homogenization as verified by unaided eye. RAP binder, RAP binder plus rejuvenators and the virgin bitumen 50/70 were also tested after laboratory aging. Standard laboratory aging procedures were used to simulate the effect of heat and air as follows. Samples were conditioned using the rolling thin-film oven test (RTFOT) which aims at simulating aging during mixing and paving (EN 12607). The samples were placed into rolling glass jars at  $163^{\circ}$  C for 85 minutes while undergoing oxidation by airflow of 400 mL/min. After the RTFOT, the samples were conditioned with the pressure aging vessel (PAV) method (EN 14769) that uses pressure and temperature, simulating long term aging in the field. Bitumen was placed into stainless steel pans and then for 20 hours in a heated PAV at 2.10 MPa. The combined aging procedures are expected to simulate mixing, laying and field aging of asphalt binders at later stages of pavement life.

#### **4. Influence of rejuvenators on the mechanical performances of reclaimed asphalt binder**

This chapter contains sections which are largely based on the content of the following paper:

These sections are indicated with an asterisk (\*).

M.C. Cavalli, M. Zaumanis, E. Mazza, M.N. Partl, L.D. Poulikakos, Effect of ageing on the mechanical and chemical properties of binder from RAP treated with bio-based rejuvenators, *Compos. Part B Eng.* 141 (2018). doi:10.1016/j.compositesb.2017.12.060.

## 4.1 Summary

Rheological tests showed how the rejuvenators may restore the mechanical properties of RAP binder. A rheological index has been proposed to show that the rejuvenators have been affected the RAP binder differently after aging. Despite their addition, physio-chemical oxidation did not reverse. Mechanical changes were not caused by chemical changes at functional groups level but a rearrangement of polar/nonpolar components. Furthermore, results obtained in this work, showed that considering the effect of aging is vital in identifying how rejuvenators affect the RAP binders long term.

## 4.2 Introduction

As described previously, generally bitumen ages due to different processes such as, oxidation, changes in molecular organization, or loss of volatiles (Lu and Isacsson 2002a; Nazzal et al. 2014). For this reason, so called “rejuvenators” are used for restoring the properties of the RAP binder. To this end, in order to have a complete picture of the effect of rejuvenators, the rheological properties of the rejuvenated RAP binder should be considered, as well as its chemical composition (dos Santos, Partl, and Poulikakos 2015). FTIR in combination with DSR for mechanical performances have been shown to be successful in analysing aging as a result of oxidation and changes in the mechanical performances as previously shown in Chapter 2 of this thesis. GPC in combination with FTIR, were found to be useful for characterizing effects of aging on the chemical structure of bitumen (Bowers et al. 2014). SARA fractioning has demonstrated an increase of polar components due to aging (Hofko et al. 2016). The objective of this study is to characterize and understand the effects of aging of RAP modified with three rejuvenators. To this end, different techniques were used such as: FTIR for investigating oxidation, GPC for determining molecular size distribution, SARA fractioning for detecting polar-nonpolar components, and DSR for analysing the mechanical time-temperature dependent behaviour.

## 4.3 Materials and Methods

The materials preparation followed what described in Chapter 3.

### 4.3.1 *Dynamic shear rheometer (\*)*

As outlined in Chapter 2, sigmoidal model was used to create mastercurves. The reference temperature  $T_{ref}$  in this study was 20° C. In order to achieve the best fit between the measured values of the complex modulus and the values described by the sigmoidal model, the shifting factor by using the WLF was used. The detailed data obtained from the shifting procedure are reported in the Appendix section of this Chapter.

According to EN 14770, for the rheological measurements, 1.5 g of each material was placed in a disc shaped silicon mould with diameters of 8 mm and 25 mm and tested with the DSR Physica MCR at temperatures between -10° C to 80° C. The 8 mm plate-plate geometry with 2 mm gap was used in strain controlled mode for the temperature range -10° C to + 40° C while the 25 mm plate-plate geometry with 1 mm gap was used for the temperature range +40° C to + 80° C as required by the standard. Each measurement was repeated four times. Testing frequencies ranged from 0.1 to 20 Hz at each temperature and were conducted in the LVE domain as shown in the Appendix section of this Chapter. The chosen frequencies were expected to simulate traffic vehicles passing during service life (Gordon D. Airey, Rahimzadeh, and Collop 2004).

### 4.3.2 *Attenuated total reflectance Fourier transform infrared spectroscopy (\*)*

The ATR-FTIR measurements were performed at room temperature in a Tensor 27 from Bruker spectrometer using a diamond crystal following the procedure described in Chapter 2. For the spectroscopy measurements, a small amount of bitumen (ca.10 mg) was placed directly on the diamond crystal with a metal spatula. The spectra were collected in the 4000 to 500  $cm^{-1}$  wave-number range with a resolution of 4  $cm^{-1}$  and each spectrum represented an accumulation of 32 spectra. The data were collected with the OPUS ® software.

### 4.3.3 *Gel permeation chromatography (\*)*

For the gel permeation chromatography experiments, an HPLC-Pump (Agilent G1310B/1260 Iso Pump) was used with column oven (SFD 12590) at a temperature of 30° C. Two detectors were utilized: a variable wavelength detector (Agilent 1260 DEABB05519) with UV signal (wavelength equal to 215 nm) and a refractive index (RI) detector (Agilent 1100/1200 G 1362A) in the range

between 1 and 1.75. As eluent solvent, high purity tetrahydrofuran, at a flow rate of 1.0 ml/min, was used. The column was composed of Agilent PL 5M-mixed C, 5 $\mu$ m, 300 x 7.5 mm with a sampling rate of 9/s and volume of injection equal to 50  $\mu$ l. The data were interpreted following what described in Chapter 2.

#### 4.3.4 Saturates Aromatics Resins Asphaltenes (SARA) fractioning (\*)

In this section, high performance liquid chromatography was used to perform SARA fractioning. Asphaltenes were separated by precipitation in n-heptane. Afterwards, maltenes were split in saturates, aromatics and resins by silica gel NH<sub>2</sub> chromatography. Saturates were split thanks to refractive index chromatography while aromatics and resins thanks to UV chromatography. The procedure followed the requirements in the American standard D 4124 – 01.

## 4.4 Results and Discussion

Aim of this section, is to show how the addition of rejuvenator could influence the mechanical performances of RAP binder. Emphasis was on the effect of aging on the overall mechanical performances.

#### 4.4.1 Rheological analysis of the unaged materials

Figure 41 left, shows the master curves of complex moduli  $|G^*|$  as function of frequency at the reference temperature of 20° C as was previously discussed in Chapter 2.

It follows that the differences between the unmodified RAP binder and the modified RAP binder are significant within the whole frequency spectrum. In particular, RAP + 5% B or RAP + 5% C had lower moduli than the virgin bitumen 50/70. Hence, it was found that at unaged state, the RAP binder modified with 5% rejuvenators B and C were mechanically softer than virgin bitumen 50/70 while RAP binder with rejuvenator A was harder in the low frequency range. The trend of the phase angle (Figure 41, right) confirmed what was shown in the rheological measurements: rejuvenator could soften the RAP binder for all frequencies.

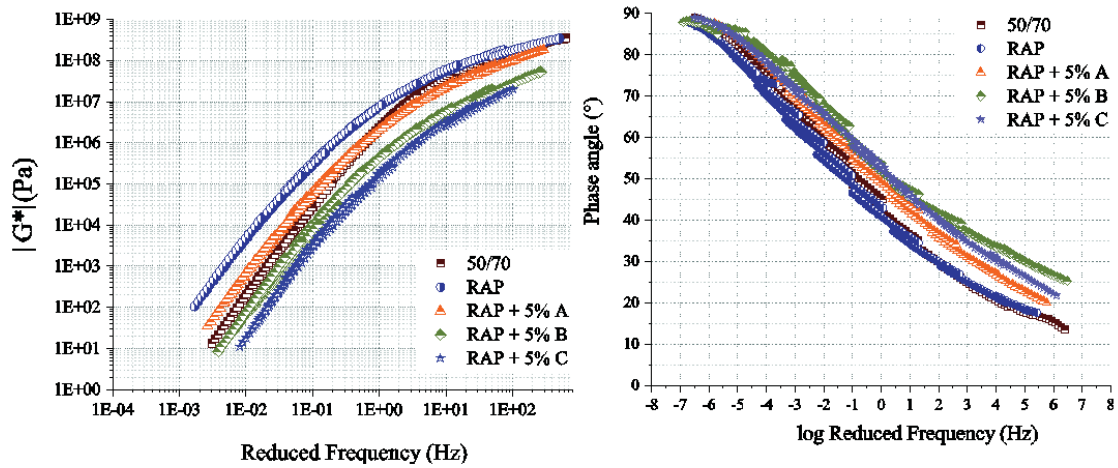


Figure 41 Dynamic shear moduli master curves for reference temperature of 20° C (left) and phase angle measurements (right) from frequency sweeps (0.1-20 Hz). The presented values are an average of four measured values.

It can be seen how RAP binder and 50/70 reached the same value of  $G^*$  (higher than 100 MPa) at high values of reduced frequency, thus lower temperature range i.e. -10° C while having a gap of one orders of magnitude at low frequencies. Moreover, rejuvenators caused a general shift downwards for all the master curves at all frequency ranges showing how at low frequencies rejuvenators could soften the RAP binder (remaining close to the mastercurve of the virgin binder) while for higher frequencies range, rejuvenators could soften the RAP binder even more than the virgin binder.

#### 4.4.2 Rheological analysis of the aged materials

After aging, the overall complex moduli of each material tested increased in comparison to the unaged materials as shown in Figure 42 and in comparison to Figure 41. It was observed that over most of the frequency range, RAP + 5% A and RAP + 5% C had similar complex moduli after aging. On the contrary, RAP + 5% B was closer to the complex moduli of the aged RAP binder indicating little improvement in mechanical stiffness after aging. The aged virgin binder 50/70 had similar values to the unaged RAP binder showing how the standard aging procedure could simulate closely the aging caused during its service life. Figure 42 left, shows how, despite the addition of rejuvenators, after aging there is in general an increase of both complex moduli and phase angle along the whole frequency range. Furthermore, the difference in the values of complex moduli at aged state is more prominent at low frequencies (higher temperatures, from +40° C to +80° C) than at high frequencies (low temperatures, from +30° C to -10° C) as the curves converge at high frequencies after aging showing that rejuvenator's effect is more prominent at high temperatures. Furthermore it can be seen from the results that aging plays a significant role in materials rheolog-

ical behaviour and should be considered when long term mechanical performance is sought. Figure 42 right shows that at low frequencies, the phase angle of the virgin bitumen is high indicating a dominance of the viscous portion of the complex modulus in comparison to the other materials. RAP + 5% A and RAP + 5% C resulted in a higher phase angle than the RAP binder alone, indicating that they could maintain the viscous portion of the complex modulus towards the values of the virgin binder which is beneficial for roads as viscosity is needed to bear traffic load conditions. A comparison of the results of unaged and aged binders clearly indicates how aging can affect the mechanical response of the rejuvenated materials.

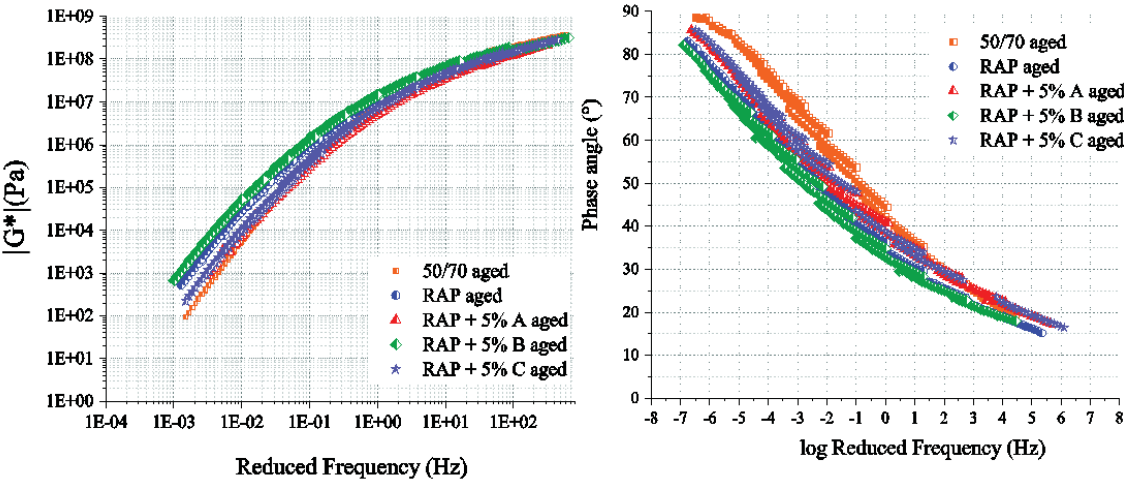


Figure 42 Master curves of complex shear moduli results of the aged materials measured (left) and phase angle measurements (right) at reference temperature of 20° C and at frequency sweeps (0.1-20 Hz). The presented values are an average of four measurements.

4.4.3 Crossover temperature at 1 Hz

As described in Chapter 2 of this thesis, at low temperatures bituminous binders are more elastic ( $G' > G''$ ) whereas at high temperatures the opposite is true.

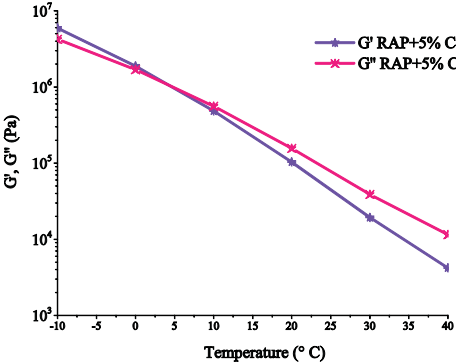


Figure 43 Example of the calculation of the crossover temperature at 1Hz.



As shown in the example in Figure 43, the interplay between the elastic and viscous components of the complex modulus undergoes a transition at some point. Defining a temperature at which this transition occurs is an important material property. As described previously in this thesis, low crossover temperature is an indication that the viscous component and the elastic component of the complex modulus are equal at low temperatures. Asphalt pavements operate in a wide temperature range, and when the pavement presents phase angle above  $45^\circ$  the binder will be more likely to flow under stress instead of cracking due to the predominant influence of the  $G''$  component. Generally, a lower crossover temperature is desired however, as binder ages, the crossover temperature increases. It is acknowledged that fatigue and thermal cracking are highly dependent on mixture properties and pavement structure, yet the flow/relaxation characteristics of the binder can attenuate or exacerbate the problem (Garcia Cucalon et al. 2018).

Results in Figure 44 indicated that rejuvenators could restore the cross over temperature of RAP binder since the crossover temperature moved towards lower temperatures in case of rejuvenator A and C. 1 Hz was chosen as a suitable value of frequency as it lies in the middle range of the frequency sweeps used for the rheological measurements (0.1-20 Hz). These results are in agreement with changes of the phase angles, where the viscous portion was more prominent for RAP + 5% B and RAP + 5% C (Figure 41, right) at lower frequency (high temperature). With the crossover temperature, it can be hypothesized that a change from elastic to viscous part appears faster in RAP + 5% B and RAP + 5% C. After the aging procedure, the crossover temperature increased for all the materials in comparison to the unaged state which can cause a reduction of ductility and elasticity (Nivitha and Murali Krishnan 2016). This resulted in an overall increase of the crossover temperature with a higher value for RAP + 5% B.

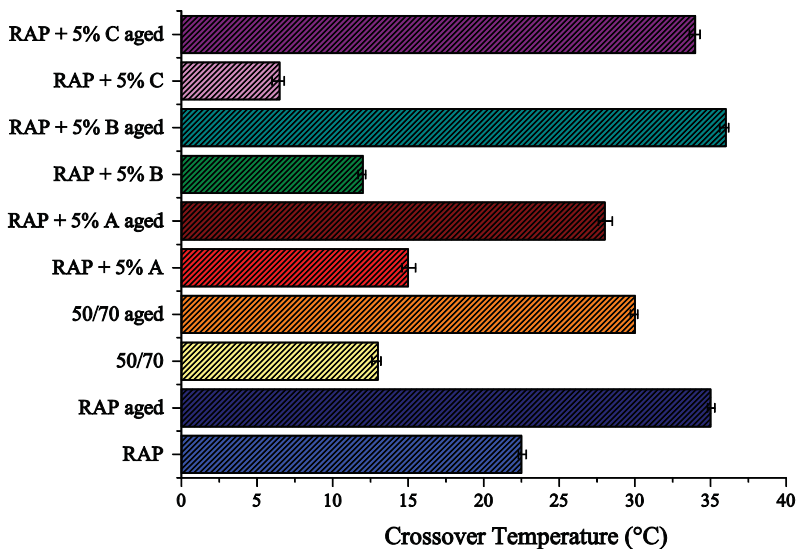


Figure 44 The crossover temperatures for the aged and unaged materials, at the frequency of 1 Hz for the different binders tested between  $-10^\circ\text{C}$  and  $+40^\circ\text{C}$ .

#### 4.4.4 Rheological aging index

In order to provide an interpretation of the results, a rheological aging index  $R_A$  was defined to incorporate the changes over a large frequency range by calculating the difference between the area under the aged and unaged master curves within a definite range of reduced frequencies chosen to ensure that the same integral limits for all calculations is used. Hence, the following equation holds:

$$R_A = \int_{-5}^{+4} \left[ \log G^* (\xi_{aged}) - \log G^* (\xi_{unaged}) \right] d\xi \quad [\text{Pa} \times \text{Hz}] \quad (21)$$

Where  $G^*$  is the complex modulus and  $\xi$  is the logarithm of the reduced frequency among the integral limits. Thus, the result of the integral, which is the area between the two master curves in double logarithmic representation, was subsequently calculated, as shown in the example in Figure 45.

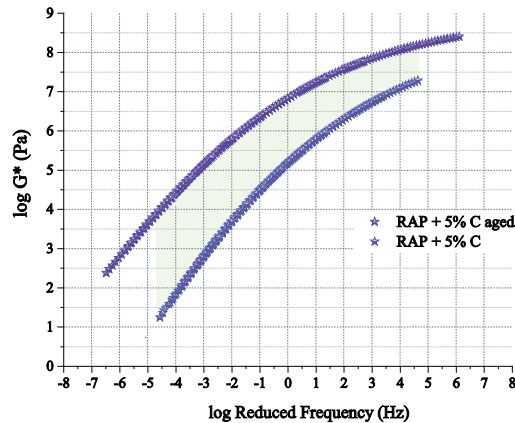


Figure 45 Principle of the rheological aging index calculation using the area between the aged and unaged master curve at reference temperature of 20° C.

The rheological index  $R_A$  demonstrates the effects of aging of the various rejuvenated RAP binders, virgin binder as well as RAP binder. As it is possible to see from Figure 46,  $R_A$  of the virgin binder 50/70 is higher than the extracted RAP binder alone, indicating that the virgin binder had aged more than the RAP binder. This is due to the fact that the RAP binder was already aged. Hence, it is subjected to less loss of volatiles and oxidation than the virgin binder. RAP + 5% B showed larger  $R_A$  indicating that the material's rheological properties, such as  $G^*$ , is highly influenced by aging compared to the others and that the difference between unaged and aged rejuvenated binders were not the same. Ranking of the aged rejuvenated RAPs from highest difference to lowest turned out as follows: RAP + 5% B, RAP + 5% C, RAP + 5% A.

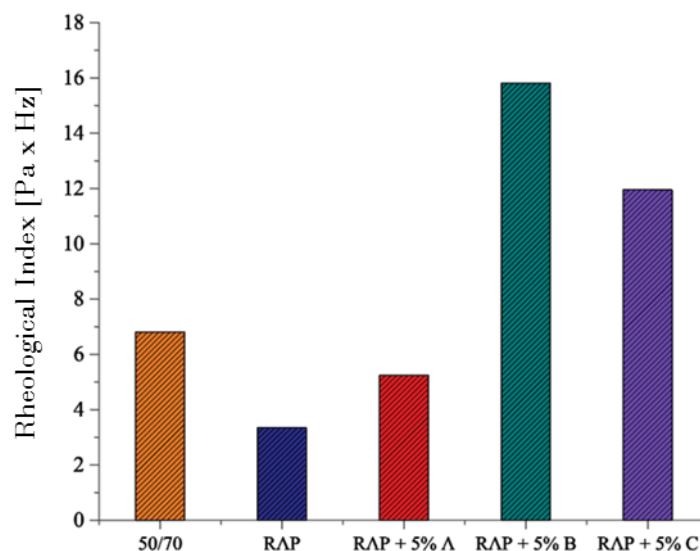


Figure 46 Variation of the rheological aging index for the different binders.

#### 4.4.5 Attenuated total reflectance-Fourier transform infrared spectroscopy

As explained in the previous chapters, the use of rejuvenators has the potential to address many issues related to the use of RAP binder, however it is important to detect any chemical changes due to the oxidation process as was outlined in Chapter 2.

#### 4.4.6 Rejuvenators composition

Additional analyses were done in order to detect differences in the rejuvenators without the addition of any bitumen compounds. Rejuvenators A and C have proven to be chemically similar while B showed significant differences as can be seen in Figure 47. As already mentioned, rejuvenator A is a vegetable oil, mainly composed of palmitic acid (saturated usually 5%), stearic acid (6% saturated), oleic acid (30% monounsaturated omega-9) and linoleic acid (59% polyunsaturated omega-6) (Raman et al. 2015). As it is possible to observe from Figure 47, rejuvenator C has some overlap in terms of chemical structure as A. Rejuvenator C is composed by tall oil fatty acids which is usually used for bio-based thermosets (White et al. 2011). Active functional groups can be introduced artificially. Rejuvenator B is a cashew nut shell oil (CNSL) which is a by-product of the cashew industry: the nut has a shell inside which is a soft honey comb structure containing a dark reddish brown viscous liquid (Toschi et al. 1993). As it is possible to see from Figure 47, the CNSL can contain a functional groups: the hydroxyl group (peak centred at  $3300\text{ cm}^{-1}$ ).

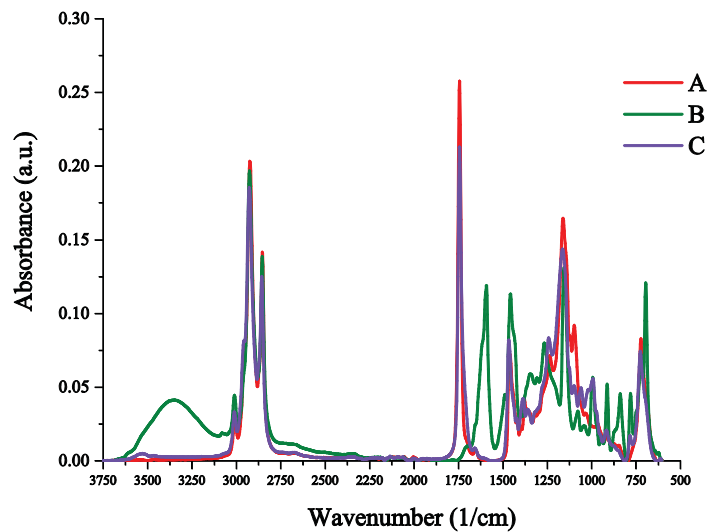


Figure 47 ATR-FTIR spectra of the plain rejuvenators A, B and C before aging.

#### 4.4.7 RAP binder with rejuvenators

Figure 48 shows the FTIR spectra for all the laboratory unaged materials showing the intensity of the spectral peaks, corresponding to the different bonds/functional groups, as a function of the wavenumber. Changes due to oxidative aging correspond to the intensity of the carbonyl (peak centred around  $1700\text{ cm}^{-1}$ ) and sulfoxide functional groups (centred around  $1030\text{ cm}^{-1}$ ), that are relevant for asphalt (Poulikakos et al. 2014). As a result of aging, functionalities are formed that increase the overall polarity of the bitumen, thus influencing bitumen rheology (Lu and Isacson 2002a). From Figure 48 follows that the spectrum of the virgin binder diverges from the binders containing RAP at two locations. The majority of the peaks of the RAP binders, even after adding 5% of the three rejuvenators, remain the same. The peaks corresponding to the aging of binders due to oxidation do not disappear although rejuvenators were added to the RAP binder belonging to the non-reversible type of aging identified by (Lu and Isacson 2002a). Chemical structures of RAP + 5% C and RAP + 5% A were found to be similar, suggesting that the chemical effect of rejuvenator C and rejuvenator A on RAP binder was similar.

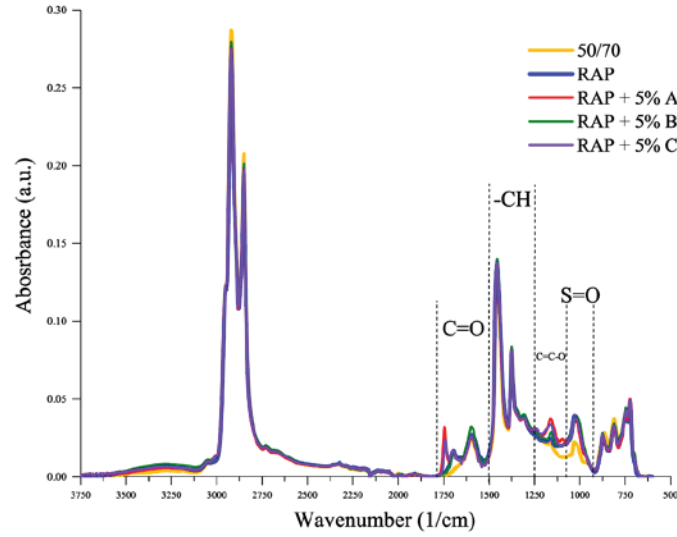


Figure 48 ATR-FTIR spectra of the virgin binder 50/70, the RAP binder and the RAP binders with rejuvenators A, B and C (5% by mass of RAP binder each).

#### 4.4.8 Carbonyl and sulfoxide indexes before and after aging (\*)

As suggested in (Marsac et al. 2014), the carbonyl and the sulfoxide indexes are calculated by dividing the area of the carbonyl and sulfoxide functional groups through the area of peaks related to the asymmetric vibration of the  $-CH$  groups. In particular, the  $CH_2$  group (centred around  $1455\text{ cm}^{-1}$ ) and to the symmetric deformation vibration of  $CH_3$  group (centred around  $1376\text{ cm}^{-1}$ ) as the latter areas do not change significantly due to aging. Hence the following equation holds:

$$\text{Carbonyl index (CI)} = \frac{\text{Area}_{\text{C=O}}}{\text{Area}_{\text{CH}_2} + \text{Area}_{\text{CH}_3}} \quad (22)$$

$$\text{Sulfoxide index (SI)} = \frac{\text{Area}_{\text{S=O}}}{\text{Area}_{\text{CH}_2} + \text{Area}_{\text{CH}_3}} \quad (23)$$

The sum of both indices (CI + SI) was used to determine the chemical aging index (CAI) before and after aging as previously proposed by other authors (Mousavi et al. 2016). Thus it holds:

$$\text{Chemical aging index (CAI)} = \text{CI} + \text{SI} \quad (24)$$

An increase in carbonyl and sulfoxide index means rising degree of oxidation in the bituminous binder, causing stiffening (Mousavi et al. 2016; Petersen and Glaser 2011). As shown in Figure 49, the unaged binders RAP + 5% A and RAP + 5% C produced a higher absorbance in the spectra at wavenumber corresponding to the carbonyl index than the plain RAP binder. This is due to the

fact that seed oil and tall oil themselves contain carboxylic groups C=O, as outlined in (Girard 1980), thereby their CI is influenced by their natural state that is not due to oxidation. As shown in Figure 49, after aging the CAI of all rejuvenated binders are similar. However, considering that the CAI of rejuvenator A and C is influenced by their natural state, it can be deduced that the CAI of aged RAP + 5% rejuvenator B is the highest. Nevertheless the CAI was not reduced after addition of rejuvenator. Therefore, it can be concluded that the addition of rejuvenators could soften the RAP binder but not breaking its chemical bonds at molecular level. As shown in the previous sections, rejuvenator alone were not affected by aging thus, the increase of both C=O and S=O groups is a result of aging of the RAP binder these results corroborate others reported such as (Lopes et al. 2016; Dondi et al. 2016).

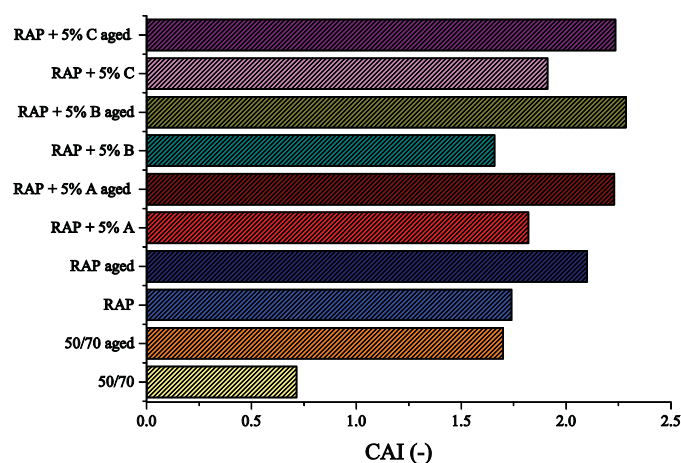


Figure 49 Comparison between the CAI of the virgin binder, RAP binder and RAP binder plus 5% by mass of rejuvenators before and after aging.

#### 4.4.9 Gel Permeation Chromatography (\*)

As outlined in Chapter 2, molecular size distribution by using GPC can be used in order to evaluate if rejuvenators modified molecular properties of RAP binder [39]. Figure 50 shows the results using two detectors that deliver different results due to their sensitivity to the different signals. The RI detector revealed some differences between the molecular size distributions of RAP binder with 5% of the three different rejuvenators. Qualitatively one can observe that, RAP + 5% A and RAP+ 5% C showed a shift from the large to the middle size as compared to RAP binder.

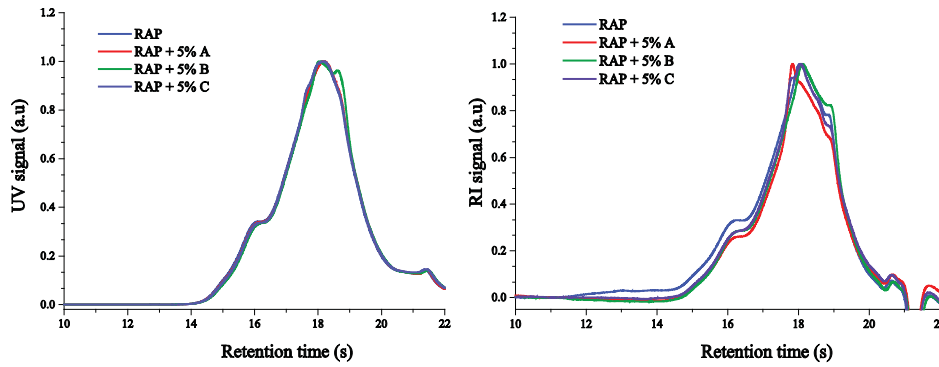


Figure 50 GPC spectra with UV (left) and RI-signals (right) of the RAP binder and the RAP binder with rejuvenator A, B and C (5% by mass of RAP binder each).

Different molecular sizes could be found with the UV detector. According to Figure 50, a difference in the RAP + 5% B has been observed showing a shift towards the smaller molecular sizes. Comparing the GPC results with the ATR-FTIR spectra, it is possible that this shift may be due to the presence of phenolic group in the rejuvenator B. In summary, rejuvenators could partially change the molecular size distribution of the RAP binders.

#### 4.4.10 SARA fractioning (\*)

Nonpolar fractions such as aromatics, which are responsible for the flexibility of the binder, tend to decrease after aging (Bonemazzi and Giavarini 1999) as was previously described in Chapter 2. As can be seen in Figure 51, the asphaltenes content of all aged binders have increased in comparison to the unaged materials. The addition of rejuvenator A, B and C could increase the content of resins in the RAP and decrease the asphaltenes, suggesting that they could partially rearrange the asphaltenes.

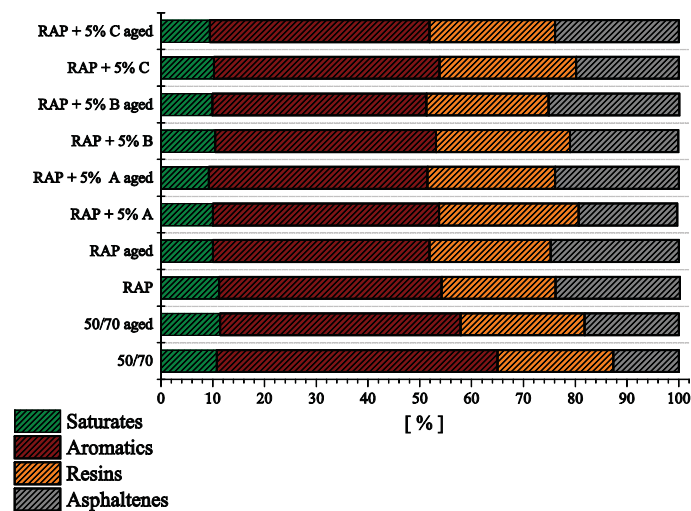


Figure 51 SARA fractioning of the virgin binder, the RAP binder and the rejuvenated RAP binder before and after aging.

From the SARA results the colloidal index (COI) can be calculated (Loeber et al. 1998), which is defined as the ratio of dispersed constituents (aromatics and resins) to flocculated constituents (saturates and asphaltenes).

Hence, the following equation holds:

$$\text{Colloidal Index (COI)} = \frac{\% \text{aromatics} + \% \text{resins}}{\% \text{saturates} + \% \text{asphaltenes}} \quad (25)$$

The colloidal index is as an indicator of sol or gel structures in bitumen. As can be observed in Figure 52, the COI increased after rejuvenation and decreased after aging. It can be hypothesized that rejuvenators could create a new agglomeration between polar and non-polar fractions in RAP binder as they were able to increase the COI of the RAP. Figure 52 shows that the COI is reduced with aging and the COI of the all aged modified RAP are similar. Despite that, the molecular interactions between the different chemical components of the RAP binder and the rejuvenators, remain very complex.

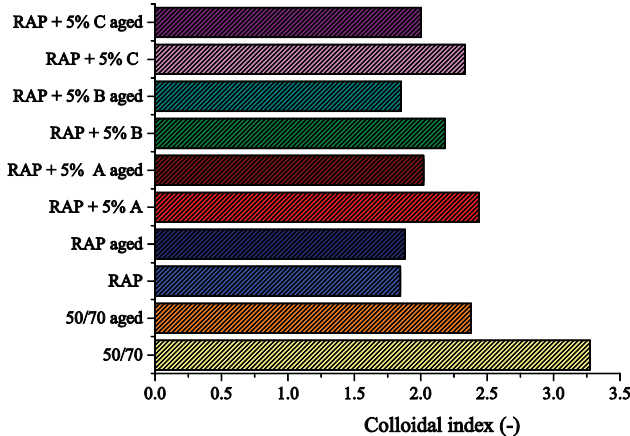


Figure 52 Colloidal index for the virgin binder, the RAP binder and the rejuvenated RAP binder before and after aging.



## 4.5 Conclusions and Perspectives

The chemical and mechanical effect of aging on rejuvenated RAP binders was studied.

Main findings from this study have been the following:

- i. The rheological analysis with the DSR confirmed that the addition of rejuvenators can cause a change in the mechanical performance of RAP. It was demonstrated how the addition of 5%, by mass of RAP binder, of rejuvenator B and 5% of rejuvenator C could reduce the complex moduli at values lower than the 50/70 virgin binder both at low and high frequencies (corresponding to high temperature and low temperatures respectively). In general, the complex moduli master curves for all of the rejuvenated binders were found to be lower than those for the RAP binder. This suggests that using asphalt binder rejuvenators when producing mixtures containing RAP would result in improving mechanical performance of RAP binder to levels similar to the virgin binder.
- ii. Aging has shown to be a fundamental aspect in analysing the material performances. After aging, the RAP + 5% A and RAP + 5% C seemed less affected by the changes of frequencies/temperature.
- iii. The rheological aging index proposed has demonstrated how the performances of all the compounds are affected by the aging process. It has demonstrated how the RAP had shown a rheological aging index lower than the 50/70 showing that the RAP is less affected by aging than the virgin binder. RAP binder + 5% A showed a lower rheological aging index while RAP + 5% B has demonstrated how the aging could increase dramatically its complex moduli both at low and high frequencies.
- iv. FTIR has confirmed that oxidation caused by aging is not a reversible process using these particular rejuvenators, and the disaggregation of oxygen bonds is not feasible even after the addition of rejuvenators. In order to have a quantitative analysis of the degree of oxidation, carboxylic group (C=O) and sulfoxide groups (S=O) were studied. C=O were found to be higher in RAP plus rejuvenator A and RAP plus rejuvenator C than in the RAP itself as vegetable seed oils alone are supposed to contain alcoholic groups. Sulfoxide groups did not decrease even after the addition of rejuvenators in the RAP binder.
- v. In GPC two different kinds of detectors were used in order to investigate any variation in the molecular size distribution. It was revealed that RAP binder with rejuvenator A and C underwent a change in the middle molecular size distribution indicating the presence of bigger molecular sizes. RAP + 5% B with UV detector has showed a shift towards the smaller molecular sizes.

In this work, it was shown that chemical aging and mechanical aging can be very different. Chemical aging as demonstrated through FTIR was stronger for the virgin binder and less for the RAP

binder whereas mechanical aging as characterized by the DSR and the rheological aging index showed lower values for RAP.

This part of the work demonstrates how a holistic approach needs to be followed where chemical and mechanical performances are used to evaluate long term performance potential of rejuvenators.

## 4.6 Appendix

### 4.6.1 Identification of the linear viscoelastic region.

The region of linear viscoelastic behaviour is defined as the region where  $G^*$  is independent of the shear stress or shear strain. The LVE region is strictly dependent on the material properties and it is not known a priori. For this reason, an amplitude sweep test for each binder was performed before the rheological measurements. The material response towards increasing stress or strain amplitude is monitored at constant frequency and temperature. In this way, it was possible to define the linear viscoelastic range as the region where both moduli are constant, and they do not depend on the amplitude of the shear strain. In particular, LVE limit is defined as the point where the complex modulus ( $G^*$ ) starts decreasing from its initial value while changing the shear rate as described in (Anderson 1994).

This procedure allows the selection of a fixed value of strain which will be used in the frequency sweep test to obtain the rheological parameters (i.e. mastercurves). During the rheological measurements, the amplitude shear strain was fixed at 1% for temperatures above 40° C and 0.5% for temperatures below 40° C, and then, the angular frequency was increased from 0.1 Hz to 20 Hz. Example of tests results for the virgin binder 50/70 as well the RAP binder can be seen in Figure 53 showing that the complex modulus does not change at small strain amplitudes.

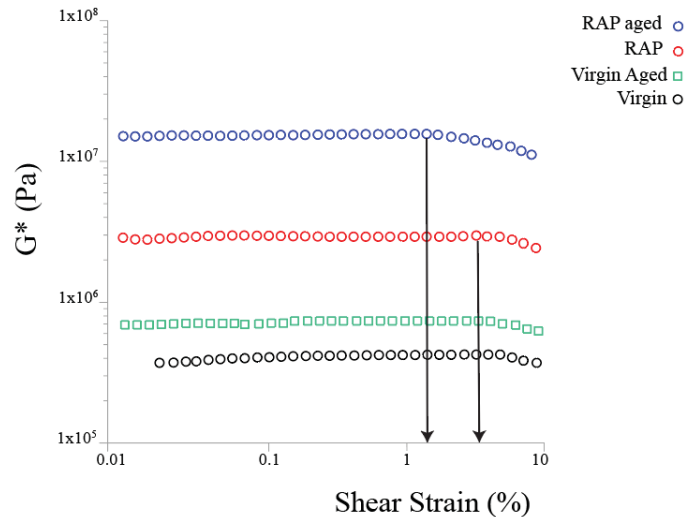


Figure 53 Complex modulus variation at different shear strains at 40° C.

#### 4.6.2 Example of data-set obtained from the rheological measurement.

As explained in Chapter 2, the amount of shifting at each temperature required to form the mastercurve, describes the temperature dependency of the material. Master curves are mathematically modelled by a sigmoidal function as can be seen in the following Figure 54.

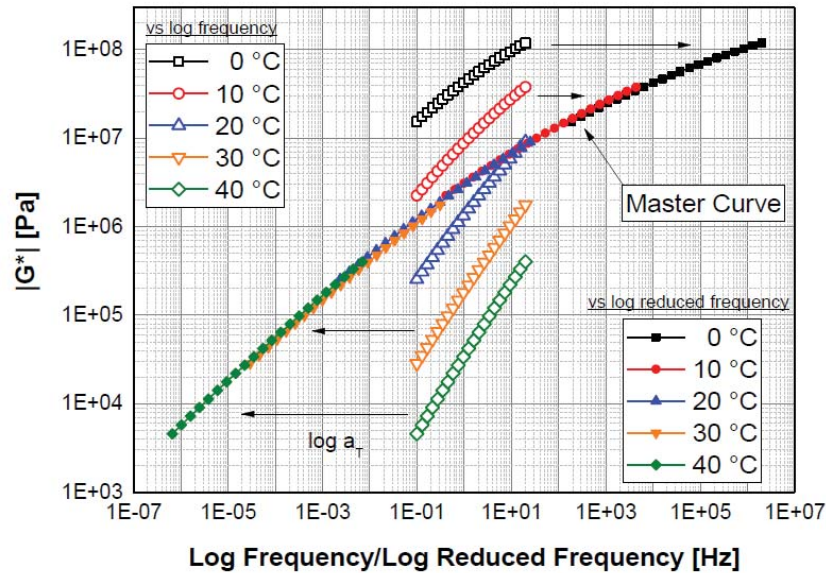


Figure 54 Data shifting to obtain a mastercurve according to the sigmoidal model with the WLF shift factor.

In the table below, parameters are presented per each binder. The considered reference temperature was 20° C.

Table 1 Parameters obtained after application of the sigmoidal model to all binders.

	$\zeta$ (log)	$\alpha$ (log)	$\beta$	$\gamma$	$C_1$	$C_2$
50/70	2.32	11.14	-1.26	0.35	13.37	107.47
RAP	13.41	12.98	-1.68	0.28	17.68	137.36
RAP + 5% A	5.25	14.11	-1.51	0.27	16.74	144.17
RAP + 5% B	3.80	11.95	-1.32	0.31	14.57	131.68
RAP + 5% C	4.55	19.68	-1.55	0.23	13.47	152.10
50/70 aged	8.99	18.06	-2.08	0.22	20.97	162.17
RAP aged	11.03	13.49	-1.75	0.28	18.02	136.36
RAP + 5% A aged	5.64	14.61	-1.70	0.23	21.55	174.80
RAP + 5% B aged	9.40	18.12	-2.27	0.23	18.76	135.90
RAP + 5% C aged	4.08	22.53	-2.06	0.20	29.09	182.66

Before obtaining the mastercurves, for each dataset, measurements were repeated four times. The standard deviation per point composing each mastercurve is presented in the below figure.

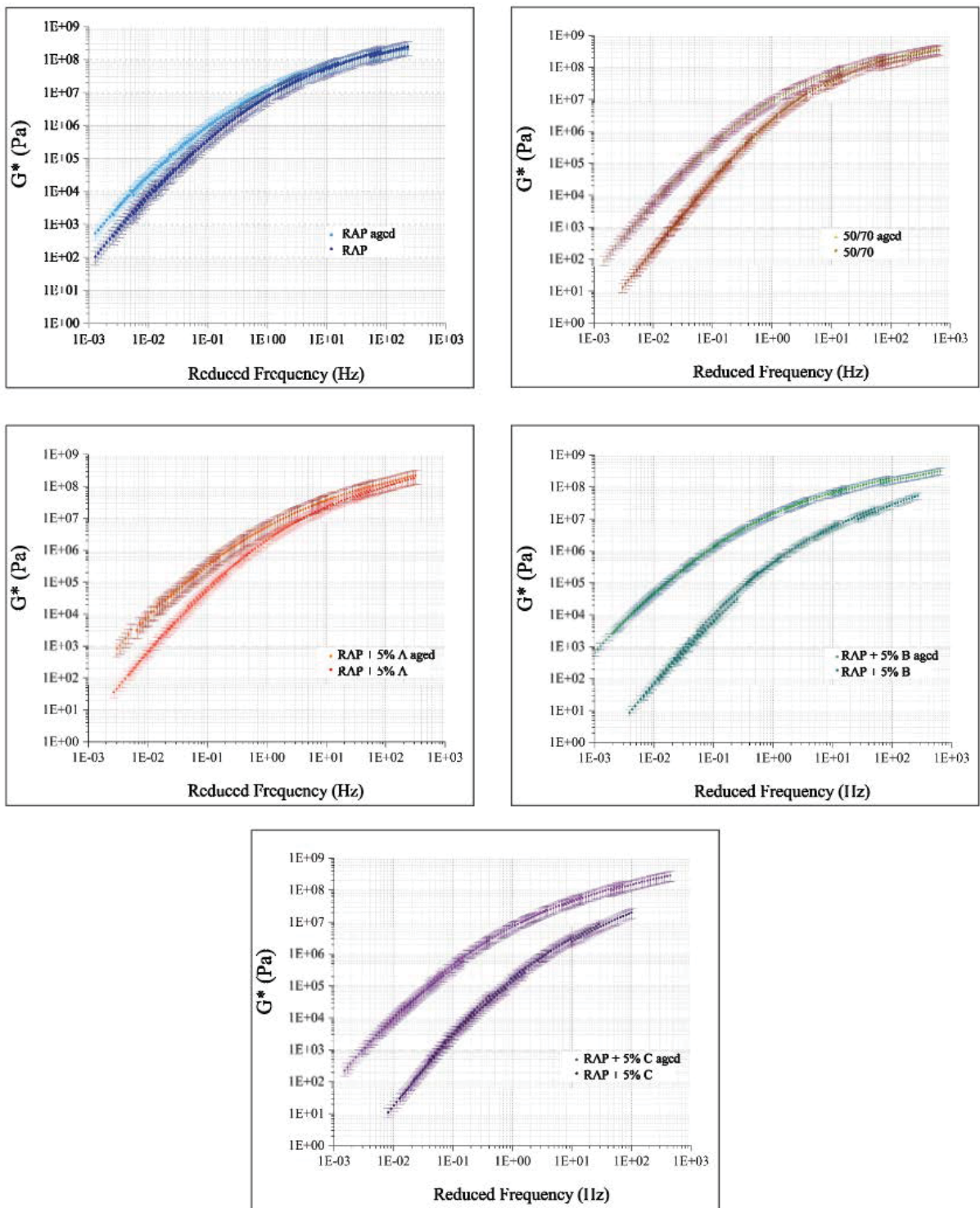


Figure 55 Mastercurves with indication of the standard deviation as average for four measurements.

#### 4.6.3 Output data for the carbonyl and sulfoxide indexes

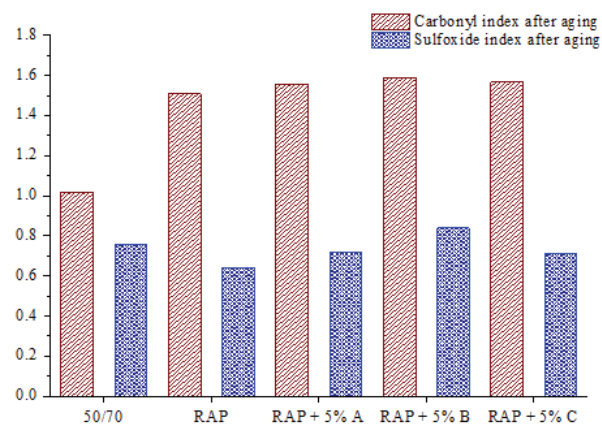
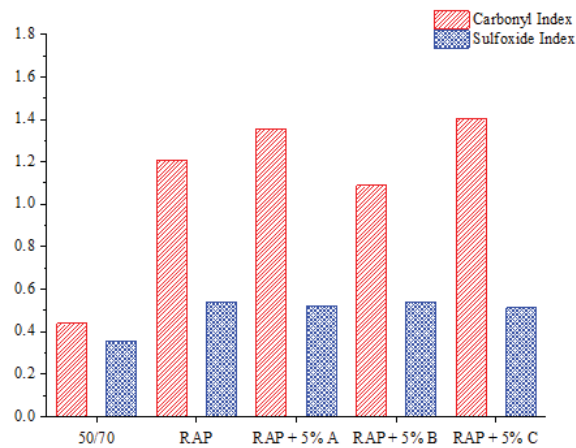


Figure 56 Comparison between the carbonyl and sulfoxide index of the virgin binder, RAP binder and RAP binder plus 5% by mass of rejuvenators before aging (top part) and after aging with RTFOT and PAV (bottom part).

## **5. Low temperature cracking behaviour of reclaimed binder with rejuvenators**

This chapter contains sections which are largely based on the content of the following paper:

Cavalli M. C., Zaumanis M., Mazza E., Partl M. N., Poulidakos L. D. (2018). Ageing effect on rheology and cracking behaviour of RAP binder with bio-based rejuvenators. *Journal of Cleaner Production*, 189, 88-97.

These sections are indicated with an asterisk (\*).

## 5.1 Summary

RAP is perceived to have lower cracking resistance than virgin asphalt concrete. Specifically, its cracking resistance at low temperature is dramatically affected by its oxidation level. Within the framework of this work, by adding bio-based rejuvenators, RAP binder mechanical performances at low temperature have been seen to be improving: fracture toughness temperature of RAP decreased after the addition of rejuvenators to a level similar of the virgin binder. However, aging has been seen as having a prominent effect for all binders at low temperature. Results were compared with additional rheological measurements and important and innovative insights on low temperature cracking behaviour of bio-based RAP have been analysed. It has been demonstrated how the addition of rejuvenator could improve the cracking performances of RAP and how aging is fundamental to investigate the rejuvenators performances.

## 5.2 Introduction

In cold climate regions, thermal cracking is one of the primary distresses in asphalt pavements, thus, preventing such kind of cracking is of great importance to ensure a long pavement lifetime. Low temperature cracking is caused by thermally induced stresses when these exceed the tensile strength of the asphalt material (Lu, Uhlback, and Soenen 2017). When the pavement is affected by thermal stresses, the bituminous binder slowly transforms from a viscoelastic material into a more elastic material. At warm temperatures, the binder is soft enough for bearing stresses, however at colder temperature, cracks generally start to propagate.

In the framework of this Ph.D. thesis, a fracture toughness test (FTT) is used as a possible alternative to traditional test method such as for example the bending beam rheometer test, for determining low temperature properties and crack susceptibility of modified RAP binders with rejuvenators. As described in Chapter 2, the so-called fracture toughness temperature ( $T_{FT}$ ), which is an indication of a material's resistance to fracture, is analysed. In this way, insight on low temperature cracking behaviour of modified RAP binder and virgin binder is given. By combining rheological measurements and FTT analysis it is shown how multiscale characterization allows identifying the effectiveness of rejuvenators in softening the RAP binder and how aging influences low temperature cracking behaviour of RAP binders modified with rejuvenators.



## 5.3 Materials and methods

Materials were selected and prepared according to what followed in Chapter 3 of this thesis.

### 5.3.1 Fracture toughness test (\*)

The fracture toughness test (FTT) is based on a European standard (European Committee for Standardization CEN TS15963, 2010). Samples were prepared by heating all binders at 110° C for 20 minutes to ensure the required viscosity for pouring the material in metal moulds without significant aging. For each binder type, pre-notched samples were created. As shown in Figure 57, the pre-notch of 5 mm depth was introduced by inserting a 0.15 mm double film polyvinyl chloride paper in the middle of the specimen. As depicted in Figure 57, in order to avoid sticking between samples, the binder's moulds were separated by a transparent film (0.125 mm) smeared with a small amount of synthetic grease.

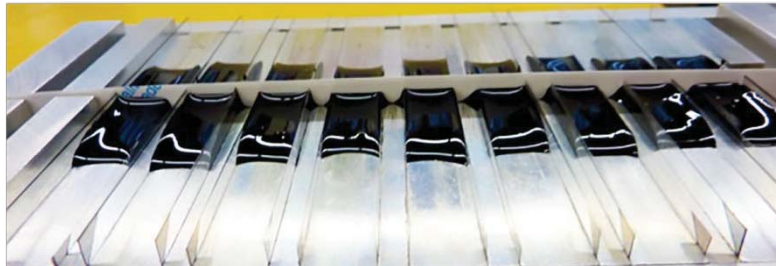


Figure 57 FTT moulds with paper to impose a pre-notch.

The specimens were then left in the ethanol (99.5 % solution) cooling bath for one hour prior to testing. Subsequently, a vertical load was applied with a constant displacement rate of 0.01 mm/s until failure of the specimen.

### 5.3.2 Dynamic shear rheometer

In the framework of this chapter, samples preparation followed the procedure outlined in Chapter 4, section 4.3.1. The chosen frequencies were expected to simulate traffic vehicles passing during service life (Gordon D. Airey, Rahimzadeh, and Collop 2004).

## 5.4 Results and Discussion

### 5.4.1 Fracture toughness at a fixed temperature

Force-displacement curves at  $-10^{\circ}\text{C}$  are shown in Figure 58 where relative standard deviation of four repetitions can be seen. In general, as expected lower force compared to other samples was needed to cause cracking in the RAP binder. Virgin binder 50/70 showed a cracking force equal to 8 N before cracking. By adding rejuvenators in the RAP binder, a higher force was necessary to start cracking compared to the RAP binder. Both RAP + 5% B and RAP + 5% C showed a force close to 9 N while RAP + 5% A needed a force of 11 N before crack initiation. Thus, after adding the rejuvenator, the maximum cracking force increased between 30% and 50% compared to the RAP binder, depending on the rejuvenator. As expected, after aging, the value of the maximum cracking force decreased (Figure 58 right). This indicates that the material becomes weaker thus, being more susceptible to low temperature cracking.

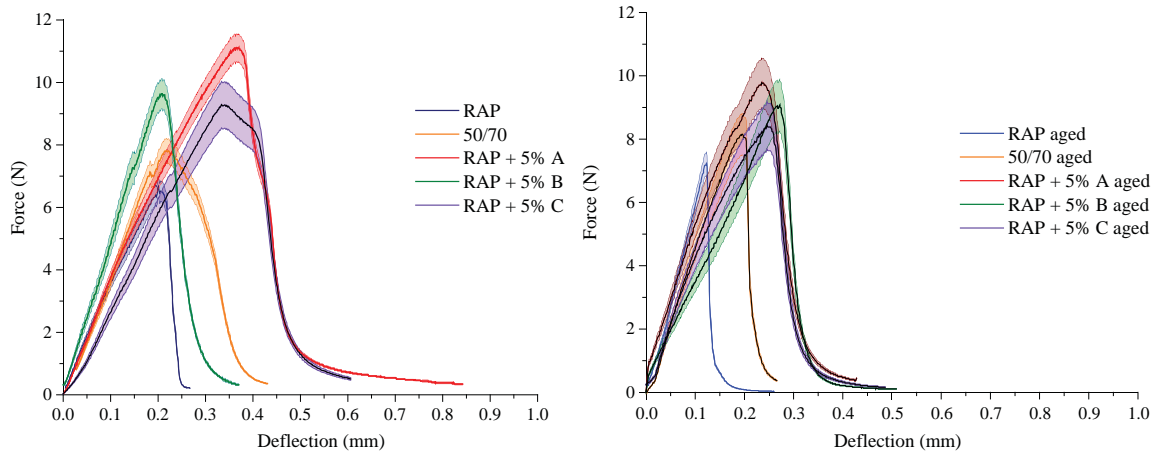


Figure 58 Example of force vs. deflection curves for all the unaged (left) and aged (right) binders at  $-10^{\circ}\text{C}$ . The curves presented are averaged of four measurements and standard deviation is presented for each point.

In order to assess low temperature behaviour resistant of the binder, a performance index is introduced. The work to fracture, as depicted in Figure 22 from Chapter 2, can be calculated from the force-displacement curve that provides a measure of cracking resistance of the binders.

As can be seen in Figure 59, after aging all the binders tested decreased their work to fracture, thus becoming more susceptible to low temperature cracking in comparison to the unaged state. These results demonstrate how aging has a significant effect on low temperature cracking behaviour. In addition, RAP binder performance at low temperature at both aged and unaged state show significant improvement after adding the rejuvenators. In particular, at unaged state, RAP + 5% A and

RAP + 5% C could increase the RAP binders work to fracture up to 50% and RAP + 5% B up to about 40%. Furthermore, at low temperature (-10° C), RAP binder appeared more sensitive to aging than the virgin binder, halving its work up to fracture. Although still higher than virgin and RAP binder, the work to fracture decreased for all modified binders. The results confirm that, despite the aging procedure, rejuvenator could improve the crack resistance of RAP binder at -10° C. In addition, the type of rejuvenator had a significant effect on fracture behaviour of the rejuvenated binders after aging and even better than virgin binder as discussed above and shown in Figure 50. Work to fracture of RAP + 5 % A was the most affected by aging. But the final result was comparable to the other rejuvenators.

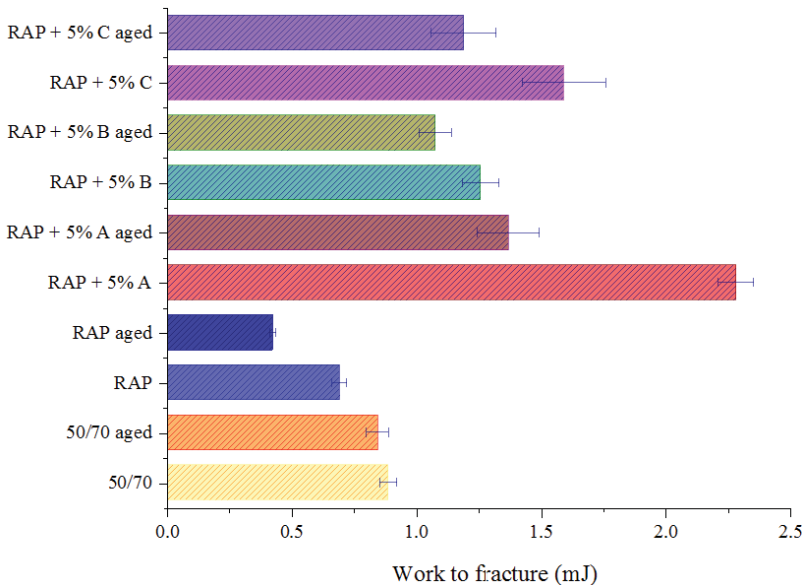


Figure 59 Work to fracture at crack initiation at -10° C before and after aging.

5.4.2 Fracture toughness temperature

To obtain a comprehensive characterization of each binder’s behaviour at low temperature, three measurements were repeated at different temperatures to determine the fracture toughness temperature (T<sub>FT</sub>). As depicted in Figure 60, increasing the temperature tends to increase the deflection, as the material gets tougher. RAP binder showed crack propagation around 0° C. Different temperatures were tested, from -15° C to 0° C and the corresponding T<sub>FT</sub> was calculated.

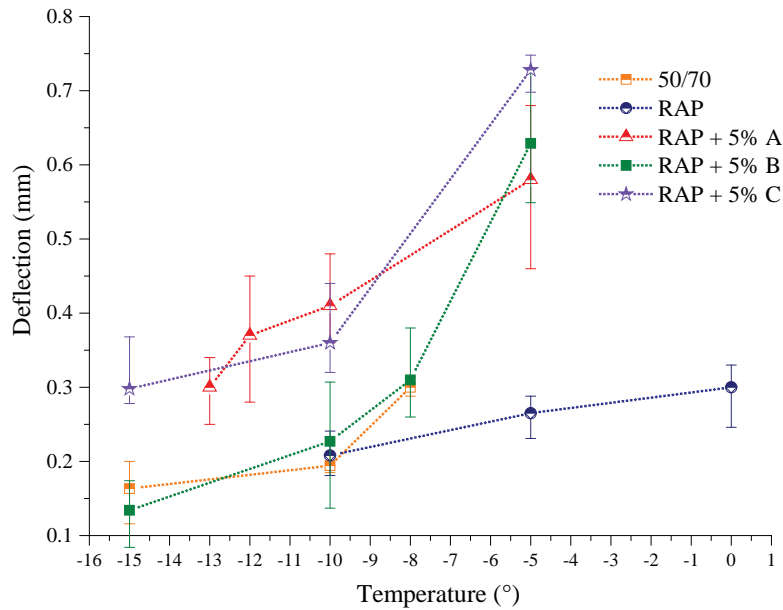


Figure 60 Deflection variation with temperature for all the binders tested at unaged state. Average and standard deviation were calculated for four measurements per sample.

As shown in Figure 61, RAP binder starts cracking around  $+0.5^{\circ}\text{C}$ . By adding rejuvenators,  $T_{FT}$  of RAP binder decreases. RAP + 5% A presented a  $T_{FT}$  equal to  $-13^{\circ}\text{C}$  ( $13.5^{\circ}\text{C}$  lower than RAP binder) while RAP + 5% B showed a  $T_{FT}$  of  $-10^{\circ}\text{C}$  and RAP + 5% C reached the prescribed displacement at  $-15^{\circ}\text{C}$ . For all rejuvenated binders it was possible to observe that cracks appear at a lower temperature (i.e. improved performance) compared to the RAP binder.

By investigation of the materials at aged state (by analysing data as for example in Figure 60), a general tendency can be seen: aging causes an increase of  $T_{FT}$  for all the binders.

In particular, RAP + 5% A and RAP + 5% C increased their  $T_{FT}$  with respect to their unaged state, by about  $4^{\circ}\text{C}$  and  $5^{\circ}\text{C}$  respectively while RAP + 5% B showed an increase of  $2^{\circ}\text{C}$ . Contrary to the unaged state discussed earlier, in aged state RAP + 5% C showed the most affected by aging in terms of FTT, however the final FTT was comparable to the other two rejuvenators.

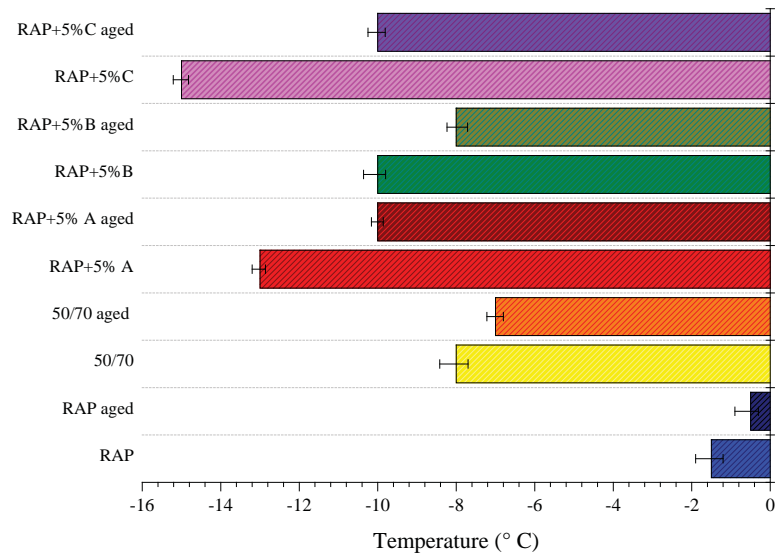


Figure 61 Fracture toughness temperature for the different materials at unaged/aged state. Average and Standard deviation was calculated for four measurements.

#### 5.4.3 Rheological measurements (\*)

Although the results from FTIR and SARA shown in Chapter 4, indicated that aging was not reversible, it is particularly important to evaluate how the addition of rejuvenators influences the rheological properties of RAP binder. In order to investigate the material's response to temperature changes, a study of the rheological properties of asphalt binders was conducted with emphasis on the phase angle variations as well as the crossover frequency. As can be seen in Figure 62, RAP binder has lower phase angle and higher complex moduli at unaged state than the other binders. The phase angle increased, especially at low temperature; e.g. for RAP+5% B at  $-10^{\circ}\text{C}$  it showed an increase of  $20^{\circ}$  with respect to the RAP binder (phase angle close to  $15^{\circ}$ ). These results show that the relationship between  $G'$  and  $G''$  can be controlled by the rejuvenators used in this study. Moreover, at  $-10^{\circ}\text{C}$ , rejuvenators contributed to increase of the phase angle. This corresponds to an increase of  $G''$ , which is desirable. At aged state, the curves of the all materials master curves tend to merge at all frequency ranges.

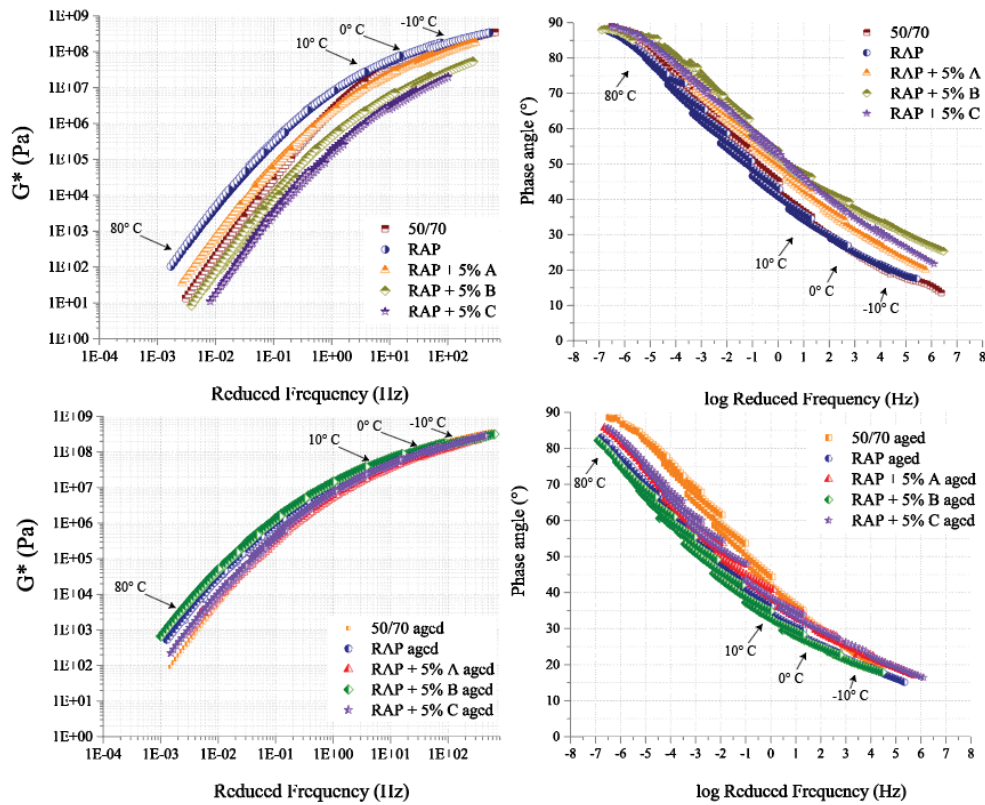


Figure 62 Modulus and phase angle master curves for all the unaged binders (on top) and the aged ones (on the bottom). Values presented are averages of four measurements.

At low temperatures bituminous binders are known to be more elastic ( $G' > G''$ ) whereas at high temperatures the opposite is true. As shown in the example in Figure 63, the interplay between the elastic and viscous component of the complex modulus undergoes a change at a precise frequency. In Chapter 3, crossover temperature was discussed in terms of the exact temperature at which the transition between elastic and viscous components occurs. Nevertheless, it is also important to analyse the so called “crossover frequency”. In other words, at a specific crossover frequency, the storage and loss moduli are equal. As a general trend, the higher the crossover frequency, the more viscous response the material will show. It can be expected that high crossover frequency at low temperature indicates a better cracking resistance.

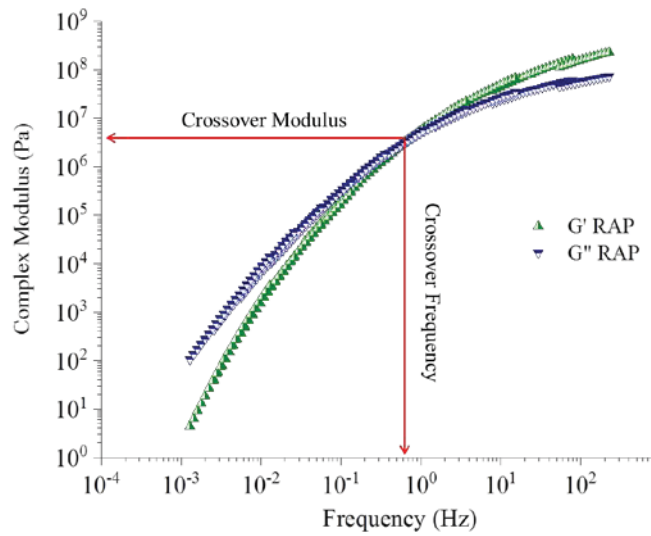


Figure 63 Example of elastic and viscous components of the complex modulus ( $G'$ ,  $G''$ ) together with the crossover frequency. The data plotted are average of four measurements.

Results in Figure 64 (in log-log scale) indicate that the rejuvenators of this study could restore the crossover frequency of RAP binder. The addition of rejuvenators into RAP binders increases the viscous components of the RAP binder, and consequently the crossover frequency shows a shift towards higher values. Nevertheless, aging had a significant effect in lowering the crossover frequency. For RAP binder, RAP + 5% A and RAP + 5% B, the transition between elastic and viscous portion appears at lower crossover frequency compared to virgin 50/70 and RAP + 5% C. Generally, it can be seen how for the modified RAP binders, aging was associated to a frequency shift rather than a change in terms of crossover moduli.

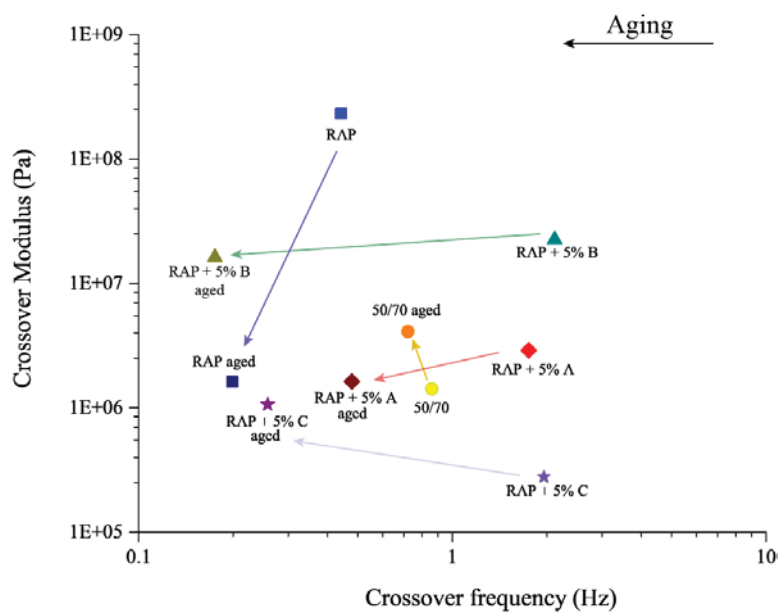


Figure 64 Crossover modulus and crossover frequency (log-log scale) for all materials tested before and after aging.

## 5.5 Conclusions and Perspectives

Low temperature is one of the most influential climatic factors for pavements with RAP and it plays a key role in crack initiation. Since RAP binder is already harder than virgin binder, rejuvenators are primarily used to restore its rheological properties. Cracking behaviour at low temperature together with rheological measurements were studied and the effect of aging on the effectiveness of three different bio-based rejuvenators was evaluated. Main findings from the fracture toughness tests have been:

- i. Rejuvenators had a positive effect on the unaged RAP binder: fracture toughness temperature ( $T_{FT}$ ) decreased after the addition of 5% rejuvenator and this decrease was rejuvenator dependent.
- ii.  $T_{FT}$  of RAP + 5% A and RAP + 5% C were more affected by aging than aged RAP + 5% B. However, after aging, RAP + 5% B showed higher  $T_{FT}$  compared to the other modified RAP binders.
- iii. Work of fracture at  $-10^{\circ}$  C showed an improvement in the behaviour of RAP binder with respect to resistance to low temperature cracking after the addition of rejuvenators, both before and after aging.

Main findings from the phase angle and crossover frequency measurements from the rheological studies in addition to those listed in Chapter 4 are:

- i. An increase in the phase angle and a shift of crossover frequency were found after addition of rejuvenators. RAP + 5% B was more influenced by aging than the other rejuvenated binders and had a lower crossover frequency than the RAP binder itself this corroborates the result enlighten in Chapter 4.

It has been observed that both rheological and fracture toughness measurements in the aged and unaged state are needed for characterizing the effect of rejuvenators on the mechanical properties. Combining different techniques delivers complementary information in restoring the mechanical properties of RAP binder with rejuvenators.



## 5.6 Appendix

### 5.6.1 Fracture toughness output data

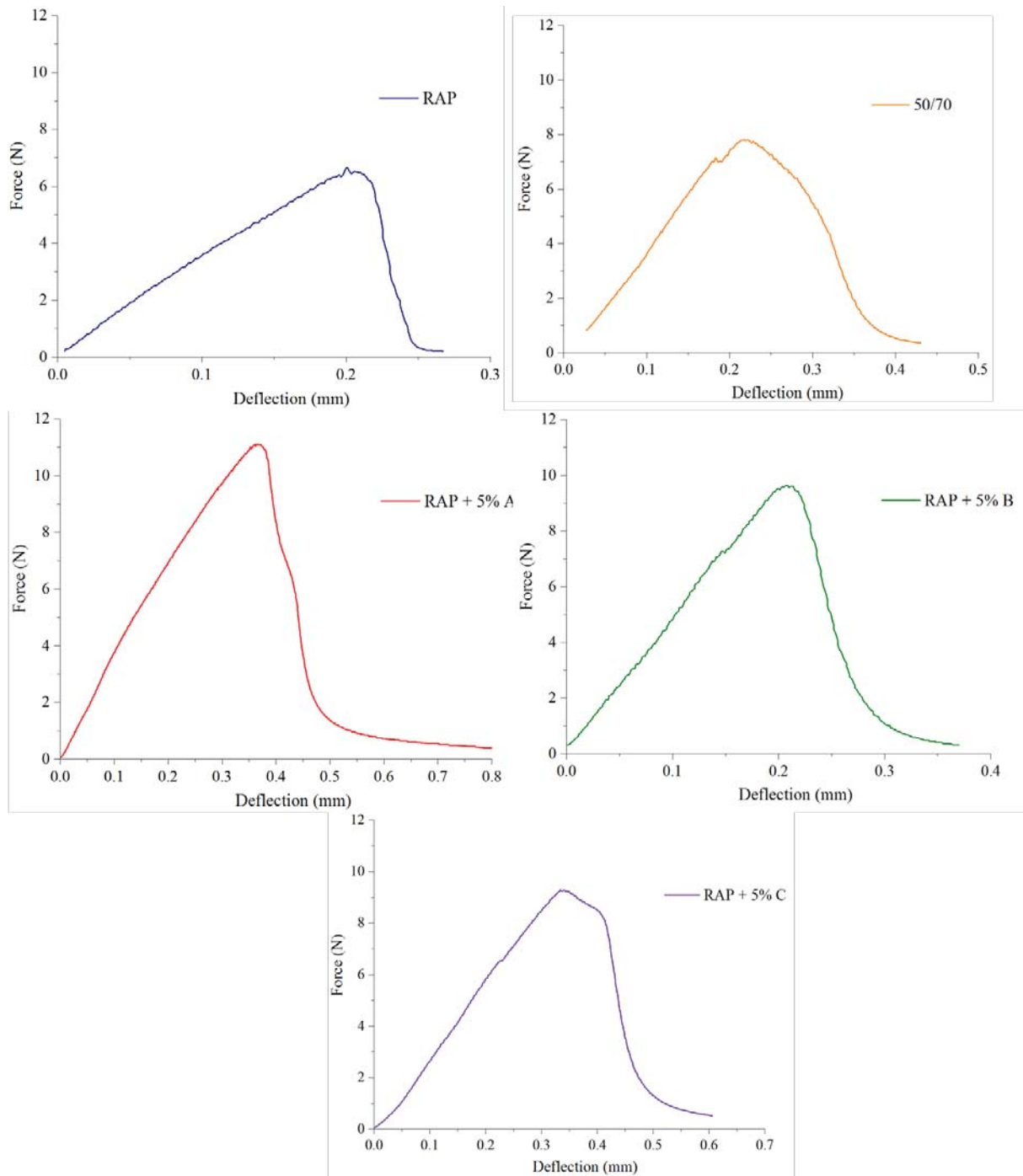


Figure 65 Example of output data for unaged binders at  $-10^{\circ}$  C.

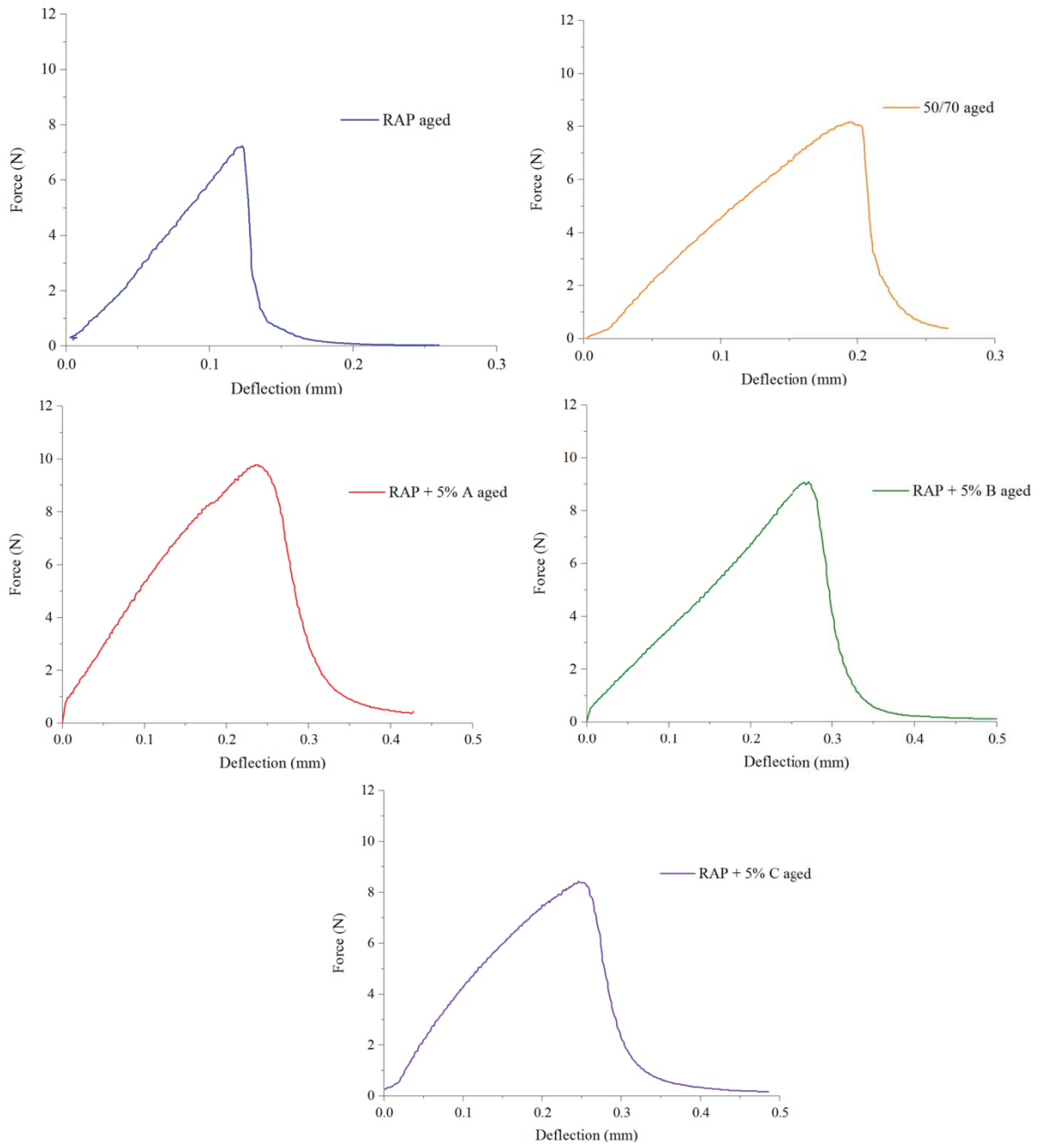


Figure 66 Example for output data for aged binders at -10° C.

## **6. Surface nano-mechanical properties of bio-modified reclaimed asphalt binder.**

This chapter contains sections which are largely based on the content of the following paper:  
Cavalli M. C., Mazza E., Zaumanis M, Partl M. N., Poulidakos L. D. Surface nano-mechanical properties of bio-modified reclaimed asphalt binder. *In preparation*.

These sections are indicated with an asterisk (\*).

## 6.1 Summary

In this work, the bio-modification of RAP binder was characterized microstructurally using atomic force microscopy (AFM). AFM was used before and after aging. Quantitative nano-mechanical mapping (QNM) showed how the addition of rejuvenators had an effect on RAP's elastic moduli. New insights on the changes of the microstructure in modified RAP binders as a function of laboratory aging have been gained. Comparison between the “bees” elastic moduli and the bulk elastic moduli for a virgin bitumen has been proposed. The results presented in this section contributed to an improved understanding of the morphological changes occurring in bio-based binders.

## 6.2 Introduction

As it was outlined in Chapter 2, AFM is a known tool capable of giving both topography and mechanical information. Recently, it was revealed that binders constituents such as asphaltenes have a consistent and measurable effect on the asphalt micro-structure that can be observed with AFM (Allen et al. 2014). A further AFM study has shown that bitumen has the tendency to show phase separation and it is highly dependent on the temperature exposure (Das et al. 2013). Moreover, the observed micro-structures under AFM have earlier been shown to be a unique and reproducible property of any specific asphalt binder (Das et al. 2016b).

Although many researches have been investigating the morphology of bitumen, the link between chemical composition and its morphology is still under debate as well as the nano-mechanical mapping which is still not univocally accepted. Aim of this study is to show different features in the RAP binder before and after the addition of the bio-based rejuvenators. Qualitative comparison between the rheological measurements and the phase contrast image has been performed as well. Afterwards, imaging of the elastic moduli at the surface has been proposed. In the last part of this chapter, an analysis of the measured elastic moduli for the “bees” has been performed and the link to the bulk properties.

## 6.3 Materials and Methods

### 6.3.1 Rejuvenation Procedure (\*)

Materials were selected and prepared as described in Chapter 3 of this thesis.

### 6.3.2 Topography imaging (\*)

As described in Chapter 2, authors followed the heat casting method procedure. Specifically, a previous protocol for AFM measurements (Soenen et al. 2014), approximately 10 mg of bitumen was spread by buttering action over a ca. 0.8x0.8 cm<sup>2</sup> area on a 1x1cm<sup>2</sup> glass slide. The glass slide was placed covered to prevent dust accumulation in a ventilated oven at 110° C for 20 minutes. The sample was left to cool for 24 hours prior to testing. Subsequently, AFM measurements were performed at room temperature. Asphalt binders' surface was analysed using an Icon3 AFM from Bruker. The data were collected using Nanoscope 8.15. The conical tip, Bruker silicon probe with Al-coating on the detector side, was type RTESPA-150A with a resonant frequency of 150 kHz and spring constant of 6 N/m, a cantilever length equal to 125 µm and width of 35 µm and a tip radius equal to 8 nm. The cantilever type was recommended by the manufacturer as the one most suitable for bitumen imaging.

The scan size was equal to 10.0 µm x 10 µm while each AFM image was built up by 512x512 pixels with a scan rate of 0.5 Hz.

### 6.3.3 Phase imaging

The samples preparation and the data collection correspond to the procedure outlined in the previous paragraph.

As described in Chapter 2, although phase images do not show the same phase scale, phase images are not related to the sample's topography rather to the samples properties. Two different domains can be distinguished in the AFM phase images (Figure 66). In order to understand how the ratio of the two domains changes, a grey scale conversion was done. This conversion was done as phase lag scale is related to changes in phase oscillation with respect to the cantilever resonant frequency which is given by the particular morphology of the sample. The aim of the conversion process was to gain qualitative information on the colour distribution. Each image, as for example Figure 67, was 10x10 µm, and corresponded to 512x512 pixels.

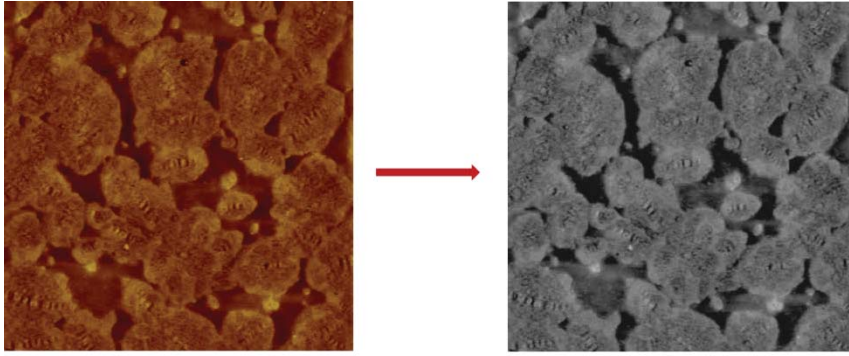


Figure 67 Corresponding grey scale image (right) of the phase image from the virgin binder 50/70 (left). Size was 10x10  $\mu\text{m}$  each image corresponding to 512x512 pixels.

Grey scale images are composed exclusively of shades of grey, varying from black at the weakest intensity to white at the strongest between 0 RGB (black) and 255 RGB (white). With the grey values ranging from 0 to 255 RGB scale, it is possible to create a histogram assigning each pixel its corresponding value. As can be seen in

Figure 68, the histogram is composed of a total of 262144 values shown as colour intensity corresponding to the total number of pixels per image. The shape of the curve obtained from the histogram has been observed as similar for all the images studied (two Gaussian curves with two peaks and two minima and). The Gaussian curves were considered for the characterization of each 8-bit image so that the algorithm was not influenced by the quantitative numerical values of the phase slag. The algorithm applied for the conversion was the same for each image with each RGB image converted in greyscale by linearly scaling (Schindelin et al. 2012).

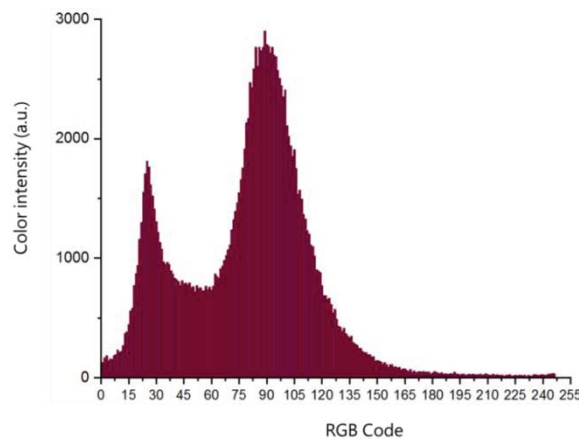


Figure 68 Histogram showing each pixel its corresponding grey scale value. On the y axis the colour intensity is reported.

Subsequently, a grey-scale threshold value for binarization is applied to create a black and white image. The threshold is applied directly at the histogram values to distinguish pixels in the image using two peaks, as can be seen in the following Figure 69.

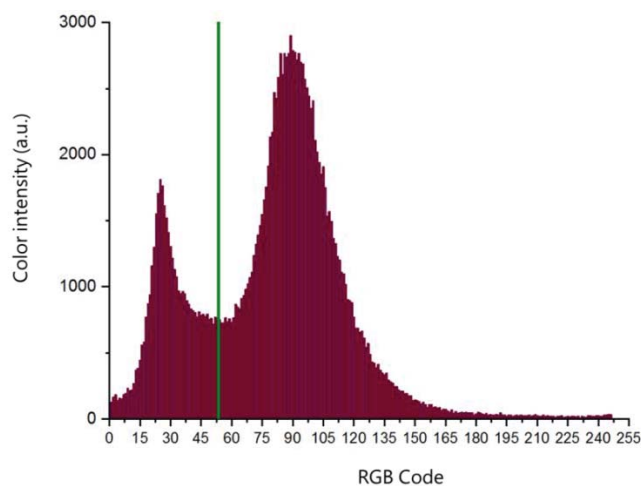


Figure 69 Histogram with the threshold to obtain a black and white image.

In the end, a black and white colour image or phase segmentation is obtained as can be seen in Figure 70. The black and white image is afterwards used to calculate the area corresponding to the white area and the area belonging to the black zones as will be described in Chapter 6. No further data processing such as noise smoothing was performed.

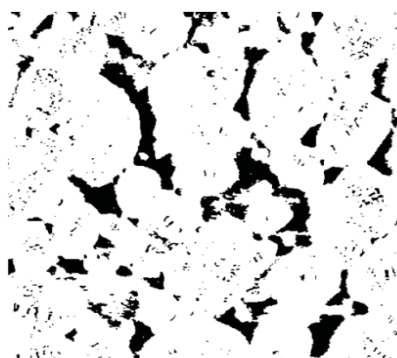


Figure 70 Black and white image of the virgin binder 50/70 after the application of the threshold.

#### 6.3.4 Force mapping (\*)

The AFM force mapping was performed on a Bruker Icon3 AFM in PeakForce quantitative nano-mechanical property mapping (QNM) mode with a Nanoscope V controller and software Nanoscope 8.15. The resulting force curves were evaluated using Nanoscope Analysis. AFM QNM scans were performed on bitumen binders at room temperature and humidity-controlled condition (RH = 40% and T = 23° C). The sample's preparation followed was described in Chapter 3. The cantilever used was the same as the one utilized for topography imaging. However, specific cantilever parameters require a calibration before performing QNM as outlined in (Yu, Burnham, and Tao 2015).

To make quantitative measurements, it is necessary to perform a cantilever calibration in order to measure the precise probe geometry and the cantilever spring constant.

The spring constant was determined by the thermal tune method (Hutter and Bechhoefer 1993). The tip radius was calibrated by using Bruker PDMS-12 sample with nominal elastic modulus of 3.5 MPa. PDMS-12 sample was recommended by the manufacturer for calibrating the RTESPA 150 A cantilever type.

QNM uses tapping mode to acquire information on nano-mechanical properties such as elastic modulus at sample's surface while simultaneously imaging sample topography at atomic scale resolution.

QNM mode measurements were performed as follows: the probe was oscillated in the vertical z-direction while at the same time the sample was scanned line by line at a rate of 1 Hz. Every image resulting from the interaction of the probe and sample, was built up of 512 per 512 pixels each. As described in Chapter 2, from the force curve, information on the elastic modulus is calculated by using the DMT modulus fitting.

## 6.4 Results and Discussion

### 6.4.1 AFM topography and phase imaging

An example of the microstructures of the virgin bitumen can be seen in Figure 71. While the topography shows the surface height morphology, the phase images provide qualitative indication of different mechanical properties among diverse domains as a result of forces resulting from the interaction between the bitumen's surface and the AFM probe. Those interactions cause a change in the cantilever's resonant frequency resulting in a phase lag which is indicated by the phase angle variations reported in the corresponding images.

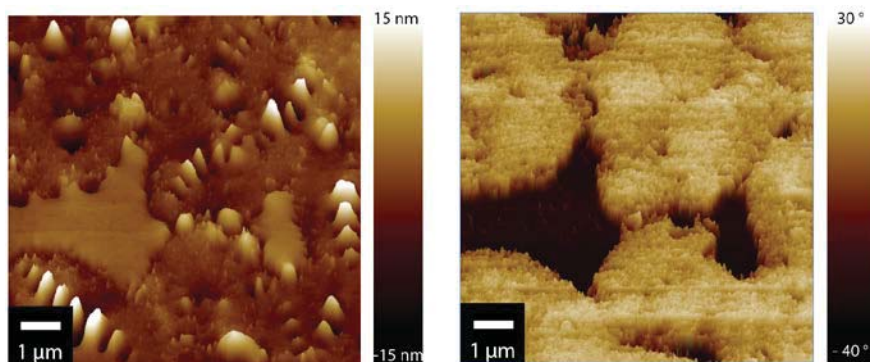


Figure 71 AFM height morphology image of the virgin binder 50/70 (left) and phase visualization (right) (image size 10 x 10 μm).



Figure 72 shows how virgin asphalt binder is not a homogenous material but contains four distinct domains topologically and two domains in the phase image indicating that two domains have similar mechanical properties. The four different zones depicted in Figure 72 are: catanaphase (“bee” shaped), periphase (around the catana shape), paraphase (matrix phase) and salphase which are phase spots and linked to the presence of non-dispersed compounds in the matrix. Wrinkling domains containing the “bee” structures (with major and minor axes of a few microns) are abundant on the surface of the virgin binder.

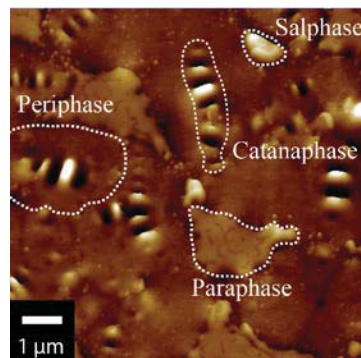


Figure 72 AFM height image showing present structures in the virgin binder 50/70. The scan size is 10 x 10 μm.

As it is possible to see the "bee" structures are absent in the RAP microstructure in Figure 73. Instead, three domains can be distinguished; two uniform matrices with few salphases appearing and in one of them as seen in the phase image. These results corroborate other investigations indicating that the "bee" structures commonly seen in the virgin binder and aged virgin binder are not present in the bitumen extracted from mixtures as the case with RAP binder (Santos, Poulikakos, and Partl 2016). As indicated in Chapter 4, the RAP used in this investigation, had an asphaltene content equal to 22%. This high content of asphaltene could be responsible for a rearrangement of the waxes, resulting in a new structure where the “bees” are absent. However it should be noted that the "bees" are generally present in aged virgin binders (Eberhardsteiner et al. 2015a). Hypothesis behind the formation of the “bees” will be reported in section 6.4.3 of this Chapter.

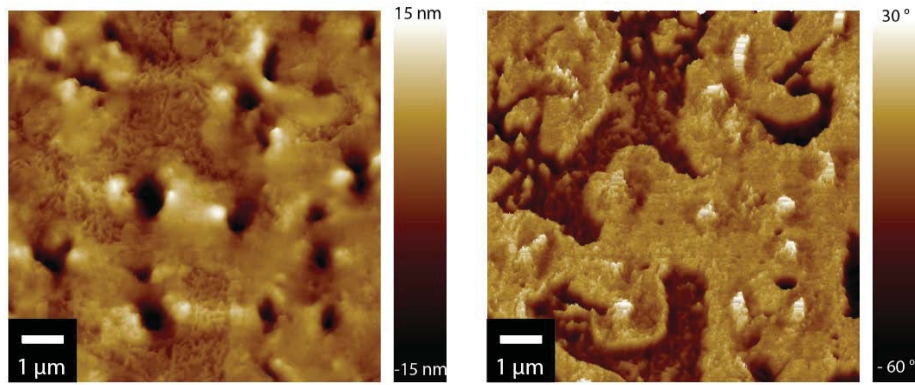


Figure 73 AFM height morphology image of the RAP binder with 22% asphaltenes (left) and its phase visualization (right) (10x10  $\mu\text{m}$ ).

As further step, rejuvenators were added to the RAP binder following the procedure described in Chapter 3 and imaged after the annealing step. As shown in Figure 74 and comparing to Figure 73, where no rejuvenator was present, the addition of rejuvenators affected the morphology of the RAP binder showing the formation of new structures which have different topography and phase images. In RAP + 5% A, the matrix phase was not homogenous presenting formation of branches which could be caused by the nucleation of waxes (Chen et al. 2007). On the contrary, RAP+ 5% B showed several salphases with hills and valleys. Spots with different mechanical properties appear in the corresponding phase image. Image of the RAP + 5% C showed evidences of several branches and ramifications similar to RAP+5%A. shows that the addition of rejuvenators do not restore the microstructure to the virgin state. This corroborates the findings in Chapter 4 as it was shown also that chemically the addition of rejuvenators do not reverse the chemical state.

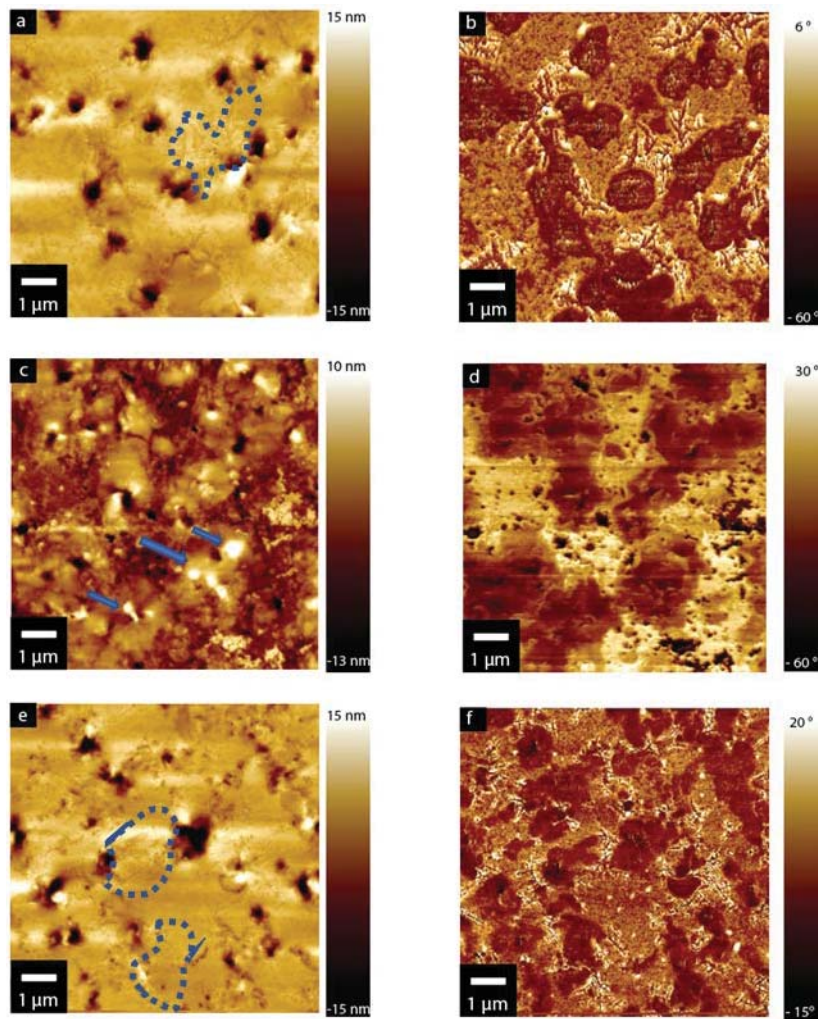


Figure 74 AFM height morphology image (10x10  $\mu\text{m}$ ) of the RAP plus 5% A (a) and corresponding phase image (b); RAP plus 5% B (c) and its phase image (d); and RAP plus 5% C (e) and its phase image (f). Branches are indicated with a dotted line while salphases are outlined with arrows.

As in Figure 75, by comparing the AFM images of the aged RAP binder and the aged virgin bitumen, it can be stated that aging can affect the morphology of both virgin binder and RAP binder. Aged virgin binder still displays “bee” structures with homogenous paraphases and less periphases, whereas the RAP binder and rejuvenated RAP binder do not. Aged RAP + 5% A and aged RAP + 5% C display similar morphologies. Assuming that the microstructure is a result of chemical interactions in the material, these results corroborate the FTIR results shown in Chapter 4 as rejuvenator A and C had similar chemical characteristics. By increasing the content of asphaltenes, as in the aged RAP binder, salphases (resulting in the phase image as white spots) are more visible than before aging (Figure 74). This could be an indication how aging the RAP binder could cause a phase separation between the fractions observed in the RAP binder morphology. As shown in Figure 75, the heterogeneity in the morphology increases. Formation of branches in aged RAP + 5%

A and aged RAP + 5% C can still be observed. Hills and valleys are visible in all the three modified RAP binder.

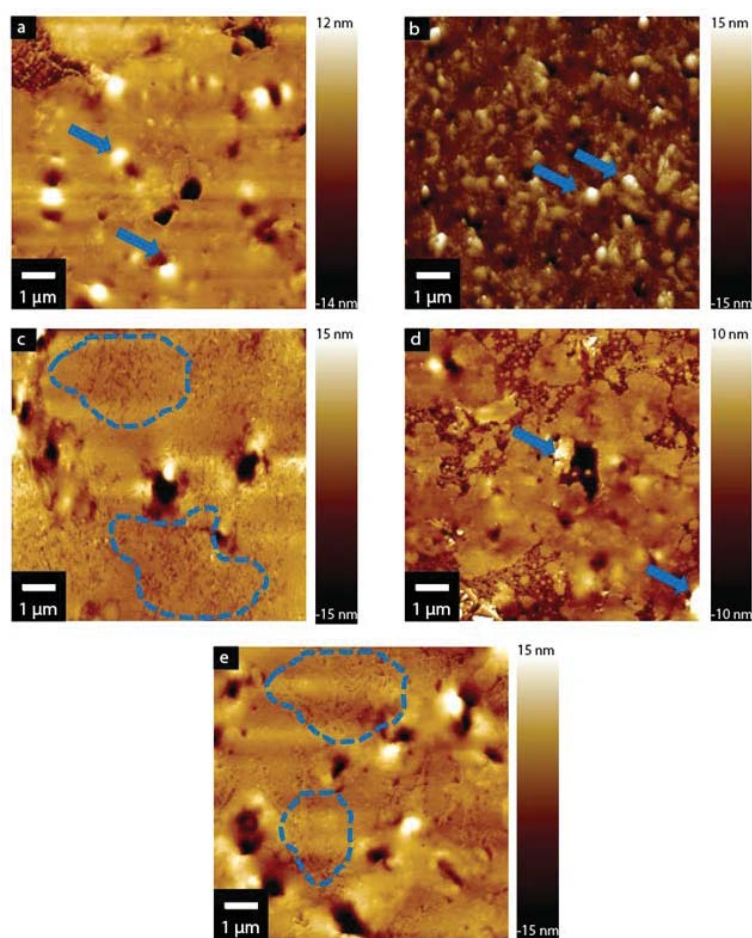


Figure 75 AFM morphology of the different rejuvenated RAP binder after aging (10 x 10 μm). From top left to bottom (clockwise): a) Aged virgin binder 50/70; b) Aged RAP binder; c) Aged RAP + 5% A; d) Aged RAP + 5% B and e) Aged RAP + 5% C. Branches are indicated with a dotted line while salphases are outlined with arrows.

As it was outlined in the “methods” section of this chapter, in order to gain qualitative information, phase images of each binder were converted in 8-bit grey scale threshold value for binarization allowing quantifying the two domains in the phase images. As can be seen in the results shown in Figure 76, RAP presented higher whiter zones compared to other binders. The general trend seen in all types of materials investigated is that aging caused an increase in the proportion of whiter/ darker i.e. harder areas.

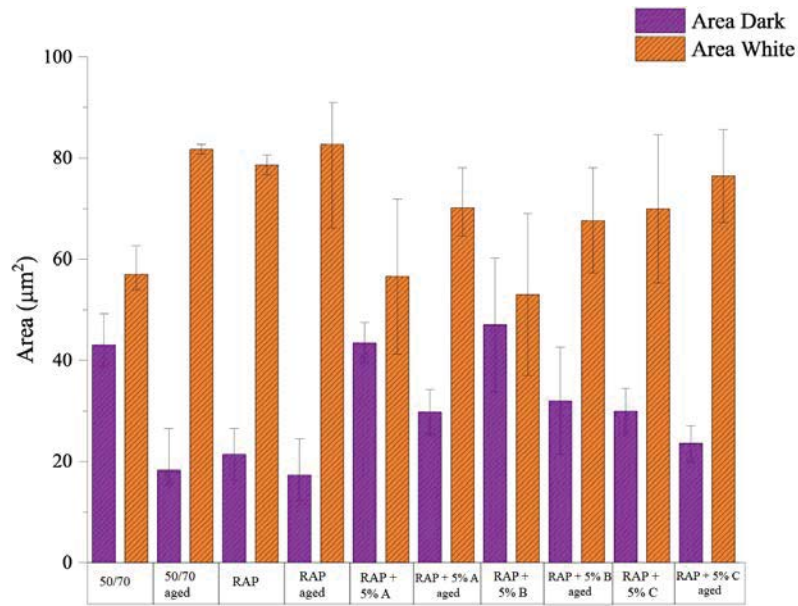


Figure 76 Area dark (relatively soft) and area white (relatively hard) for each binder and its relative standard deviation. The standard deviation was calculated over five areas in five different images.

In addition, the ratio between the dark and the white area for each binder was compared with the complex shear modulus  $G^*$  obtained by rheological measurement in own previous investigation (Cavalli et al. 2018) and reported in Chapter 4. The  $G^*$  used in Figure 77 was obtained at 20° C at a frequency equal to quasi-static condition (0.1 Hz) for the purpose of demonstration, however as discussed in Chapter 4 over the whole frequency range the trend is similar i.e. there is an increase in the value of complex modulus with aging. These values were chosen in order to have a qualitative comparison with the sample condition during AFM measurements (room temperature equal to 22° C and quasi-static conditions). In Figure 77, a general trend can be seen: aging causes a lower ratio of dark/white and an increase in complex moduli. The plot presented shows how there's a qualitative link between the images showing cantilever phase slag and the bulk properties in terms of complex moduli.

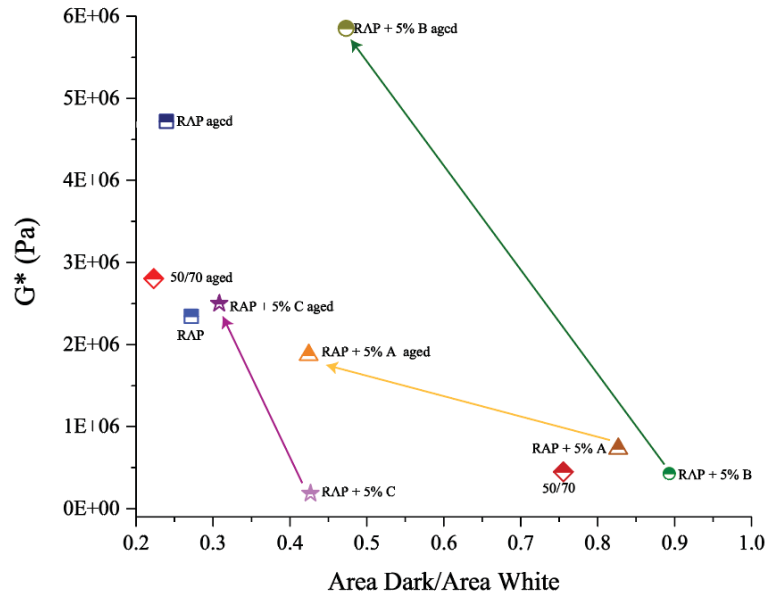


Figure 77  $G^*$  and ratio between the dark are and the white area for each binder.

#### 6.4.2 Quantitative nano-mechanical mapping

QNM imaging was done following the procedure described in detail Chapter 2. As can be seen a sample of the results shown in Figure 78, all four images show two distinct domains with different mechanical properties similar to the phase images shown in the previous section. The virgin binder images both unaged and aged, show a softer paraphase surrounding the “bee” structures. On the contrary, RAP binder images appear generally brighter with few softer spots. General observation can be made: on average RAP binder's Young's moduli at the surface are higher than the virgin binder both at unaged and aged state. As can be seen in Figure 78, after aging the Young's moduli for both RAP binder and virgin binder increase. In particular, in Figure 78 a) and c) it's possible to observe how after aging, “bees” appear smaller and with higher elastic moduli. In Figure 78 b) and c), it's shown how the morphology of RAP binder doesn't change significantly after aging however, in this specific case, its elastic modulus increases. As can be seen in Figure 80, the median elastic modulus passed from 128 MPa up to 190 MPa.

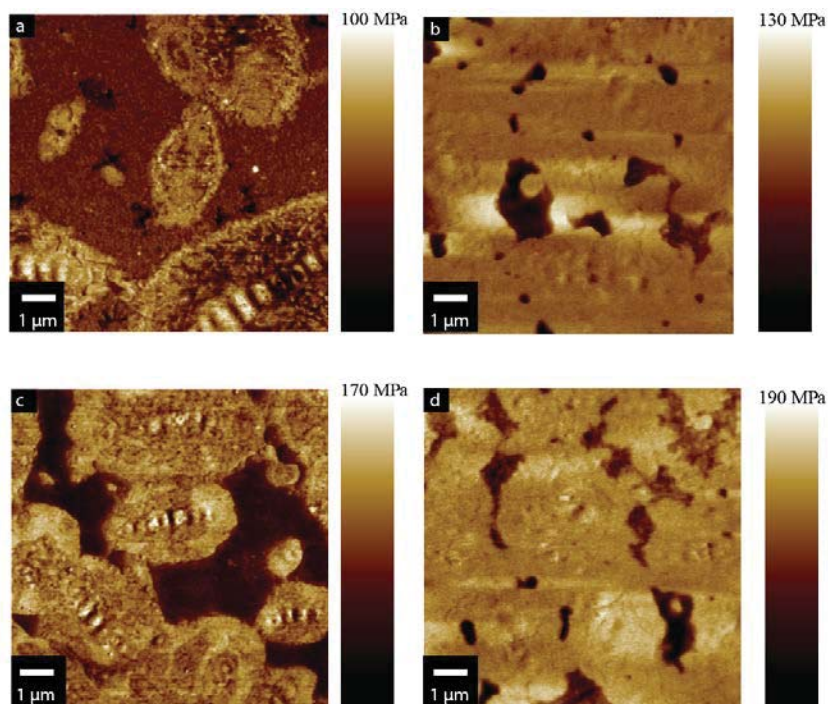


Figure 78 AFM QNM images (10 x 10  $\mu\text{m}$ ). a) Virgin binder 50/70 unaged; b) RAP binder unaged; c) Virgin binder 50/70 aged; d) RAP binder aged.

Figure 77 shows an example of the QNM images for rejuvenated RAP in unaged and aged states. As shown in this figure, Figure 79, RAP plus 5% A and RAP plus 5% C show the same branch formations discussed in the previous section by tapping mode. In addition, QNM mode demonstrates how branch formations are softer than the matrix in terms of elastic moduli. All the rejuvenated binders at unaged state, show lower elastic moduli than the RAP binder. This can be an indication of the softening potential of rejuvenators in reducing the surface's moduli of the RAP binder. As shown in Figure 79, RAP plus 5% B presents topography similar to the RAP binder with higher Young's moduli than the other two modified binders, indicating that rejuvenator B was less effective in reducing the modulus of the surface at micro scale as was demonstrated by rheological measurements in Chapter 4. As indicated in Figure 79 from d) to f), all binders increase their elastic moduli at the surface after laboratory aging. In particular, RAP plus 5% B was more affected by aging than the other two binders corroborating results in Chapter 4.

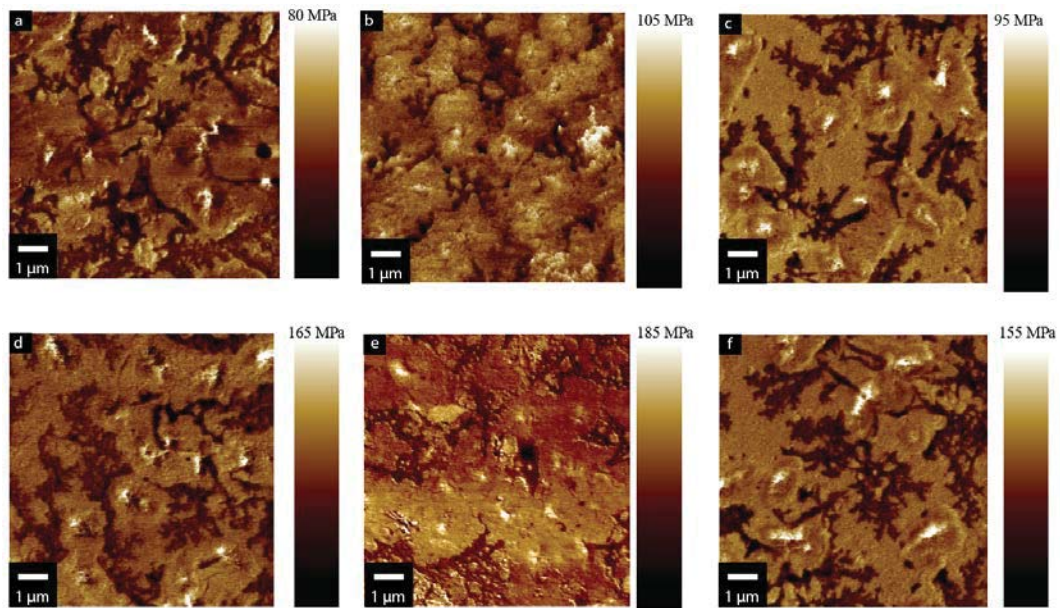


Figure 79 AFM QNM images (10 x 10  $\mu\text{m}$ ). From top left clockwise: a) RAP + 5% A b) RAP + 5% B c) RAP + 5% C d) RAP + 5% A aged e) RAP + 5% B aged f) RAP + 5% C aged.

The data obtained with QNM measurements, were used to create Gaussian functions describing the distribution of the elastic moduli as average of five different images. In addition, cumulative distribution functions for each binder were calculated. As can be observed in Figure 80, at unaged stage, the RAP binder presented a broader range of elastic moduli compared to the other binders. RAP binder modulus was overall higher while RAP plus 5% B and virgin binder 50/70 had similar trend. At unaged stage, RAP plus 5% B and RAP plus 5% C showed higher softening potential of the RAP binder moduli. After aging, there is a general shift of the entire Gaussian curves towards higher elastic moduli. Generally, despite aging, RAP plus 5% A and RAP plus 5% C showed lower elastic moduli than all the other binders. Furthermore, comparing the unaged and aged states of the binders shows that the RAP plus 5% C had lower aging susceptibility (peak Modulus 95 MPa at unaged stage and 155 MPa at aged stage). However, in general it can be observed how each rejuvenated RAP increases its Young's modulus after aging. On the contrary, RAP binder peak modulus increases from 120 MPa (unaged stage) to 180 MPa.



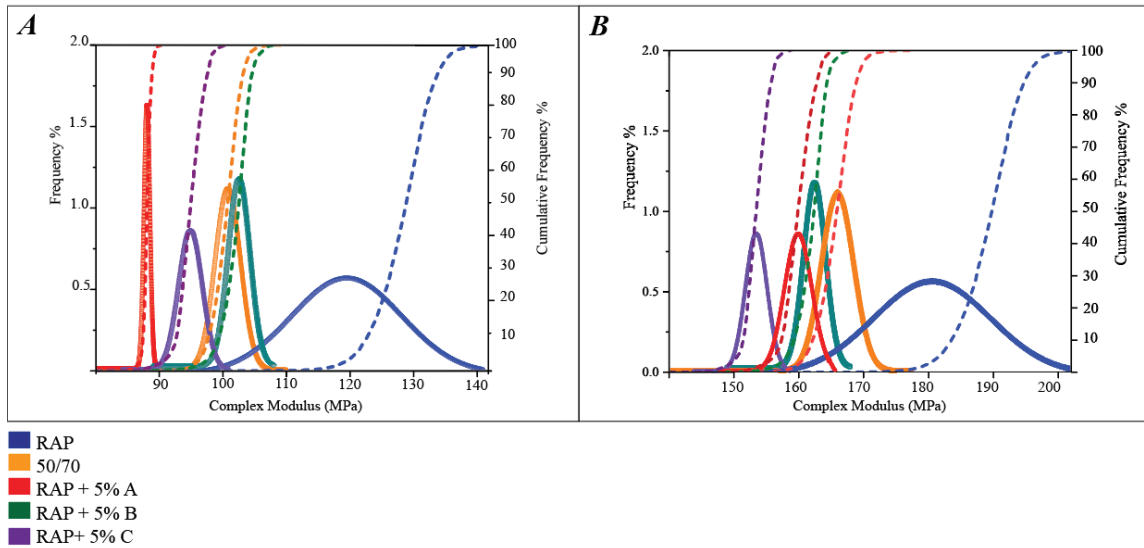


Figure 80 Gaussian distribution and cumulative frequency curve for unaged binders (A, left) aged binders (B, right). Data were obtained as average of five different images per binder.

Similar results were obtained by analysing the 50<sup>th</sup> percentile values of elastic moduli also shown in Fig 78 in the cumulative distribution function at the surface with the QNM method. As can be seen in Figure 81, before aging, all rejuvenated binders showed lower elastic moduli. After aging, the elastic moduli of the surface on average increased for all binders. However, it can be noticed in unaged state, how as a general trend, the elastic moduli of all rejuvenated binders appeared lower than the RAP binder corroborating the results outlined in Chapter 4 for bulk measurements with DSR.

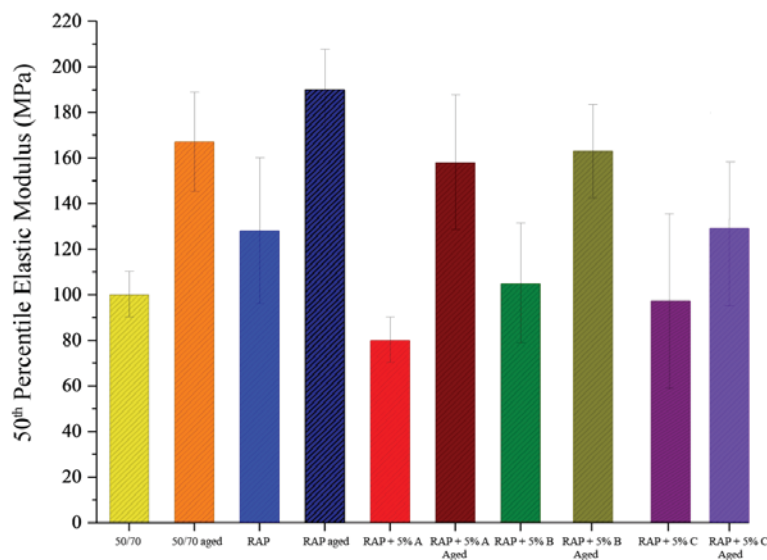


Figure 81 50<sup>th</sup> percentile elastic modulus for all binders with standard deviation calculated as average of five measurements.

As described in Chapter 4, for all frequencies ranges, at the bulk RAP + 5% A and RAP + 5% C had similar complex moduli after aging. It was shown how despite the addition of rejuvenators, after aging there is in general an increase of both complex moduli and phase angle. However, complex moduli results at quasi static load conditions (i.e. 0.1 Hz) for 20° C, as shown in Chapter 4 Figure 41, were in the range 0.1 (unaged RAP + 5% C) and 10 MPa (aged RAP binder). At the surface, the elastic moduli presented a range between 80 (unaged RAP + 5% A) and 200 MPa (aged RAP binder). Thus, it has been confirmed how there are two orders of magnitude difference between the bulk and the surface moduli of the softer and harder material respectively.

6.4.3 Comparison of the bulk and surface properties of the “bees” structures

Aim of this section is to validate the hypothesis that “bees” are stiffer domain in a compliant substrate (in this case the bitumen at the bulk) by using QNM measurements. As can be seen in Figure 82, virgin binder 50/70 presents wrinkled surface structures known as “bee” structures presenting undulated patterns which are not perfectly regular. However, the system can be simplified in sinusoidal wrinkles composed by certain wavelength  $\lambda_0$ , and a maximum amplitude  $A_0$ .

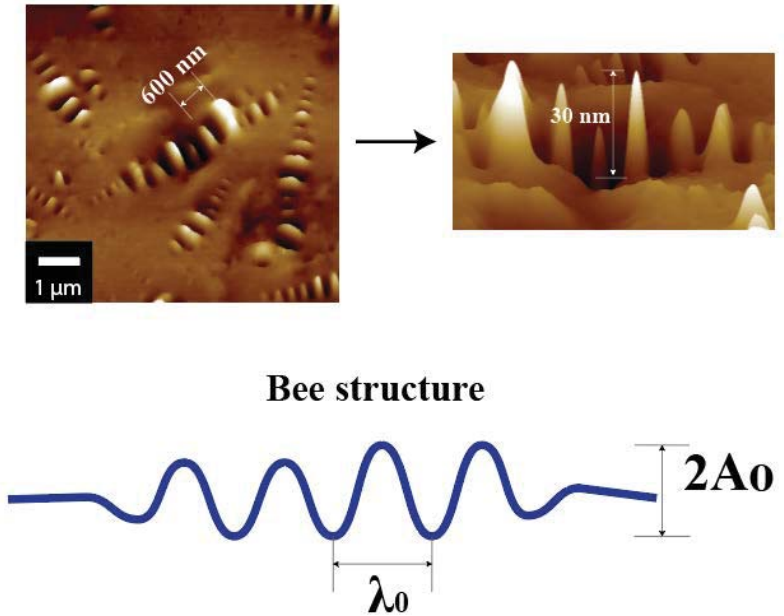


Figure 82 Top part: AFM topography image of the virgin binder 50/70 with corresponding measurement of wavelength  $\lambda_0$  and maximal amplitude  $2A_0$  of the “bee” structure. Bottom part: representation of the “bee” structure with corresponding wavelength  $\lambda_0$  and the maximum amplitude  $2A_0$ .

Many studies have been done in the past to understand the origin behind the process of the “bees” formation. Nowadays, the most widely accepted hypothesis is that the “bees” are wrinkled film of

crystallized paraffin (Lyne, Wallqvist, and Birgisson 2013). It has been observed that stiff laminated films on viscoelastic substrates have shown the formation of wrinkled structures on the surface when the material was subjected to certain compressive strain (Jiang et al. 2007). In this study, when such a system is subjected to a lateral compressive strain designated as  $\varepsilon_{load}$ , the stiff film is less able to support the strain than the soft substrate.

If  $\varepsilon_{load}$  exceeds a defined critical compressive strain called  $\varepsilon_{cr}$ , the film buckles and transforms some of the lateral compressive strain into bending and normal strain in order to reduce the total elastic strain energy. Subsequently, the thin film buckles into highly regular, sinusoidal wrinkles with specific wavelength  $\lambda_o$  and amplitude  $A_o$ . The values of  $\lambda_o$  and  $A_o$  depend on the film thickness  $h$  and the plane-strain moduli of the film  $\bar{E}_{film}$  and the substrate  $\bar{E}_{substrate}$ . (Jiang et al. 2007)

The research in (Hung and Fini 2015) showed the validity of this assumption for a bitumen presenting “bees”.

By applying this model to the “bee” structures,  $\varepsilon_{load}$  can be replaced with  $\varepsilon_{bee}$  which can be identified as the compressive strain that is purported to cause the thin film to wrinkle into “bees”.

In the limit of small deformations,  $\lambda_o$  and  $A_o$  are given by the following equations (Jiang et al. 2007):

$$\lambda_o = 2\pi h \left( \frac{\bar{E}_{film}}{\bar{E}_{substrate}} \right)^{\frac{1}{3}} \quad (26)$$

$$A_o = h \sqrt{\frac{\varepsilon_{bee}}{\varepsilon_{cr}} - 1} \quad (27)$$

For the purpose of discussion,  $A_o$  is considered as the highest amplitude. Based on this model, when the compressive strain  $\varepsilon_{bee}$  exceeds the critical strain  $\varepsilon_{cr}$ , the film buckles into sinusoidal wrinkles. In the hypothesis of small deformations (Im and Huang 2005),  $\varepsilon_{cr}$  is given by the following equation (Jiang et al. 2007):

$$\varepsilon_{cr} = \frac{1}{4} \left( \frac{3\bar{E}_{substrate}}{\bar{E}_{film}} \right)^{\frac{2}{3}} \quad (28)$$

Combining Equation (26) and Equation (27), the magnitude of the compressive strain  $\varepsilon_{bee}$  that creates the wrinkled “bees” can be calculated from a measurement of the ratio between  $A_o$  and  $\lambda_o$ . Subsequently, by inserting those values in Equation (28) it is conceivable to calculate  $\varepsilon_{bee}$  as follows (Hung and Fini 2015):

$$\varepsilon_{bee} = \varepsilon_{cr} + \left( \pi \frac{A_o}{\lambda_o} \right)^2 = \frac{1}{4} \left( \frac{3\bar{E}_{substrate}}{\bar{E}_{film}} \right)^{\frac{2}{3}} + \left( \pi \frac{A_o}{\lambda_o} \right)^2 \quad (29)$$

As depicted in Figure 82, the values of  $A_0$  and  $\lambda_o$ , depend on the “bees” geometry. For the case studied, as average among five “bees” the maximum  $A_0$  was found to be equal to 15 nm while the wavelength  $\lambda_o$  equal to 600 nm. These values found agreement with averaged “bees” dimensions as reported in previous works (Hung and Fini 2015).

As described previously, the formulation of the plain strain moduli  $\bar{E}_{film}$  and  $\bar{E}_{substrate}$  are the following:

$$\bar{E} = E^*/(1 - \nu^2) \quad (30)$$

where  $E$  is the measured elastic modulus and  $\nu$  is the Poisson’s ratio.

In order to obtain  $\bar{E}_{substrate}$ , it is necessary to convert the complex modulus  $G^*$  values into its corresponding  $\bar{E}_{substrate}$  values.

$G^*$  values used in this section were obtained for quasi static conditions at room temperature by using the DSR following sample preparation outlined in Chapter 3.

For quasi-static condition (0.1 Hz) at 20° C, virgin bitumen has generally a Poisson’s ratio equal to 0.40 (Di Benedetto, Delaporte, and Sauzéat 2007).

The elastic modulus  $E$  can be calculated by using the following equation:

$$E^* = 2G^*(1 + \nu) \quad (31)$$

Thus, by substituting Equation (32) into Equation (31), it is possible to obtain  $\bar{E}_{substrate}$ .

In the same way,  $\bar{E}_{film}$  is obtained by inserting in Equation (31) the corresponding median elastic modulus which was obtained by QNM as it was described in Chapter 2 with corresponding values in Figure 80. Results are summarized in the below Table 2.

Table 2 Results obtained from the rheological measurements with corresponding elastic modulus as well elastic modulus obtained after AFM QNM.

Material	$G^*$ (MPa)	$E^*$ (MPa)	$\bar{E}_{\text{substrate}}$ (MPa)	$\bar{E}_{\text{film}}$ (MPa)	$\frac{\bar{E}_{\text{film}}}{\bar{E}_{\text{substrate}}}$
50/70 unaged	0.44	1.23	1.46	119.04	81
50/70 aged	2.43	6.80	8.10	202.38	25
RAP unaged	2.34	6.55	7.80	154.76	20
RAP aged	5.16	14.44	17.2	226.19	13

As can be observed in Figure 82, the ratio  $\frac{A_0}{\lambda_0}$  was found to be equal to 0.025. Thus,  $\varepsilon_{cr}$  has resulted to be 0.028 for the unaged 50/70 while for the aged material  $\varepsilon_{cr}$  has been measured equal to 0.054. According to Equation (29), the following compressive strain  $\varepsilon_{\text{bee}}$  can be obtained: for example, for the unaged 50/70,  $\varepsilon_{\text{bee}}$  was equal to 3.40% and 6.08% for the aged case.

For  $\varepsilon_{cr}$  to be a reasonable value, the film should be significantly stiffer than the substrate ( $\bar{E}_{\text{film}} > \bar{E}_{\text{substrate}}$ ) i.e. (Hung and Fini 2015) used properties from the literature and estimated the ratio  $\frac{\bar{E}_{\text{film}}}{\bar{E}_{\text{substrate}}}$  for bitumen to be in the order of magnitude of 100. As shown in Table 2, from QNM measurements, RAP binder film in comparison to the substrate did not show such a significant difference as the virgin binder. From Table 2, the ratio was 80 and 25 for the unaged and aged virgin binder respectively where it was observed formation of “bees” whereas when this ratio was 20 and 13 for the unaged and aged RAP respectively, no “bee” structures formed. This can be contributing to the fact that no “bee” structures have formed on the surface of the RAP binder.

The significance of this ratio for the “bee” formation should be further investigated. The origin of a softer substrate can be caused by processes originating during for example the cooling of the sample (Hung and Fini 2015). The validation of the hypothesis of stiff wrinkled system (“bees”) on compliant substrate (virgin bitumen bulk) can confirm the difference observed in terms of elastic moduli between the bulk elastic modulus (average equal to 0.44 MPa and 2.43 MPa for the unaged and aged virgin binder respectively as in Figure 41) and the surface’s elastic modulus (as depicted in Figure 81, equal to 100 MPa for the unaged virgin and 170 MPa for the aged virgin binder).

## 6.5 Conclusions and outlook

Atomic force microscopy (AFM) has been utilized to characterize the topography and phase information and the elastic moduli at the surface of all binders studied in this thesis. Each material was analysed before and after laboratory aging. Main findings from the AFM studies have been the following:

- i. RAP binder and virgin binder display significantly different microstructures; the four domains including “bee” structures do not form in RAP binder microstructure.
- ii. Addition of rejuvenators does not reverse the microstructure of the RAP binder to that of virgin binder corroborating the chemical characterizations shown in Chapter 4.
- iii. Generally, the microstructures show four domains topographically while two distinct domains in the phase image. It has been observed that the two different domain in the phase images corresponded to zones with different mechanical properties.
- iv. In the topography images, aging caused a reduction of periphase which was associated to the softer part of the microstructure.
- v. The addition of two types of rejuvenators (A and C) could create new branches at the surface of the RAP binder.
- vi. A correlation between phase images (qualitative mechanical properties) and rheological measurements have been hereby proposed.
- vii. Quantitative nano-mechanical mapping of elastic moduli along samples’ surface was possible. Generally, surface’s elastic moduli ranged from 80 MPa up to 200 MPa.
- viii. In general, RAP binder was stiffer than the other binders. The addition of rejuvenators decreased the elastic moduli of the RAP binder. As a result of aging, the surface elastic moduli of all binder increased. Using the Gaussian distribution of the surface moduli it was shown how rejuvenators A and C showed less aging susceptibility.
- ix. “Bees” were observed to be composed of periodic ripples with wavelength and amplitude. Surface modulus was consistently higher than the bulk modulus contributing to the formation of the “bee” structures.

In conclusion, the addition of rejuvenators results in the formation of new structures on the surface of the RAP binder. This work can be seen as first attempt to correlate nano-mechanical properties at the surface with the bulk properties of modified asphalt binders. It was found that precise relations between the materials mechanical properties before and after aging exist. In addition, it has been demonstrated how rejuvenators could soften the RAP’s binder both at the bulk and at the surface. Aging has been seen as a key parameter when studying these kinds of relations.

## 7. Overall conclusions and outlook

Pavements continually oxidize and age during their performance life, leading to durability issues as a result of the increase in stiffness and brittleness and their lower ability to withstand stresses. Bio-based rejuvenated pavement materials are a building material made of reclaimed asphalt binder and specific products called rejuvenators. Rejuvenators are products designed to restore original properties of oxidized binders. The reason behind the choice of a bio-based rejuvenator is dual: firstly, asphalt rejuvenators are used for the creation of environmentally friendly roads and secondly bio-based rejuvenators have the added benefit of respecting the environmental sustainability. This thesis dealt with the investigation of the applications of three different bio-based rejuvenators in reclaimed asphalt. Rejuvenator called “A” a natural seed oil; rejuvenator designated as “B” a cashew-nut shell based oil and rejuvenator “C” a tall based oil with the first one being a common vegetable oil while the others commercially available rejuvenators for asphalt. The first part of the thesis was focused on the effect of aging. The developed study demonstrated how aging had a significant effect on the chemical and on the rheological properties of the rejuvenated RAP binders. Rheological measurements showed that all investigated rejuvenators could enhance the mechanical properties of RAP binders to a level similar to the unaged state. However, only two rejuvenators (A and C) could after laboratory aging mechanically restore the aged RAP binder to a level similar of the aged virgin binder, showing significant differences in the modulus and phase angle results compared to rejuvenator B. Furthermore, it has been shown how mechanical changes due to rejuvenators were not caused by changes at chemical bonds/functional groups level, which were detected with Fourier transform infrared spectroscopy, but rather due to a rearrangement at higher molecular scale such as polar/nonpolar components (analysed with saturates, aromatics, resins, asphaltenes fractioning). This part of the work demonstrated that rejuvenators are able to restore the mechanical properties albeit aging and rejuvenator type play an important role.

In the second part of the thesis, the focus was on low temperature mechanical behaviour of the modified binders. Cracking behaviour at low temperature together with rheological measurements was analysed and the effect of aging on the effectiveness of the bio-based modification has been evaluated. Specifically, rheological measurements performed with dynamic shear rheometer (DSR) were combined with fracture toughness test (FTT). It was observed how rejuvenators had a positive effect on the unaged RAP binder: fracture toughness temperature decreased after the addition of 5% rejuvenator and this decrease was rejuvenator dependent. Specifically, rejuvenator A and C showed better performances in restoring the RAP binder rather than rejuvenator B. Work to fracture at  $-10^{\circ}\text{C}$  showed a significant improvement in the fracture toughness of RAP binder after the addition of rejuvenators, both before and after ageing. However, it has been demonstrated how ag-

ing had a significant impact on the low temperature performances of all binders. This part of the investigation showed how rejuvenators were effective in restoring fracture toughness properties at low temperature however; aging had a significant impact which must be taken into account.

It has always been a challenge to identify the origin behind the appearance of the bee-shaped micro-structures at the binder's surface. The third part of this thesis has investigated fundamental aspects related to the microstructure of bio-based rejuvenated binders. Atomic force microscopy (AFM) has been carried out on the modified binders before and after aging. In particular, it was shown that the morphology of RAP binder and virgin binder are not the same and it changed after the addition of rejuvenators but the virgin microstructure was not restored. Rejuvenators A and C caused the formation of new branches along the surface of the RAP binder. On the contrary, rejuvenator B showed a similar morphology to the one of the RAP binder. Subsequently, phase images (qualitative mechanical information) were correlated with the complex bulk modulus ( $G^*$ ). This result showed how the morphology is affected by aging resulting in an increase of stiffer area of the surface microstructure. The increase in the surface modulus followed a similar trend to an increase of the sample's bulk modulus  $G^*$  showing a direct relationship between surface properties and bulk properties. Using quantitative nano-mechanical mapping (QNM) at the binders' surface Young's moduli along samples' surface were measured with AFM. In general, RAP binder was stiffer than the virgin and rejuvenated RAP binders. The addition of rejuvenators decreased the elastic moduli of the RAP binder however, as a result of aging, the elastic moduli of all binders increased. Gaussian distribution of the surface moduli showed that rejuvenators A and C showed less aging susceptibility as it was confirmed by rheological measurements. In addition, a hypothesis on the formation of the "bee" structures in the virgin binder has been developed. A correlation between the bulk complex modulus  $E^*$  (from rheological measurements) and elastic modulus  $E$  (from AFM measurements) have been carried out. In the framework of this thesis, the origin of the microstructures lies in the fact that there is a difference between the surface and bulk properties that results in the formation of microstructures caused by the processes originating during for example the heating/cooling of the sample. In conclusion, in this thesis the topic of bio-based modification of RAP binder has been studied from three different perspectives: by exploring fundamental aspects; by studying the enhancement of the mechanical and rheological performances, chemical characterizations and in the end, the effects of rejuvenators on the RAP's morphology. As discussed in first part of this thesis, this project was part of a larger study titled "fully sustainable asphalt concrete". Results of this Ph.D. dissertation have been used to perform tests on the mixture scale. In particular, 100% recycled mixtures have been designed by balancing two performance-based properties of asphalt: rutting using French wheel tester and cracking using semi-circular bend test. Two different RAP grading curves were used with two binder contents each. It has been observed how 100% RAP mixtures could not satisfy the conventional volumetric and Marshal test requirements.



However, performance-based balanced design procedure using French Rutting test and so called “flexibility index” from semi-circular bend test was found practical and provided the expected trends as a result of changes in mix design. It was also found that by changing different mixture parameters it is possible to ensure that 100% recycled asphalt mixtures provide similar performance to conventional asphalt which is designed for roads with design traffic volume of up to 300 equivalent single axis loads. Based on the positive experience of using performance-based mixture tests to balance cracking and rutting, it is recommended to consider such an approach as part of mixture design procedure when dealing with reclaimed asphalt.

Ideally, efforts should be made to avoid waste of natural resources such as crude oil and virgin aggregates thus, correctly understanding the complex asphalt system is vital nowadays. The identification of a suitable rejuvenator capable of improving the performances of RAP binder is a key aspect that allow development of effective rejuvenators with long term effect and thereby the design of durable high RAP mixtures. Future works should aim at achieving the same performances between a virgin binder and a bio-modified RAP binder with approaches that could be defined as green and environmentally friendly. In particular, the possibility to create rejuvenators able to chemically reverse aging should be further investigated. Up to now, standardized procedures regarding the rejuvenator selection dosage are also not very well developed.

From this study, it was concluded that aging is a fundamental aspect to be considered. Thus, in a future perspective, to evaluate the degree of binder which is activated by the rejuvenators, aging should be a key parameter to be analysed. In particular, a further study could be conducted by focusing on enhancing the rejuvenators’ potential by exploring fundamental aspects such as their interaction with the RAP binder at molecular level through for example molecular dynamics studies. This could provide a feasible way to get the molecular interactions behind the asphalt materials, which is still very largely unknown. In addition, AFM has been found to be a useful tool to analyse topology and nano-mechanical information. However, as it was outlined in the thesis, several questions remained open. Particularly, focus should be made in finding precise explanations on the “bees” formation. An important aspect is the chemical nature of the microstructures. Furthermore, aspects to be considered are the implementation of accurate models to predict the elastic modulus when using atomic force microscopy.

In summary, it was demonstrated that the achieved results showed how aging can be associated with different chemo-mechanical mechanisms. These findings can demonstrate how a multi scale characterization is fundamental in understanding the rejuvenation effect and aging influences the chemical, mechanical and microstructural evolution of asphalt binders that can aid in designing new materials.

## Bibliography

- Airey, G.D. 1997. "Rheological Characteristics of Polymer Modified and Aged Bitumens. Doctoral Dissertation." Retrieved from "The University of Nottingham" Bibliography database.
- Airey, Gordon D., Behzad Rahimzadeh, and Andrew C. Collop. 2004. "Linear Rheological Behavior of Bituminous Paving Materials." *Journal of Materials in Civil Engineering* 16 (3): 212–20. doi:10.1061/(ASCE)0899-1561(2004)16:3(212).
- Al-Khateeb, Ghazi G., and Khaled Z. Ramadan. 2015. "Investigation of the Effect of Rubber on Rheological Properties of Asphalt Binders Using Superpave DSR." *KSCE Journal of Civil Engineering* 19 (1). Korean Society of Civil Engineers: 127–35. doi:10.1007/s12205-012-0629-2.
- Ali, Ayman W., Yusuf A. Mehta, Aaron Nolan, Caitlin Purdy, and Thomas Bennert. 2016. "Investigation of the Impacts of Aging and RAP Percentages on Effectiveness of Asphalt Binder Rejuvenators." *Construction and Building Materials* 110 (May). Elsevier Ltd: 211–17. doi:10.1016/j.conbuildmat.2016.02.013.
- Allen, R. Grover, Dallas N. Little, Amit Bhasin, and Charles J. Glover. 2014. "The Effects of Chemical Composition on Asphalt Microstructure and Their Association to Pavement Performance." *International Journal of Pavement Engineering* 15 (1). Taylor & Francis: 9–22. doi:10.1080/10298436.2013.836192.
- Amani, Mohammad J., Murray R. Gray, and John M. Shaw. 2014. "The Phase Behavior of Athabasca Bitumen+toluene+water Ternary Mixtures." *Fluid Phase Equilibria* 370: 75–84. doi:10.1016/j.fluid.2014.02.028.
- Anderson, David. 1994. "Binder Characterization, Vol. 3: Physical Properties", SHRP-A-369, Strategic Highways Research Program." *Report of the National Research Council*. Washington, D.C., 494.
- Baek, Sung-Hyun, Jun-Pyo Hong, Sung Un Kim, Jung-Soon Choi, and Kwang-Woo Kim. 2011. "Evaluation of Fracture Toughness of Semirigid Asphalt Concretes at Low Temperatures." *Transportation Research Record: Journal of the Transportation Research Board* 2210 (1): 30–36. doi:10.3141/2210-04.
- Bailey, H K, and S E Zoorob. 2012. "The Use of Vegetable Oil as a Rejuvenator for Asphalt Mixtures." *Transportation Research Record*, no. A5EE–161. <https://trid.trb.org/view.aspx?id=1216714>.
- Benedetto, H. Di, B. Delaporte, and C. Sauzéat. 2007. "Three-Dimensional Linear Behavior of Bituminous Materials: Experiments and Modeling." *International Journal of Geomechanics* 7 (2): 149–57. doi:10.1061/(ASCE)1532-3641(2007)7:2(149).

- Benedetto, H. Di, Manfred N. Partl, L Francken, and Chantal De la Roche. 2001. “Stiffness Testing for Bituminous Mixtures.” *Materials and Structures* 34: 66–70. doi:10.1007/BF02481553.
- Binnig, G, C Quate, and C Gerber. 1986. “Atomic Force Microscope.” *Physical Review Letters*. doi:10.1103/PhysRevLett.56.930.
- Bird, R. Byron, Warren E. Stewart, and Edwin N. Lightfoot. 2007. *Transport Phenomena*. J. Wiley.
- Boltzmann, L. 1871. “Zur Priorität Der Auffindung Der Beziehung Zwischen Dem Zweiten Hauptsatze Der Mechanischen Wärmetheorie Und Dem Principe Der Kleinsten Wirkung.” *Annalen Der Physik* 219: 211–30.
- Bonemazzi, F, and C Giavarini. 1999. “Shifting the Bitumen Structure from Sol to Gel.” *Journal of Petroleum Science and Engineering* 22 (1): 17–24. doi:10.1016/S0920-4105(98)00052-7.
- Bowers, Benjamin F., Baoshan Huang, and Xiang Shu. 2013. “New Method for Detecting Asphalt Contamination within Fine Aggregate Medium through Chemical Testing.” *Journal of Materials in Civil Engineering* 25 (2): 252–56. doi:10.1061/(ASCE)MT.1943-5533.0000594.
- Bowers, Benjamin F., Jason Moore, Baoshan Huang, and Xiang Shu. 2014. “Blending Efficiency of Reclaimed Asphalt Pavement: An Approach Utilizing Rheological Properties and Molecular Weight Distributions.” *Fuel* 135. Elsevier Ltd: 63–68. doi:10.1016/j.fuel.2014.05.059.
- Cannone Falchetto, Augusto, Mugurel I Tuross, and Mihai O Marasteanu. 2012. “Investigation on Asphalt Binder Strength at Low Temperatures.” *Road Materials and Pavement Design* 13 (4): 804–16. doi:10.1080/14680629.2012.735793.
- Cappella, B., and G. Dietler. 1999. “Force-Distance Curves by Atomic Force Microscopy.” *Surface Science Reports* 34 (1–3). North-Holland: 1–104. doi:10.1016/S0167-5729(99)00003-5.
- Cavalli, M.C., Manfred N. Partl, and Lily D. Poulikakos. 2017. “Measuring the Binder Film Residues on Black Rock in Mixtures with High Amounts of Reclaimed Asphalt.” *Journal of Cleaner Production* 149 (April): 665–72. doi:10.1016/j.jclepro.2017.02.055.
- Cavalli, M.C., M. Zaumanis, E. Mazza, M.N. Partl, and L.D. Poulikakos. 2018. “Effect of Ageing on the Mechanical and Chemical Properties of Binder from RAP Treated with Bio-Based Rejuvenators.” *Composites Part B: Engineering* 141 (May): 174–81. doi:10.1016/j.compositesb.2017.12.060.
- Chen, Wuhua, Zongchang Zhao, Xiaodong Zhang, and Lijuan Wang. 2007. “Thermodynamic Phase Equilibria of Wax Precipitation in Crude Oils.” *Fluid Phase Equilibria* 255 (1): 31–36. doi:10.1016/j.fluid.2007.03.015.
- Cheung, C. Y., and D. Cebon. 1997. “Deformation Mechanisms of Pure Bitumen.” *Journal of Materials in Civil Engineering* 9 (3): 117–29. doi:10.1061/(ASCE)0899-1561(1997)9:3(117).

- Christensen, R. M. 1982. “Theory of Viscoelasticity.” *Journal of Applied Mechanics* 38 (3): 720. doi:10.1115/1.3408900.
- D. Tranchida, Z. Kiflie, and S. Piccarolo. 2007. “Atomic Force Microscope Nano Indentations to Reliably Measure the Young’s Modulus of Soft Matter.” *Modern Research and Educational Topics in Microscopy*.
- Daniel, J.S., Y.R. Kim, S. Brown, G. Rowe, G. Chehab, and G. Reinke. 2002. “Development of a Simplified Fatigue Test and Analysis Procedure Using a Viscoelastic, Continuum Damage Model.” In *Asphalt Paving Technology: Association of Asphalt Paving Technologists- Proceedings of the Technical Sessions*, 71:619–50.
- Das, Prabir Kumar, Hassan Baaj, Susan Tighe, and Niki Kringos. 2016a. “Atomic Force Microscopy to Investigate Asphalt Binders: A State-of-the-Art Review Atomic Force Microscopy to Investigate Asphalt Binders: A State-of-the-Art Review.” *Road Materials and Pavement Design* 17 (3): 693–718. doi:10.1080/14680629.2015.1114012.
- . 2016b. “Atomic Force Microscopy to Investigate Asphalt Binders: A State-of-the-Art Review.” *Road Materials and Pavement Design* 17 (3). Taylor & Francis: 693–718. doi:10.1080/14680629.2015.1114012.
- Das, Prabir Kumar, Niki Kringos, Viveca Wallqvist, and Björn Birgisson. 2013. “Micromechanical Investigation of Phase Separation in Bitumen by Combining Atomic Force Microscopy with Differential Scanning Calorimetry Results.” *Road Materials and Pavement Design* 14: 25–37. doi:10.1080/14680629.2013.774744.
- Dealy, J, and D Plazek. 2009. “Time-Temperature Superposition—a Users Guide.” *Rheol. Bull.* <http://www.chem.mtu.edu/~fmorriso/cm4655/DealyPlazekTimeTempSuper2009.pdf>.
- Derjaguin, B., V. Muller, and Y. Toporov. 1975. “Effect of Contact Deformations on the Adhesion of Particles.” *Journal of Colloid And Interface Science* 53 (2). Academic Press: 314–26. doi:10.1016/0021-9797(75)90018-1.
- Desseaux, Solenne, Salomé dos Santos, Thomas Geiger, Philippe Tingaut, Tanja Zimmermann, Manfred N. Partl, and Lily D. Poulikakos. 2018. “Improved Mechanical Properties of Bitumen Modified with Acetylated Cellulose Fibers.” *Composites Part B: Engineering* 140 (May). Elsevier: 139–44. doi:10.1016/J.COMPOSITESB.2017.12.010.
- Dickinson, E. J., and H. P. Witt. 1974. “The Dynamic Shear Modulus of Paving Asphalts as a Function of Frequency.” *Transactions of the Society of Rheology* 18 (4). The Society of Rheology: 591–606. doi:10.1122/1.549349.
- Dobson, G., C. Monismith, V. Puzinauskas, and H. Busching. 1969. “THE DYNAMIC MECHANICAL PROPERTIES OF BITUMEN.” *Transportation Research Record*. <https://trid.trb.org/view/101205>.
- Dokukin, Maxim E., and Igor Sokolov. 2012. “Quantitative Mapping of the Elastic Modulus of

- Soft Materials with HarmoniX and PeakForce QNM AFM Modes.” *Langmuir* 28 (46): 16060–71. doi:10.1021/la302706b.
- Dondi, G., F. Mazzotta, A. Simone, V. Vignali, C. Sangiorgi, and C. Lantieri. 2016. “Evaluation of Different Short Term Aging Procedures with Neat, Warm and Modified Binders.” *Construction and Building Materials* 106: 282–89. doi:10.1016/j.conbuildmat.2015.12.122.
- Dourado, Erico R., Bianca S. Pizzorno, Laura M G Motta, Renata A. Simao, and Leni F M Leite. 2014. “Analysis of Asphaltic Binders Modified with PPA by Surface Techniques.” *Journal of Microscopy* 254 (3): 122–28. doi:10.1111/jmi.12123.
- Eaton, Peter, and Paul West. 2010. *Atomic Force Microscopy*. Oxford University Press. doi:10.1093/acprof:oso/9780199570454.001.0001.
- Eberhardsteiner, Lukas, Josef Füssl, Bernhard Hofko, Florian Handle, Ronald Blab, and Hinrich Grothe. 2016. “Micromechanical Description of Bitumen Aging Behavior.” Springer, Dordrecht, 411–21. doi:10.1007/978-94-017-7342-3\_33.
- Eberhardsteiner, Lukas, Josef Füssl, Bernhard Hofko, Florian Handle, Markus Hospodka, Ronald Blab, and Hinrich Grothe. 2015a. “Influence of Asphaltene Content on Mechanical Bitumen Behavior: Experimental Investigation and Micromechanical Modeling.” *Materials and Structures* 48 (10). Springer Netherlands: 3099–3112. doi:10.1617/s11527-014-0383-7.
- . 2015b. “Towards a Microstructural Model of Bitumen Ageing Behaviour.” *International Journal of Pavement Engineering* 16 (10): 939–49. doi:10.1080/10298436.2014.993192.
- Edwards, Y, and P Redelius. 2003. “Rheological Effects of Waxes in Bitumen.” *Energy & Fuels* 17 (3): 511–20. doi:10.1021/ef020202b.
- Eicher, Theophil, Siegfried Hauptmann, and Andreas Speicher. 2003. *The Chemistry of Heterocycles*. Weinheim, FRG: Wiley-VCH Verlag GmbH & Co. KGaA. doi:10.1002/352760183X.
- Elkashef, Mohamed, Joseph Podolsky, R. Christopher Williams, and Eric W. Cochran. 2017. *Introducing a Soybean Oil-Derived Material as a Potential Rejuvenator of Asphalt through Rheology, Mix Characterisation and Fourier Transform Infrared Analysis*. *Road Materials and Pavement Design*. doi:10.1080/14680629.2017.1345781.
- European Committee for Standardization CEN. 2010. “CEN TS15963. Bitumen and Bituminous Binders. Determination of the Fracture Toughness Temperature by a Three Point Bending Test on a Notched Specimen.”
- Ferry, J D. 1980. “Viscoelastic Properties of Polymers.” *Polymer*, 641. doi:10.1016/0032-3861(81)90360-8.
- Fleig, G. E. 1969. *Gel Permeation Chromatography: A Study of Column Geometry - Gordon Elmer Fleig - Google Libri*. Edited by Cornell University.
- Freund, M, and G. Mozes. 1982. *Paraffin Products: Properties, Technologies, Applications*. Elsevier

Scientific Pub. Co.

- Garcia Cucalon, Lorena, Fawaz Kaseer, Edith Arámbula-Mercado, Amy Epps Martin, Nathan Morian, Sara Pournoman, and Elie Hajj. 2018. “The Crossover Temperature: Significance and Application towards Engineering Balanced Recycled Binder Blends.” *Road Materials and Pavement Design*, March. Taylor & Francis, 1–22. doi:10.1080/14680629.2018.1447504.
- Garcia, R., C. J. Gómez, N. F. Martínez, S. Patil, C. Dietz, and R. Magerle. 2006. “Identification of Nanoscale Dissipation Processes by Dynamic Atomic Force Microscopy.” *Physical Review Letters* 97 (1). American Physical Society: 016103. doi:10.1103/PhysRevLett.97.016103.
- García, Ricardo, Javier Tamayo, and Alvaro San Paulo. 1999. “Phase Contrast and Surface Energy Hysteresis in Tapping Mode Scanning Force Microscopy.” *Surface and Interface Analysis* 27 (5–6). John Wiley & Sons, Ltd.: 312–16. doi:10.1002/(SICI)1096-9918(199905/06)27:5/6<312::AID-SIA496>3.0.CO;2-Y.
- Gawrys, Keith L., and Peter K. Kilpatrick. 2004. “Asphaltene Aggregation: Techniques for Analysis.” *Instrumentation Science and Technology* 32 (3): 247–53. doi:10.1081/CI-120030536.
- Girard, J.E. 1980. *Practical Organic Chemistry. Nature*. Vol. 284. doi:10.1038/284083b0.
- Gómez Castro, Carlos Javier, N. F. Martínez, Shivprasad Patil, Christian Dietz, R. Magerle, Ricardo American Physical Society., Carlos Javier Gómez Castro, et al. 2006. *Physical Review Letters*. American Physical Society. <http://digital.csic.es/handle/10261/18705>.
- Gong, Minghui, Jun Yang, Jiayun Zhang, Haoran Zhu, and Tianzhi Tong. 2016. “Physical–chemical Properties of Aged Asphalt Rejuvenated by Bio-Oil Derived from Biodiesel Residue.” *Construction and Building Materials* 105 (February). Elsevier: 35–45. doi:10.1016/J.CONBUILDMAT.2015.12.025.
- Hertz, H. R. 1882. “Ueber Die Beruehrung Elastischer Koerper.” *Gesammelte Werke*.
- Hill, Brian, Daniel Oldham, Behzad Behnia, Elham H. Fini, William G. Buttlar, and Henrique Reis. 2018. “Evaluation of Low Temperature Viscoelastic Properties and Fracture Behavior of Bio-Asphalt Mixtures.” *International Journal of Pavement Engineering* 19 (4). Taylor and Francis Ltd.: 362–69. doi:10.1080/10298436.2016.1175563.
- Hofko, B., L. Eberhardsteiner, J. Füssl, H. Grothe, F. Handle, M. Hospodka, D. Grossegger, S.N. Nahar, A.J.M. Schmets, and A. Scarpas. 2016. “Impact of Maltene and Asphaltene Fraction on Mechanical Behavior and Microstructure of Bitumen.” *Materials and Structures/Materiaux et Constructions* 49 (3): 829–41. doi:10.1617/s11527-015-0541-6.
- Hooke, Robert. 1678. *Lectures de Potentia Restitutiva*.
- Huang, Baoshan, Guoqiang Li, Dragan Vukosavljevic, Xiang Shu, and Brian Egan. 2005. “Laboratory Investigation of Mixing Hot-Mix Asphalt with Reclaimed Asphalt Pavement.” *Transportation Research Record: Journal of the Transportation Research Board* 1929 (Figure 1). Transportation Research Board of the National Academies : 37–45. doi:10.3141/1929-05.

- Huang, Shin-Che. 2008. "Rubber Concentrations on Rheology of Aged Asphalt Binders." *Journal of Materials in Civil Engineering* 20 (3): 221–29. doi:10.1061/(ASCE)0899-1561(2008)20:3(221).
- Huang, Shin-Che, and W. Grimes. 2010. "Influence of Aging Temperature on Rheological and Chemical Properties of Asphalt Binders." *Transportation Research: Journal of the Transportation Research Board*. doi:10.3141/2179-05.
- Huang, Shin Che, and Adam T. Pauli. 2008. "Particle Size Effect of Crumb Rubber on Rheology and Morphology of Asphalt Binders with Long-Term Aging." *Road Materials and Pavement Design* 9 (1): 73–95. doi:10.1080/14680629.2008.9690108.
- Huang, Shin Che, Qian Qin, R. Will Grimes, Adam Troy Pauli, and Ron Glaser. 2015. "Influence of Rejuvenators on the Physical Properties of RAP Binders" 43 (3). ASTM International: 594–603. doi:10.1520/JTE20130314.
- Hung, Albert M., and Elham H. Fini. 2015. "AFM Study of Asphalt Binder 'Bee' Structures: Origin, Mechanical Fracture, Topological Evolution, and Experimental Artifacts." *RSC Advances* 5 (117): 96972–82. doi:10.1039/C5RA13982A.
- Hung, Albert M., Adrian Goodwin, and Elham H. Fini. 2017. "Effects of Water Exposure on Bitumen Surface Microstructure." *Construction and Building Materials* 135 (March): 682–88. doi:10.1016/j.conbuildmat.2017.01.002.
- Hung, Albert M, Masoumeh Mousavi, Farideh Pahlavan, and Ellie H Fini. 2017. "Intermolecular Interactions of Isolated Bio-Oil Compounds and Their Effect on Bitumen Interfaces." *ACS Sustainable Chemistry & Engineering* 5 (9): 7920–31. doi:10.1021/acssuschemeng.7b01462.
- Hutter, Jeffrey L., and John Bechhoefer. 1993. "Calibration of Atomic-Force Microscope Tips." *Review of Scientific Instruments* 64 (7): 1868–73. doi:10.1063/1.1143970.
- Im, S. H., and R. Huang. 2005. "Evolution of Wrinkles in Elastic-Viscoelastic Bilayer Thin Films." *Journal of Applied Mechanics* 72 (6). American Society of Mechanical Engineers: 955. doi:10.1115/1.2043191.
- Jäger, A., R. Lackner, Ch. Eisenmenger-Sittner, and R. Blab. 2004. "Identification of Four Material Phases in Bitumen by Atomic Force Microscopy." *Road Materials and Pavement Design* 5 (sup1). Taylor & Francis Group : 9–24. doi:10.1080/14680629.2004.9689985.
- Jennings, P.W., J.A.S. Pribanic, T.M. Mendes, and J.A. Smith. 1992. "HIGH PERFORMANCE GEL PERMEATION CHROMATOGRAPHY IN THE CHARACTERIZATION OF SELF-ASSEMBLIES IN ASPHALT. I." *Fuel Science and Technology International* 10 (4–6). Taylor & Francis Group : 809–23. doi:10.1080/08843759208916022.
- Jiang, H., D.-Y. Khang, J. Song, Y. Sun, Y. Huang, and J. A. Rogers. 2007. "Finite Deformation Mechanics in Buckled Thin Films on Compliant Supports." *Proceedings of the National Academy of Sciences* 104 (40): 15607–12. doi:10.1073/pnas.0702927104.

- Jongepier, R, B Kuilman, R J Schmidt, V P Puzinauskas, and F S Rostler. 1969. “Characteristics of the Rheology of Bitumens.” *Transportation Research Record*.
- Kang, Hailan, Yinyin Tang, Lei Yao, Feng Yang, Qinghong Fang, and David Hui. 2017. “Fabrication of Graphene/Natural Rubber Nanocomposites with High Dynamic Properties through Convenient Mechanical Mixing.” *Composites Part B: Engineering* 112: 1–7. doi:10.1016/j.compositesb.2016.12.035.
- Karlsson, Robert, and Ulf Isacsson. 2003. “Application of FTIR-ATR to Characterization of Bitumen Rejuvenator Diffusion.” *Journal of Materials in Civil Engineering* 15 (2): 157–65. doi:10.1061/(ASCE)0899-1561(2003)15:2(157).
- Karlsson, Robert, Ulf Isacsson, and Jonas Ekblad. 2007. “Rheological Characterisation of Bitumen Diffusion.” *Journal of Materials Science* 42 (1). Springer US: 101–8. doi:10.1007/s10853-006-1047-y.
- Kim, Kwang W., Kyongae Kim, Young S. Doh, and Serji N. Amirkhanian. 2006. “Estimation of RAP’s Binder Viscosity Using GPC without Binder Recovery.” *Journal of Materials in Civil Engineering* 18 (4): 561–67. doi:10.1061/(ASCE)0899-1561(2006)18:4(561).
- Kim, S. H., M. T. Dugger, and K. L. Mittal. 2010. *Adhesion Aspects in MEMS-NEMS*. Taylor and Francis.
- Kim, Y Richard. 2009. “Modeling of Asphalt Concrete.” *Transportation Research Record*, 1–7. doi:10.1036/007146462X.
- Klein, Geoffrey C., Annelie Angström, Ryan P. Rodgers, and Alan G. Marshall. 2006. “Use of Saturates/Aromatics/Resins/Asphaltenes (SARA) Fractionation To Determine Matrix Effects in Crude Oil Analysis by Electrospray Ionization Fourier Transform Ion Cyclotron Resonance Mass Spectrometry.” *Energy & Fuels* 20 (2): 668–72. doi:10.1021/ef050353p.
- Kolarik, Jan, and Alessandro Pegoretti. 2008. “Proposal of the Boltzmann-like Superposition Principle for Nonlinear Tensile Creep of Thermoplastics.” *Polymer Testing* 27 (5): 596–606. doi:10.1016/j.polymertesting.2008.03.002.
- Lackner, Roman, and Markus Spiegl. 2005. “Is Low-Temperature Creep of Asphalt Mastic Independent of Filler Shape and Mineralogy?—arguments from Multiscale Analysis.” *Journal of Materials in Civil Engineering* 17 (5): 485–91. doi:10.1061/(ASCE)0899-1561(2005)17:5(485).
- Lesueur, Didier. 2008. “The Colloidal Structure of Bitumen: Consequences on the Rheology and on the Mechanisms of Bitumen Modification.” *Advances in Colloid and Interface Science* 145 (1–2). Elsevier: 42–82. doi:10.1016/j.cis.2008.08.011.
- Lian, Hsienjen, Jiuun Ren Lin, and Teh Fu Yen. 1994. “Peptization Studies of Asphaltene and Solubility Parameter Spectra.” *Fuel* 73 (3): 423–28. doi:10.1016/0016-2361(94)90097-3.
- Lin, Juntao, Jinxiang Hong, Chong Huang, Jiaping Liu, and Shaopeng Wu. 2014. “Effectiveness



- of Rejuvenator Seal Materials on Performance of Asphalt Pavement.” *Construction and Building Materials* 55 (March). Elsevier: 63–68. doi:10.1016/J.CONBUILDMAT.2014.01.018.
- Lindon, John C., George E. Tranter, and David W. Koppenaal. 1999. *Encyclopedia of Spectroscopy and Spectrometry*. Elsevier Ltd.
- Loeber, L., G. Muller, J. Morel, and O. Sutton. 1998. “Bitumen in Colloid Science: A Chemical, Structural and Rheological Approach.” *Fuel* 77 (13). Elsevier: 1443–50. doi:10.1016/S0016-2361(98)00054-4.
- Loeber, L., O. Sutton, J. Morel, J.-M. Valleton, and G. Muller. 1996. “New Direct Observations of Asphalts and Asphalt Binders by Scanning Electron Microscopy and Atomic Force Microscopy.” *Journal of Microscopy* 182 (1). Blackwell Science Ltd: 32–39. doi:10.1046/j.1365-2818.1996.134416.x.
- Lopes, Manuela, Virginie Mouillet, Liedi Bernucci, and Thomas Gabet. 2016. “The Potential of Attenuated Total Reflection Imaging in the Mid-Infrared for the Study of Recycled Asphalt Mixtures.” *Construction and Building Materials* 124: 1120–31. doi:10.1016/j.conbuildmat.2016.08.108.
- Lu, Xiaohu, and Ulf Isacsson. 2002a. “Effect of Ageing on Bitumen Chemistry and Rheology.” *Construction and Building Materials* 16 (1). Elsevier: 15–22. doi:10.1016/S0950-0618(01)00033-2.
- . 2002b. “Effect of Ageing on Bitumen Chemistry and Rheology.” *Construction and Building Materials* 16 (1). Elsevier: 15–22. doi:10.1016/S0950-0618(01)00033-2.
- Lu, Xiaohu, Petri Uhlback, and Hilde Soenen. 2017. “Investigation of Bitumen Low Temperature Properties Using a Dynamic Shear Rheometer with 4 Mm Parallel Plates.” *International Journal of Pavement Research and Technology* 10 (1). Elsevier: 15–22. doi:10.1016/J.IJPRT.2016.08.010.
- Lyne, Åsa Laurell, Viveca Wallqvist, and Björn Birgisson. 2013. “Adhesive Surface Characteristics of Bitumen Binders Investigated by Atomic Force Microscopy.” *Fuel* 113 (November). Elsevier: 248–56. doi:10.1016/j.fuel.2013.05.042.
- Mainardi, F., and G. Spada. 2011. “Creep, Relaxation and Viscosity Properties for Basic Fractional Models in Rheology.” *The European Physical Journal Special Topics* 193 (1). Springer-Verlag: 133–60. doi:10.1140/epjst/e2011-01387-1.
- Mangiafico, Salvatore, Herve Di Benedetto, Cedric Sauzeat, Francois Olard, Simon Pouget, and Luc Planque. 2016. “Effect of Colloidal Structure of Bituminous Binder Blends on Linear Viscoelastic Behaviour of Mixtures Containing Reclaimed Asphalt Pavement.” *Materials and Design* 111: 126–39. doi:10.1016/j.matdes.2016.07.124.
- Mangiafico, Salvatore, Cédric Sauzéat, Hervé Di Benedetto, Simon Pouget, François Olard, and Luc Planque. 2017. “Complex Modulus and Fatigue Performances of Bituminous Mixtures

- with Reclaimed Asphalt Pavement and a Recycling Agent of Vegetable Origin.” *Road Materials and Pavement Design* 18 (2): 315–30. doi:10.1080/14680629.2016.1213509.
- Marsac, Paul, Nathalie Piérard, Laurent Porot, Wim Van den bergh, James Grenfell, Virginie Mouillet, Simon Pouget, et al. 2014. “Potential and Limits of FTIR Methods for Reclaimed Asphalt Characterisation.” *Materials and Structures* 47 (8): 1–14. doi:doi:10.1617/s11527-014-0248-0.
- Masson, J. F., Roger M. Leblanc, and J. Margeson. 2006. “Bitumen Morphologies by Phase-Detection Atomic Force Microscopy.” *Journal of Microscopy* 221 (1): 17–29. doi:10.1111/j.1365-2818.2006.01540.x.
- Mastrofini, D, and M. Scarsella. 2000. “The Application of Rheology to the Evaluation of Bitumen Ageing.” *Fuel* 79 (9). Elsevier Science Ltd: 1005–15. doi:10.1016/S0016-2361(99)00244-6.
- Menapace, Ilaria, Lorena Garcia Cucalon, Fawaz Kaseer, Edith Arámbula-Mercado, Amy Epps Martin, Eyad Masad, Gayle King, et al. 2018. “Effect of Recycling Agents in Recycled Asphalt Binders Observed with Microstructural and Rheological Tests.” *Construction and Building Materials* 158 (January). Elsevier: 61–74. doi:10.1016/J.CONBUILDMAT.2017.10.017.
- Mitchell, David L., and James G. Speight. 1973. “The Solubility of Asphaltenes in Hydrocarbon Solvents.” *Fuel* 52 (2): 149–52. doi:10.1016/0016-2361(73)90040-9.
- Mokhtari, Ali, Hosin David Lee, R. Christopher Williams, C. Allan Guymon, Jon P. Scholte, and Scott Schram. 2017. “A Novel Approach to Evaluate Fracture Surfaces of Aged and Rejuvenator-Restored Asphalt Using Cryo-SEM and Image Analysis Techniques.” *Construction and Building Materials* 133 (February). Elsevier: 301–13. doi:10.1016/J.CONBUILDMAT.2016.12.075.
- Mousavi, Masoumeh, Farideh Pahlavan, Daniel Oldham, Shahrzad Hosseinnezhad, and Ellie H Fini. 2016. “Multiscale Investigation of Oxidative Aging in Biomodified Asphalt Binder.” *The Journal of Physical Chemistry*. doi:10.1021/acs.jpcc.6b05004.
- Murali Krishnan, J, and KR Rajagopal. 2003. “Review of the Uses and Modeling of Bitumen from Ancient to Modern Times.” *Applied Mechanics Reviews* 56 (2): 149. doi:10.1115/1.1529658.
- National Asphalt Pavement Association. 2010. “Reclaimed Asphalt Pavement - Material Description.” *Transportation Research Record*.
- Navarro, F. J., P. Partal, M. García-Morales, F. J. Martínez-Boza, and C. Gallegos. 2007. “Bitumen Modification with a Low-Molecular-Weight Reactive Isocyanate-Terminated Polymer.” *Fuel* 86 (15): 2291–99. doi:10.1016/j.fuel.2007.01.023.
- Nazzal, Munir D., Walaa Mogawer, Savas Kaya, Thomas Bennert, M Asce, Walaa Mogawer, F Asce, Savas Kaya, and Thomas Bennert. 2014. “Multiscale Evaluation of the Composite Asphalt Binder in High–Reclaimed Asphalt Pavement Mixtures.” *Journal of Materials in*

- Civil Engineering* 26 (7): 04014019. doi:10.1061/(ASCE)MT.1943-5533.0000825.
- Nivitha, M. R., and J. Murali Krishnan. 2016. “What Is Transition Temperature for Bitumen and How to Measure It?” *Transportation in Developing Economies* 2 (1). Springer International Publishing: 3. doi:10.1007/s40890-015-0009-y.
- Oldham, Daniel, Albert Hung, Mahour M. Parast, and Ellie H. Fini. 2018. “Investigating Bitumen Rejuvenation Mechanisms Using a Coupled Rheometry-Morphology Characterization Approach.” *Construction and Building Materials* 159 (January). Elsevier: 37–45. doi:10.1016/J.CONBUILDMAT.2017.10.113.
- Oliveira, Joel R.M., Hugo M.R.D. Silva, Carlos M.G. Jesus, Liliana P.F. Abreu, and Sara R.M. Fernandes. 2013. “Pushing the Asphalt Recycling Technology to the Limit.” *International Journal of Pavement Research and Technology* 6 (2): 109–16. doi:10.6135/ijprt.org.tw/2013.6(2).109.
- Ouyang, Chunfa, Shifeng Wang, Yong Zhang, and Yinxi Zhang. 2006. “Improving the Aging Resistance of Styrene–butadiene–styrene Tri-Block Copolymer Modified Asphalt by Addition of Antioxidants.” *Polymer Degradation and Stability* 91 (4). Elsevier: 795–804. doi:10.1016/J.POLYMDEGRADSTAB.2005.06.009.
- Pahlavan, Farideh, Masoumeh Mousavi, Albert Hung, and Ellie H Fini. 2016. “Investigating Molecular Interactions and Surface Morphology of Wax-Doped Asphaltenes.” *Phys. Chem. Chem. Phys.* 18 (13): 8840–54. doi:10.1039/C5CP07180A.
- Pahlavan, Farideh, Masoumeh Mousavi, Albert M. Hung, and Elham H. Fini. 2018. “Characterization of Oxidized Asphaltenes and the Restorative Effect of a Bio-Modifier.” *Fuel* 212 (January). Elsevier: 593–604. doi:10.1016/J.FUEL.2017.10.090.
- Pauli, A T, R W Grimes, A G Beemer, T F Turner, and J F Branthaver. 2011. “Morphology of Asphalts, Asphalt Fractions and Model Wax-Doped Asphalts Studied by Atomic Force Microscopy.” *International Journal of Pavement Engineering* 12 (4). Taylor & Francis Group : 291–309. doi:Doi 10.1080/10298436.2011.575942.
- Pedersen, K. S., A. Fredenslund, and P. Thomassen. 1989. *Properties of Oils and Natural Gases*. Gulf Pub. Co., Book Division.
- Petersen, J. Claine. 2000. “Chapter 14 Chemical Composition of Asphalt as Related to Asphalt Durability.” In *Developments in Petroleum Science*, 40:363–99. doi:10.1016/S0376-7361(09)70285-7.
- Petersen, J. Claine, and Ronald Glaser. 2011. “Asphalt Oxidation Mechanisms and the Role of Oxidation Products on Age Hardening Revisited.” *Road Materials and Pavement Design* 12 (4): 795–819. doi:10.1080/14680629.2011.9713895.
- Pfeiffer, J. Ph., and R. N. J. Saal. 1940. “Asphaltic Bitumen as Colloid System.” *The Journal of Physical Chemistry* 44 (2). American Chemical Society: 139–49. doi:10.1021/j150398a001.

- Poel, C Der Van. 1954. "A General System Describing the Viscoelastic Properties of Bitumens and Its Relation to Routine Test Data." *Journal of Applied Chemistry* 4 (5): 221–36. doi:10.1002/jctb.5010040501.
- Porot, L., D. Broere, M. Wistuba, and J. Grönniger. 2017. "Asphalt and Binder Evaluation of Asphalt Mix with 70% Reclaimed Asphalt." *Road Materials and Pavement Design* 18 (sup2). Taylor and Francis Ltd.: 66–75. doi:10.1080/14680629.2017.1304259.
- Poulikakos, Lily D., Salomé dos Santos, Moises Bueno, Simon Kuentzel, Martin Hugener, and Manfred N. Partl. 2014. "Influence of Short and Long Term Aging on Chemical, Microstructural and Macro-Mechanical Properties of Recycled Asphalt Mixtures." *Construction and Building Materials* 51. Elsevier Ltd: 414–23. doi:10.1016/j.conbuildmat.2013.11.004.
- Raman, Noor Azah Abdul, Mohd Rosli Hainin, Norhidayah Abdul Hassan, and Farid Nasir Ani. 2015. "A Review on the Application of Bio-Oil as an Additive for Asphalt." *Jurnal Teknologi* 72 (5): 105–10. doi:10.11113/jt.v72.3948.
- Read, John, David. Whiteoak, Robert N. (Robert Newell) Hunter, Shell Bitumen., and Whiteoak D. Read J. 2003. "The Shell Bitumen Handbook." *Thomas Telford Publishing*. Thomas Telford, 460.
- Redelius, P.G. 2000. "Solubility Parameters and Bitumen." *Fuel* 79 (1): 27–35. doi:10.1016/S0016-2361(99)00103-9.
- Redelius, Per G. 2006. "The Structure of Asphaltenes in Bitumen." *Road Materials and Pavement Design* 7 (sup1): 143–62. doi:10.1080/14680629.2006.9690062.
- Ritchie, Robert O. 2011. "The Conflicts between Strength and Toughness." *Nature Materials* 10 (11). Nature Publishing Group: 817–22. doi:10.1038/nmat3115.
- Rodríguez-Alloza, Ana María, Juan Gallego, and Felice Giuliani. 2017. "Complex Shear Modulus and Phase Angle of Crumb Rubber Modified Binders Containing Organic Warm Mix Asphalt Additives." *Materials and Structures* 50 (1). Springer Netherlands: 77. doi:10.1617/s11527-016-0950-1.
- Roylance, David. 2011. *Engineering Viscoelasticity*. Massachusetts Institute of Technology Publisher.
- Santos, Salomé dos, Manfred N. Partl, and Lily D. Poulikakos. 2015. "From Virgin to Recycled Bitumen: A Microstructural View." *Composites Part B: Engineering* 80: 177–85. doi:10.1016/j.compositesb.2015.05.042.
- Santos, Salomé dos, Lily D. Poulikakos, and Manfred N. Partl. 2016. "Crystalline Structures in Tetracosane–asphaltene Films." *RSC Adv.* 6 (47). The Royal Society of Chemistry: 41561–67. doi:10.1039/C6RA03708A.
- Schindelin, Johannes, Ignacio Arganda-Carreras, Erwin Frise, Verena Kaynig, Mark Longair,

- Tobias Pietzsch, Stephan Preibisch, et al. 2012. "Fiji: An Open-Source Platform for Biological-Image Analysis." *Nature Methods* 9 (7). Nature Publishing Group: 676–82. doi:10.1038/nmeth.2019.
- Shen, Junan, Serji Amirkhanian, and Boming Tang. 2007. "Effects of Rejuvenator on Performance-Based Properties of Rejuvenated Asphalt Binder and Mixtures." *Construction and Building Materials* 21 (5). Elsevier: 958–64. <https://www.sciencedirect.com/science/article/pii/S095006180600050X>.
- Snyder, Lloyd Robert. 1969. "Determination of Asphalt Molecular Weight Distributions by Gel Permeation Chromatography." *Analytical Chemistry* 41 (10). American Chemical Society: 1223–27. doi:10.1021/ac60279a028.
- Soenen, Hilde, Jeroen Besamusca, Hartmut R. Fischer, Lily D Poulidakos, Jean-Pascal Planche, Prabir K. Das, Niki Kringos, James R A Grenfell, Xiaohu Lu, and Emmanuel Chailleux. 2014. "Laboratory Investigation of Bitumen Based on Round Robin DSC and AFM Tests." *Materials and Structures* 47 (7): 1205–20. doi:10.1617/s11527-013-0123-4.
- Speight, James G. 2014. *The Chemistry and Technology of Petroleum*. CRC Press, Taylor and Francis.
- Storm, David A., Eric Y. Sheu, and Maureen M. DeTar. 1993. "Macrostructure of Asphaltenes in Vacuum Residue by Small-Angle X-Ray Scattering." *Fuel* 72 (7): 977–81. doi:10.1016/0016-2361(93)90295-D.
- Swanson, John M. 1942. "A Contribution to the Physical Chemistry of the Asphalts." *Journal of Physical Chemistry* 46 (1): 141–50. doi:10.1021/j150415a017.
- Toschi, T. Gallina, M. F. Caboni, G. Penazzi, G. Lercker, and P. Capella. 1993. "A Study on Cashew Nut Oil Composition." *Journal of the American Oil Chemists' Society* 70 (10): 1017–20. doi:10.1007/BF02543029.
- Tschoegl, Nicholas W. 1989. "Linear Viscoelastic Response." In *The Phenomenological Theory of Linear Viscoelastic Behavior*, 35–68. Berlin, Heidelberg: Springer Berlin Heidelberg. doi:10.1007/978-3-642-73602-5\_2.
- Tung, L. H. 1966. "Method of Calculating Molecular Weight Distribution Function from Gel Permeation Chromatograms." *Journal of Applied Polymer Science* 10 (3): 375–85. doi:10.1002/app.1966.070100303.
- Weigel, S., and D. Stephan. 2017a. "Modelling of Rheological and Ageing Properties of Bitumen Based on Its Chemical Structure." *Materials and Structures* 50 (1). Springer Netherlands: 83. doi:10.1617/s11527-016-0957-7.
- . 2017b. "Relationships between the Chemistry and the Physical Properties of Bitumen." *Road Materials and Pavement Design*, June. Taylor & Francis, 1–15. doi:10.1080/14680629.2017.1338189.

- White, Kristopher, Nikki Lorenz, Tom Potts, W. Roy Penney, Robert Babcock, Amber Hardison, Elizabeth A. Canuel, and Jamie A. Hestekin. 2011. "Production of Biodiesel Fuel from Tall Oil Fatty Acids via High Temperature Methanol Reaction." *Fuel* 90 (11): 3193–99. doi:10.1016/j.fuel.2011.06.017.
- Williams, Malcolm L., Robert F. Landel, and John D. Ferry. 1955. "The Temperature Dependence of Relaxation Mechanisms in Amorphous Polymers and Other Glass-Forming Liquids." *Journal of the American Chemical Society* 77 (14). American Chemical Society: 3701–7. doi:10.1021/ja01619a008.
- Witczak, M. W., and O. A. Fonseca. 1996. "Revised Predictive Model for Dynamic (Complex) Modulus of Asphalt Mixtures." *Transportation Research Record* 1540 (1): 15–23. doi:10.3141/1540-03.
- Xu, Meng, Junyan Yi, Decheng Feng, Yudong Huang, and Dongsheng Wang. 2016. "Analysis of Adhesive Characteristics of Asphalt Based on Atomic Force Microscopy and Molecular Dynamics Simulation." *ACS Applied Materials and Interfaces* 8 (19): 12393–403. doi:10.1021/acsami.6b01598.
- Yao, Hui, Zhanping You, Liang Li, Chee Huei Lee, David Wingard, Yoke Khin Yap, Xianming Shi, and Shu Wei Goh. 2013. "Rheological Properties and Chemical Bonding of Asphalt Modified with Nanosilica." *Journal of Materials in Civil Engineering* 25 (11): 1619–30. doi:10.1061/(ASCE)MT.1943-5533.0000690.
- Yu, Xiaokong, Nancy A. Burnham, and Mingjiang Tao. 2015. "Surface Microstructure of Bitumen Characterized by Atomic Force Microscopy." *Advances in Colloid and Interface Science* 218. Elsevier B.V.: 17–33. doi:10.1016/j.cis.2015.01.003.
- Yu, Xiaokong, Martins Zaumanis, Salome Dos Santos, and Lily D. Poulikakos. 2014. "Rheological, Microscopic, and Chemical Characterization of the Rejuvenating Effect on Asphalt Binders." *Fuel* 135. Elsevier Ltd: 162–71. doi:10.1016/j.fuel.2014.06.038.
- Zaumanis, Martins, Rajib B. Mallick, and Robert Frank. 2014. "Determining Optimum Rejuvenator Dose for Asphalt Recycling Based on Superpave Performance Grade Specifications." *Construction and Building Materials* 69 (October): 159–66. doi:10.1016/j.conbuildmat.2014.07.035.
- Zhao, Sheng, Benjamin Bowers, Baoshan Huang, Xiang Shu, M Asce, Xiang Shu, and A M Asce. 2014. "Characterizing Rheological Properties of Binder and Blending Efficiency of Asphalt Paving Mixtures Containing RAS through GPC." *Journal of Materials in Civil Engineering* 26 (5): 941–46. doi:10.1061/(ASCE)MT.1943-5533.0000896.

